NATIONAL TECHNICAL UNIVERSITY of ATHENS
SCHOOL of ELECTRICAL and COMPUTER ENGINEERING

DIVISION of COMMUNICATION, ELECTRONIC and INFORMATION ENGINEERING
ELECTRONIC SENSORS LAB

DEVELOPMENT OF A DEW POINT SENSOR BASED ON CHILLED MIRROR HYGROMETER TECHNOLOGY

DIPLOMA THESIS

Panagiotis A. Sarafis

Supervisor: John N. Avaritsiotis
Professor of N.T.U.A.

Athens, June 2010

Εθνικο Μετσοβιο Πολυτεχνειο
Τμημα Ηλεκτρολογων Μηχανικων και Μηχανικων Υπολογιστων

Τομεας Επικοινωνιων, Ηλεκτρονικης και Συστηματων
Εργαστηριο Ηλεκτρονικων Αισθητηρων

ΜΕΛΕΤΗ ΚΑΙ ΚΑΤΑΣΚΕΥΗ ΑΙΣΘΗΤΗΡΑ ΣΗΜΕΙΟΥ ΔΡΟΣΟΥ ΒΑΣΙΣΜΕΝΟΥ ΣΤΗΝ ΤΕΧΝΟΛΟΓΙΑ ΨΥΧΡΟΥ ΚΑΘΡΕΦΤΗ

ΔΙΠΛΩΜΑΤΙΚΗ ΕΡΓΑΣΙΑ

Παναγιώτης Α. Σαράφης

Επιβλέπων: Ιωάννης Ν. Αβαριτσιώτης
Καθηγητής Ε.Μ.Π.

ΕΘΝΙΚΟ ΜΕΤΣΟΒΙΟ ΠΟΛΥΤΕΧΝΕΙΟ
ΣΧΟΛΗ ΗΛΕΚΤΡΟΛΟΓΩΝ ΜΗΧΑΝΙΚΩΝ
ΚΑΙ ΜΗΧΑΝΙΚΩΝ ΥΠΟΛΟΓΙΣΤΩΝ
ΤΟΜΕΑΣ ΕΠΙΚΟΙΝΩΝΙΩΝ, ΗΛΕΚΤΡΟΝΙΚΗΣ
ΚΑΙ ΣΥΣΤΗΜΑΤΩΝ
ΕΡΓΑΣΤΗΡΙΟ ΗΛΕΚΤΡΟΝΙΚΩΝ ΑΙΣΘΗΤΗΡΩΝ

ΜΕΛΕΤΗ ΚΑΙ ΚΑΤΑΣΚΕΥΗ ΑΙΣΘΗΤΗΡΑ ΣΗΜΕΙΟΥ ΔΡΟΣΟΥ ΒΑΣΙΣΜΕΝΟΥ ΣΤΗΝ ΤΕΧΝΟΛΟΓΙΑ ΨΥΧΡΟΥ ΚΑΘΡΕΦΤΗ

ΔΙΠΛΩΜΑΤΙΚΗ ΕΡΓΑΣΙΑ

Παναγιώτης Α. Σαράφης

Επιβλέπων: Ιωάννης Ν. Αβαριτσιώτης
Καθηγητής Ε.Μ.Π.

Εγκρίθηκε από την τριμελή εξεταστική επιτροπή την -εισάγετε ημερομηνία-.

.....	.....	.....
Ιωάννης Ν. Αβαριτσιώτης	Ελευθέριος Καγιάφας	Βασίλειος Λούμος
Καθηγητής Ε.Μ.Π.	Καθηγητής Ε.Μ.Π.	Καθηγητής Ε.Μ.Π.

Αθήνα, Ιούνιος 2010.

.....
Παναγιώτης Α. Σαράφης
(Διπλωματούχος Ηλεκτρολόγος Μηχανικός και Μηχανικός Υπολογιστών ΕΜΠ)

Abstract

Humidity is the second most important environmental variable after temperature. Monitoring and controlling humidity is a quite crucial matter in a wide field of applications concerning industry (e.g. pharmaceutical, automotive, food processing, silicon fabrication), meteorology, medicine and many more.

Measurements on moisture and humidity can be achieved through several sensing mechanisms either physical or chemical. One of the main methods that can be used, is the measurement of the water vapour condensation temperature or else the "Dew Point Temperature". In the first chapter of this thesis a brief review of the available technologies is presented, whereas in the second one the operation of the Chilled Mirror Hygrometer (CMH) is described in detail. CMH is the most fundamental and accurate way of sensing humidity and is used in activities where accuracy and traceability are needed.

In the next chapters, the design and the development of the CMH is explained. Temperature control is based on thermoelectrical devices, while dew detection is achieved through a reflectivity sensor. The control and readout systems are based on a AVR microcontroller (ATmega32) which is synchronizing the attached devices and establishes communication with a computer via an RS-232 port. The final assembly consists of independent sensing and readout systems and can be used for distanced measurements.

An accuracy of $\delta T < \pm 0.2^oC$ and a detection range between $-25^oC < T_{DP} < 60^oC$ were achieved. Supplementary research was conducted on the optimization of the operating algorithms, the results of which are presented inside. The assembly meets the specifications of the commercial CMH, whereas the construction cost is around the one tenth of the current commercial value.

The main part of the sensor's development was carried out during the participation in the CMS -Compact Muon Solenoid- experiment in CERN, Geneva. In this context, the study and the development of this sensor was always targeted in radioactive-environment applications.

Keywords : Chilled Mirror Hygrometer, Dew Point, Thermoelectric Cooling, Humidity, Environmental Sensor, CERN

Περίληψη

Η υγρασία είναι το δεύτερο πιο σημαντικό μέγεθος, μετά την θερμοκρασία, για την περιγραφή του περιβάλλοντος. Η παρακολούθηση και ο έλεγχος της υγρασίας είναι μία αρκετά κρίσιμη παράμετρος για ένα ευρύ πεδίο εφαρμογών, όπως η βιομηχανία (π.χ. αυτοκινητοβιομηχανία, φαρμακοβιομηχανία, επεξεργασία τροφίμων, επεξεργασία πυριτίου), η μετεωρολογία, η ιατρική κ.α.

Η μέτρηση της υγρασίας μπορεί να επιτευχθεί μέσα από αρκετές μεθόδους αίσθησης είτε φυσικές είτε χημικές. Ένας από τους πιο κυριότερους μηχανισμούς είναι ο εντοπισμός της θερμοκρασίας υγροποίησης των ατμοσφαιρικών υδρατμών, ή αλλιώς του "σημείου δρόσου". Στο πρώτο κεφάλαιο γίνεται μία σύντομη ανασκόπηση των υπαρχουσών τεχνολογιών ενώ στο δεύτερο, μία λεπτομερής παρουσίαση της λειτουργίας του υγρομέτρου ψυχρού καθρέφτη (Chilled Mirror Hygrometer - CMH). Το υγρόμετρο ψυχρού καθρέφτη είναι ο πιο θεμελιώδης και ακριβής τρόπος μέτρησης της υγρασίας και χρησιμοποιείται σε εφαρμογές όπου η ακρίβεια και η συμβατότητα είναι αναγκαίες.

Στα επόμενα κεφάλαια επεξηγείται ο σχεδιασμός και η κατασκευή του CMH . Ο έλεγχος της θερμοκρασίας στηρίζεται σε θερμοηλεκτρικές συσκευές, ενώ η ανίχνευση του δρόσου γίνεται μέσω ενός αισθητήρα ανακλαστικότητας. Το κύκλωμα ελέγχου και ανάγνωσης είναι βασισμένο στον μικροελεγκτή AVR (ATmega32) ο οποίος συγχρονίζει τις επί μέρους συσκευές και διασυνδέει τον αισθητήρα με έναν Η/Υ μέσω της θύρας RS-232.Η τελική κατασκευή έχει ανεξάρτητα κυκλώματα αίσθησης και επεξεργασίας και είναι κατάλληλη να χρησιμοποιηθεί σε μετρήσεις εξ αποστάσεως.

Η επιτευχθείσα ακρίβεια μέτρησης είναι της τάξης του $\delta T < \pm 2^oC$ και το εύρος ανίχνευσης $-25^oC \leqslant T_{DP} \leqslant 60^oC$. Επιπλέον έρευνα διεξήχθη για τη βελτιστοποίηση των αλγορίθμων λειτουργίας, της οποίας τα αποτελέσματα παρουσιάζονται στο αντίστοιχο κεφάλαιο. Η τελική κατασκευή ανταποκρίνεται στις προδιαγραφές των εμπορικών CMH, ενώ το κόστος κατασκευής ανέρχεται στο ένα δέκατο της τιμής τους.

Το κύριο μέρος της ανάπτυξης του αισθητήρα συνέβη κατά τη διάρκεια συμμετοχής στο πείραμα CMS -Compact Muon Solenoid- στο ερευνητικό ίδρυμα CERN, στη Γενεύη της Ελβετίας. Σε αυτό το πλαίσιο, η μελέτη και η κατασκευή αυτού του αισθητήρα έχει γίνει με κύριο άξονα τη χρήση του σε ραδιενεργό περιβάλλον.

Λέξεις Κλειδία : Υγρόμετρο Ψυχρού Καθρέφτη, Σημείο Δρόσου, Θερμοηλεκτρική Ψύξη, Υγρασία, Περιβαλλοντικός Αισθητήρας, CERN

Acknowledgements

The current diploma thesis had started in the Electronic Sensors Lab of the Electrical and Computer Engineering School of N.T.U.A, with Professor John Avaritsiotis acting as supervisor. Its main part was continued in CERN, Geneva under the supervision and cooperation of Researcher Andromachi Tsirou and Professor Piero Giorgio Verdini.

I would like to express my warmest acknowledgements to the three of them, for encouraging and helping me to get involved in the field of electronic sensors. Without them and their valuable knowledge, I would be neither able nor motivated to study this very interesting combination of theory and technology. Especially, I would like to thank them for trusting and providing me with the unique chance of participating in the CMS experiment that is taking place in CERN. Also, I owe special thanks to Mr. Apostolos Psarros from the Electronic Sensors Lab for his help in solving technical problems that had arisen during the implementation.

Of course, I cannot forget my family, which with great efforts, has been standing by me, since the beginning of my life.

Last, but not least, I would like to thank all my fellow students and collaborators, who helped in solving various small and big problems -either practical or theoretical- during this project. Particularly, Cristos Spatharakis, Julia Giasemi, Grigoris Piperagkas, Nikos Nikoleris, Efi Vokali and Athina Gerangelou for spending much of their personal time, each one of them in his specific field.

Panagiotis A. Sarafis

Ευχαριστίες

Η παρούσα διπλωματική εργασία ξεκίνησε στο Εργαστήριο Ηλεκτρονικών Αισθητήρων της Σχολής Ηλεκτρολόγων Μηχανικών και Μηχανικών Υπολογιστών του Ε.Μ.Π., υπό την επίβλεψη του Καθηγητή Ιωάννη Αβαριτσιώτη. Κατά το μεγαλύτερο μέρος της, συνεχίστηκε στο ερευνητικό κέντρο του CERN στη Γενεύη της Ελβετίας, υπό την επίβλεψη και τη συνεργασία της Ερευνήτριας Ανδρομάχης Τσίρου και του Καθηγητή Piero Giorgio Verdini.

Θα ήθελα να εκφράσω τις θερμές μου ευχαριστίες και στους τρεις για την παρότρυνση και τη βοήθεια που μου έδωσαν στην ενασχόληση με τον τομέα των ηλεκτρονικών αισθητήρων. Χωρίς αυτούς και την πολύτιμη γνώση τους, δεν θα είχα ούτε την έμπνευση ούτε τη δυνατότητα να μελετήσω αυτόν τον πολύ ενδιαφέροντα συνδυασμό θεωρίας και τεχνολογίας. Ιδιαιτέρως, θα ήθελα να τους ευχαριστήσω που με εμπιστεύτηκαν και μου έδωσαν την ευκαιρία, ο καθένας από τη μεριά του, να συμμετέχω στο πείραμα CMS που διεξάγεται αυτή τη στιγμή στο CERN. Επίσης, θα ήθελα να ευχαριστήσω τον κ. Απόστολο Ψαρρό από το Εργαστήριο Ηλεκτρονικών Αισθητήρων για τη συμβολή του στην επίλυση των τεχνικών προβλημάτων που ανέκυψαν κατά τη διάρκεια της υλοποίησης.

Δεν θα μπορούσα να μην ευχαριστήσω την οικογένεια μου που, με πολύ κόπο, με στήριξε και συνεχίζει να με στηρίζει καθ'όλη τη διάρκεια των σπουδών και της ζωής μου.

Τέλος, θα ήθελα να ευχαριστήσω όλους τους συμφοιτητές και συνεργάτες που βοήθησαν στην επίλυση μικρών και μεγάλων προβλημάτων -είτε πρακτικών, είτε θεωρητικών- που ανέκυπταν κατά τη διάρκεια της εργασίας. Ιδιαιτέρως, τους Χρήστο Σπαθαράκη, Ιουλία Γιασεμή, Γρηγόρη Πιπεράγκα, Νίκο Νικολέρη, Ευθυμία Βόκαλη και Αθηνά Γεραγγέλου, που, χωρίς φειδώ του προσωπικού τους χρόνου, με στήριξαν σε όλους τους επιμέρους τομείς.

Παναγιώτης Α. Σαράφης

Contents

List of Figures

Chapter 1

Overview of the Humidity Sensing Technology

1.1 Introduction

Humidity is an important environmental variable that expresses the amount of water vapour that is included in the air. As it is well known, water vapour is a natural component of air and a universal solvent playing an important role in a wide range of applications. It can impact many chemical reactions and the mechanical properties of many hygroscopic materials. Monitoring humidity is vital for a wide variety of applications as silicon wafer processing, rear window defoggers in automotive industry, respiratory equipment, sterilizers, incubators, pharmaceutical processing and biological products in medical field. In agriculture humidity sensors are used for green-house air-conditioning, dew prevention, soil moisture monitoring and cereal storage. In domestic applications humidity is important for applications such as intelligent control of living environment in building, cooking control for microwave ovens, intelligent laundry and many relative subjects. In general industry humidity sensing is used for chemical gas purification, dryers, ovens, film desiccation, textile production and food processing.

Moreover humidity monitoring is crucial in complicated electronic systems that operate in very low temperatures and there is high risk of water condensation. Such systems can exist either in space and aeronautic industry, in particle detectors or in the nuclear factories. In these applications special sensors are required that should be very reliable, stable and resistant to extreme environmental conditions (e.g. exposure to chemicals, heavy irradiation, extremely low and extremely high temperatures).

A good sensor should combine the following features : (a) Good sensitivity over a wide range of humidity and temperature conditions (b) Short response time (c) Good reproducibility (d) Small hysterisis (e) Resistance against harsh environments (e.g. contaminants, magnetic field, radiation) (f) Negligible temperature dependence (g) Low cost (h) Small size - easily integrated.

In this chapter a brief review on the existing humidity sensors will be pre-

Market Segment	Application	T Range(^oC)	RH range (%)
Indoor Comfort	Winter	22	30-70
	Summer	24	30-70
Manufacturing			
-Electronics	ESD Control	22	30-70
-Semiconductors	Clean Rooms	21	36-39
-Food Processing	Food Dehydration	50-100	0-50
-Printing	Web-Printing		40-55
-Materials	Dryers	5-100	0-50
Medical	Operating room	20-25	50-80
	Infant incubator	10-30	50-80
Automotive	Window defogger	-20-80	50-100
	Windscreen wipers	-20-80	50-100
Meteorology	Weather radiosondes	-50-50	0-100

Table 1.1: The applications of water vapour sensing

sented with emphasis in the most efficient and competitive technologies. The definitions concerning hygrometry terms like Relative Humidity (RH), Dew/Frost Point (DP/FP), etc. are explained in Appendix A.

1.2 Humidity Sensors Classification

The main methods of measuring RH and dew-point vary between generic resistive, capacitive, optical and mass sensitive concepts. Most of them are based on the microscopic properties of certain materials (e.g. miniaturized sensors that use a sensitive thin film as in most capacitive, resistive sensors) and some other on more generalized macroscopic mechanisms of RH measurement and dew-point detection (e.g. Chilled Mirror Hygrometers, Wet Bulb Hygrometers).

A prerequisite to understand several of these water vapour sensing mechanisms is to explain the properties of the humidity sensitive material that they employ as a sensing element. These materials are usually used in thin films that change their electrical/mechanical properties according to water vapour variations. This transformation is performed in a three-step process :

1. physical/chemical interaction of the vapour with the film surface

2. surface and bulk modifications of the film due to water vapour

3. electrical measurement of a key electrical/mechanical property of the film that changes due to its interaction with water vapour.

Chemical vapour interacts with the film surface through three mechanisms : adsorption, coordination chemical or chemisorption.

Adsorption involves a weak interaction between the vapour and the surface of the sensing material via Van der Waals forces or acid-base reactions. Van der Waals forces are based on a low energy dynamic balance between molecular attractive and repulsive forces involving reaction of energies of the order of 0-10kJ/mole. Acid-base reactions between the target gas and the sensing element react with higher energies, although usually lower than 40kJ/mole. Depending on the structure of the film (e.g. affinity to water, bulk porosity), water may be absorbed into the bulk through diffusion or capillary action.

Chemical Coordination involve films containing metal-ligand complexes, such as metallophtalocyanines.

Chemisorption involves strong vapour-film interactions where chemical bonds are broken and formed with reaction energies over 300kJ/mole.

A key element to prolong the lifetime of a humidity sensor is to build it on reversible low energy reactions rather than on irreversible high energy. This point fits ideally to the first two low-energy mechanisms, as mentioned above. On the other hand chemisorption reactions are usually irreversible and may require extra thermal energy input to regenerate the sensing ability of the film.

The main materials that are used as sensing films in the commercial humidity sensors are ceramics, polymers and poly-electrolytes. The variation of the properties of these materials permits their use as capacitive or resistive humidity sensors, depending on the specific properties of the material and the sensor's operation concept.

1.2.1 Capacitive Humidity Sensors

Capacitive-based water vapour sensors are the most widely commercialized humidity sensors in today's marketplace and are mainly targeted to measure RH. Capacitive humidity sensors are usually constructed with interdigitated electrodes that are covered with a humidity-sensitive material. The total capacitance for this layout is the sum of the fringing capacitances between adjacent fingers where the sensing element is acting as a dielectric layer. However, the most common design configuration consists of a parallel plate capacitor with two polymer layers. The top polymer is a porous film that actually acts as a mechanical filter against contamination, dust and dirt. An upper electrode is patterned and deposited on top of the sensing film. A lower electrode layer resides between the sensing film and the silicon substrate. Variations of this design exist either without the porous filter or with various electrode geometries to optimize sensor performance.

Depending on the application of the humidity sensor the sensor readout could be distanced resulting in a high capacitance induced by the long cables. The necessity of a basic signal conditioning circuit near the sensor is prominent. This circuit should use a method to transform capacitance into voltage and can be achieved

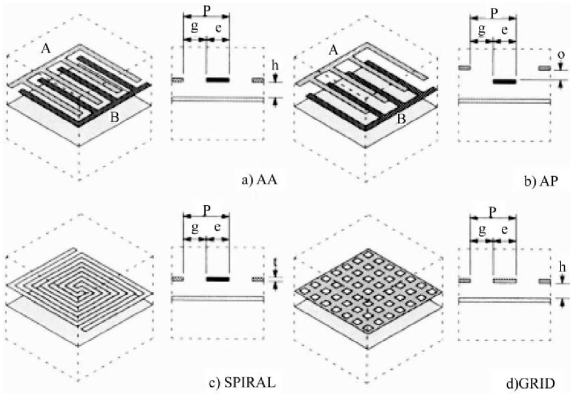

Figure 1.1: Electrodes for capacitive humidity sensors as presented by Korvink et al. [1]

through a frequency to voltage converter. Thus, this is the main disadvantage of this configuration as the environment of several applications (i.e. space, nucleat) can be extremely hostile to electronics which are exposed to it.

1.2.2 Resistive Humidity Sensors

Resistive sensors operate in a similar way as the capacitive thin film sensors measuring the change in the conductivity of a sensitive film due to the uptake of water vapour. Another class of resistive RH sensors exploits the volumetric changes of polymeric films as a function of humidity. At the bottom lies a humi-sensitive polymer film while above there is an arrangement of piezoresistors (usually in a Wheatstone bridge configuration). Water absorption causes polymer swelling which induces an extra strain on a piezoresistors, transducing the polymer deflection into an output voltage. An advantage of this sensor over the rest resistive and capacitive sensors is that the polymeric film can be electrically isolated from the sensing electrodes, leaving apart the possibility of strong effects on the accuracy and long term stability of capacitive sensors when the film is in electrical contact with the electrodes [2].

One of the most representative sensors of that type is HMX-2000 by Hygrometrix and it was the one that was thoroughly studied as it proved to be quite radiation resistant and suitable for humidity monitoring inside the CMS Silicon Strip Tracker.

1.2.3 Mass Sensitive Humidity Sensors

Quartz Crystal Microbalance (QCM)

The most widely known gravimetric humidity sensor is the Quartz Crystal Microbalance (QCM)[3]. Thin plates of piezoelectric quartz have resonance (thickness-or and shear-mode) frequencies in the MHz-range. Coated with a hygroscopic layer,

the change of frequency acts as a measure for the humidity. The change of the frequency, Δf, can be approximated with the equation of Sauerbrey, assuming that the adsorbed vapour behaves like a rigid mass:

$$\Delta f = -2\frac{f_o}{A\sqrt{\mu\rho}}\Delta m$$

where A is the surface area, f_o the nominal frequency, μ the shear modulus, ρ the density and Δm the change of mass caused by the adsorption.

The resonance frequency of the quartz crystal depends not only on the mass change but also on the viscosity of the gas, the stress of the film, the pressure, and the temperature. In usual measurements where the water vapour concentration is detected under a constant gas flow condition, all but the temperature effect are not significant. Therefore, stabilization of the temperature of a quartz crystal is very important in respect to the sensitivity and the accuracy of the measurements. However by using a non-coated reference resonator, cross-sensitivities of pressure and temperature can be compensated and minimized.

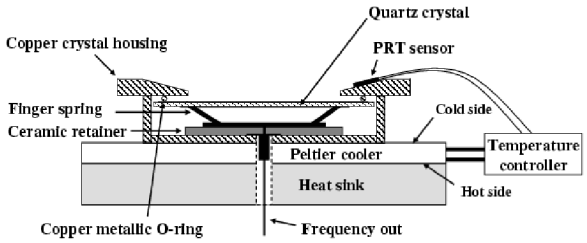

Figure 1.2: Layout of the QCM humidity sensor structure as constructed by Su Yong Kwon [4]

Evidently, the properties -response time, sensitivity, and hysteresis- of the QCM are largely dependent on the applied hygroscopic film. A few interesting devices have recently been presented, e.g. with fullerene layers [5], with sol-gel-derived silica coatings [6] and with polyimide [7]. In addition, porous ceramics have been used, such as for instance Al_2O_3. With this technique mass differences as small as $10^{-8} - 10^{-10} gr$ can be detected, proving that these devices are particularly efficient for very low humidity concentrations.

Surface Acoustic Wave (SAW)

Another use of the mass loading effect occurs in SAW devices. These devices may increase considerably the accuracy of humidity measurements because of their dual ability to detect due deposition and to measure the temperature with great accuracy. Here, the phase velocity of surface waves is changed in the presence of adsorbed vapour. SAW devices have particular application not only in microanalytical systems but in temperature and pressure sensors as well [8].

The operation of a SAW humidity sensor can be described as follows. Surface acoustic waves are launched onto the SAW sensor delay path via the reverse piezoelectric effect when an RF signal, at the microsensor's center frequency, is applied

to the input interdigitated transducers (IDT). This creates a series of SAWs which travel across the delay path to the output IDT where they are converted back into an electrical signal. The device can consist of two IDT pairs, i.e. either one emitter and one receiver, or it may additionally contain two reflector electrodes on either side of the IDT which compose a SAW-resonator or SAW-filter.

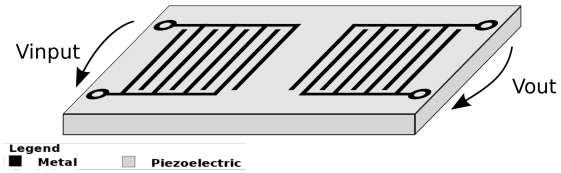

Figure 1.3: The typical construction of a SAW device on a piezoelectric material

The microsensor is cooled down with the use of a thermoelectric cooler. As the cooling proceeds condensation forms on its surface affecting the properties of the channel between the two IDT. The same effect is achieved if a hygroscopic material is placed in between the two IDT. As the environmental humidity rises up the amount of water vapour that will get adsorbed increases affecting the SAW velocity and attenuation. The relative change of the phase velocity ν can be measured either as a phase or a frequency difference, i.e.

$$\frac{\Delta\nu}{\nu_o} - \frac{\Delta\phi}{\phi_o} = \frac{\Delta f}{f_o}$$

or

$$\frac{\Delta\nu}{\nu_o} = -\frac{\pi h \nu_0^2}{2\lambda}\Delta\rho(A_x^2 + A_y^2 + A_z^2)$$

where h is the thickness of the film, ν_o the nominal velocity, $\Delta\rho$ the mass loading, λ the acoustic wavelength and A_i (i = x, y or z) the normalised displacement amplitudes of the SAW.

Adsorption of vapour on a hygroscopic film placed in between the IDT changes both the amplitude and the phase of the SAW. The sensitivity of the device can be improved by etching a membrane structure, as this will lead to larger deflection and smaller acoustic losses into the bulk.

1.2.4 Fibre-Optic Humidity Sensors

The physical background of optical humidity sensors is a harmonic electromagnetic wave with amplitude E_o, frequency ω and phase ϕ or else $E(t) = E_o cos(\omega t + \phi)$. Information about the air humidity can be achieved through the amplitude, the polarisation, the frequency or the phase of the wave. Another application of optical techniques makes use of the absorption wavelength of water; when light is passed through a gas, the absorption of certain wavelengths provides information about the composition. Adsorbed water can change both the amplitude and the polarization of an incident optical signal.

Interferometric sensors

Optical interferometry is a powerful and versatile tool that has been applied in optical fibre sensing to yield high performance sensors. The sensing mechanism relies on the perturbation of the phase properties of the light signal travelling in the optical fibre introduced by an external environment. The detection of the phase change is realised by mixing the signal of interest with a reference signal, consequently converting the phase difference between the two signals into an optical intensity change. Various interferometer configurations such as the Mach-Zehnder, Michelson, Sagnac and Fabry-Perot can be used to perform the detection.

One of the earliest fibre-optic interferometric humidity sensors was demonstrated by Mitschke [9]. The proposed sensor design consists of a structure at the tip of the optical fibre that will act as a Fabry-Perot interferometer (see Figure 1.4). The interference between the optical signals reflected by the mirror at both ends of the cavity gives rise to a spectral response which maximizes its intensity output (resonances) at specific wavelengths. As the refractive index of the cavity material has a dependence on humidity, the resonance is therefore shifted in response to humidity change and can be conveniently detected by performing intensity measurement at a fixed wavelength.

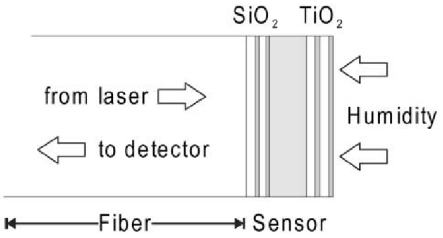

Figure 1.4: A prototype fibre-optic Fabry-Perot interferometric humidity sensor as designed by Mitschke [9]

The Fabry-Perot cavity in the proposed design was created by a layer of TiO_2 sandwiched in between two partially reflecting mirrors, with the thickness of the cavity optimised to match the operation at the wavelength of the input diode laser source. The demonstrated sensor suffers from cross-sensitivity to temperature which can be corrected using a suitable compensation scheme. Nevertheless, it showed a good response between 0 and 80%RH and a response time of less than a minute.

In-fibre grating sensors

Fibre grating is a UV-created periodic structure in the fibre which modulates the refractive index of the core. This procedure can be generally classified in two main categories depending on the grating period; Fiber Bragg Grating (FBG) and Long-Period Fibre Grating (LPFG).

The LPFG (Fig. 1.5b) can be employed as a general refractive index sensor and used in conjunction with chemical selective materials to create a species-specific chemical sensor. Thus this forms a very attractive, refractive-index-based, chemical sensing mechanism which has been employed in the detection of a variety of chemical species.

The FBG-based sensors (Fig. 1.5a), on the other hand, are on the whole used predominantly for the monitoring of physical parameters such a temperature, strain or pressure. A common approach to use a FBG as a humidity sensor is to select a material selectively sensitive to water vapour and capable of inducing mechanical deformation as it interacts with moisture. This is done to produce a secondary strain-induced change that will be measured through the FBG sensor. The selection of the sensing materials for a FBG chemical sensor is therefore more stringent than LPFG as it should not only be responsive to vapour but also be able to deform in order to induce strain on the FBG.

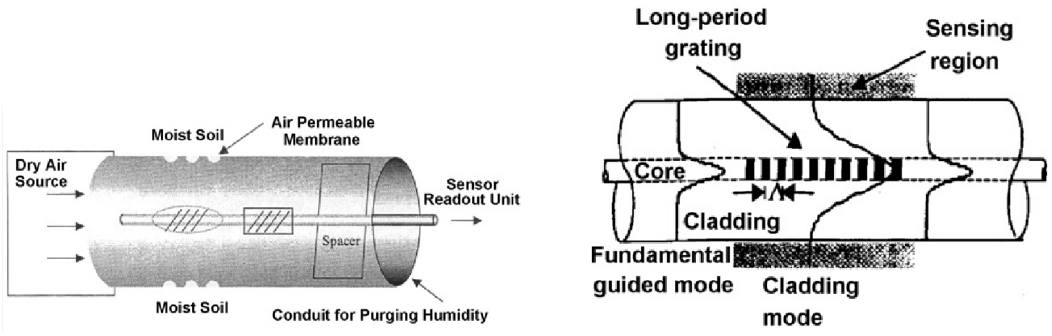

(a) (b)

Figure 1.5: a. Description of a FBG humidity sensor [10] b. Description of a LPFG humidity sensor [11]

Refractive index change

Refractive index change is another approach frequently used in the fibre-optic sensing. The main idea of this device is that the refractive index of the cladding is varying with humidity affecting the light propagation. As it can be seen in Figure 1.6 the cladding is replaced by a humidity sensitive material which varies its refractive index according to the amount of water vapour contained in the air. This fluctuation forces a leaky propagation mode resulting in gradual signal attenuation which is the basis of humidity detection.

A similar application that relies on the same mechanism is the use of a side-polished optical fibre with a humidity sensitive overlay. A typical example of such a sensor is the one demonstrated by Alvarez-Herrero [12]. The flat surface that is parallel to the fibre axis is polished back to remove the cladding. Side-polishing should be followed by the immobilization of fibre through the use of a rigid material

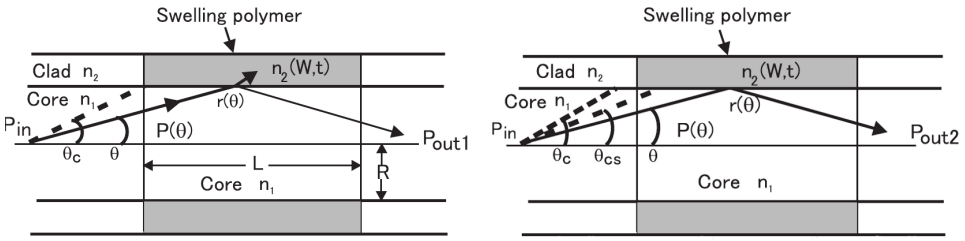

(a) $n_2 > n_1$ Leaky (b) $n_2 < n_1$ Guided

Figure 1.6: The basic concept of a refractive index humidity sensor

that will prohibit the induction of parasitic effects to the final signal and form the substrate for the humidity sensitive overlay (in this case TiO_2). The humidity dependent optical response of the sensor is monitored through a wideband spectrum consisting of the resonance bands which satisfy the phase matching conditions [1].

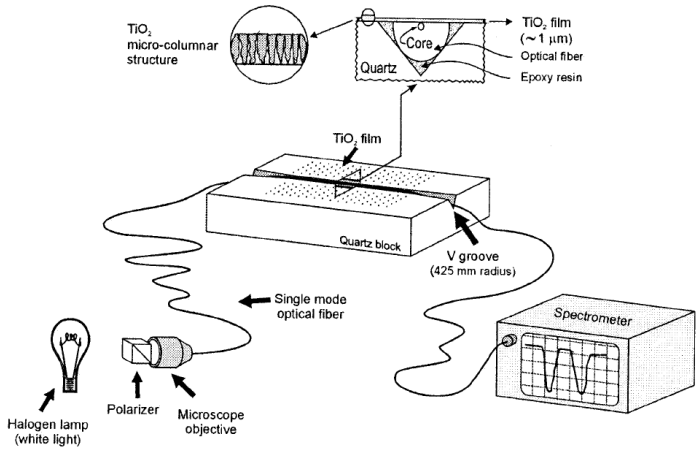

Figure 1.7: Experimental setup for measuring humidity induced resonance wavelength shift of a side-polished optical fibre [12]

1.2.5 Wet and Dry Bulb Psychrometer

A simple and relatively low cost method which has been popular for humidity measurements is the wet and dry bulb psychrometer. It consists of a pair of matched electrical thermometers one of which is covered with a damp wick to determine the wet bulb temperature and the other one is free to measure the temperature of the sampled gas (dry bulb temperature). The dry bulb temperature is simply the temperature of the air, whereas the wet bulb temperature is the temperature achieved

[1]This happens when the refractive index of the guided mode equals to that of the highest order mode of the overlay resulting in the optical coupling between the fibre and the overlay

as a result of water evaporation and latent heat transfer. The difference of these two temperatures is called wet-bulb depression and is in one-to-one match with relative humidity. Examples of such measuring device are the sling psychrometer which operates by whirling the device through the air to obtain the temperature readings and the Assman psychrometer, a similar device with a fan attached to the unit to provide air flow.

(a) (b)

Figure 1.8: a. Assman psychrometer concept of operation b. Sling psychrometer

The accuracy of a wet and dry bulb psychrometer is strongly dependent on the accuracy of the thermometers, thus the use of precise and reliable Resistance Temperature Detector (RTD) is very common. In general psychrometer is a fundamental measurement system and, if properly calibrated and operated, can provide with very accurate, reliable and repeatable measurements. For this reason wet and dry bulb psychrometers have been used in the past as a fundamental calibration standard.

1.2.6 Infrared optical absorption hygrometer

Transmission of infrared and ultraviolet radiation through a gaseous medium is not uniform at all wavelengths. Selective absorption of radiation occurs in certain bands which are characteristic of the particular gas that radiation is crossing. The operation of the infrared psychrometer is based exactly on this scheme, as the presence of water vapour affects the absorption of the light beam. This absorption is maximum in bands in bands centered at $2.7\mu m$ and $6.3\mu m$.

Operation of an IR hygrometer is mainly based on a differential dual-wavelength absorption method. A primary wavelength is selected in the bands where optical absorption is strong and a secondary nearby wavelength where absorption is negligible (reference signal). The ratio of these two signals expresses the normalised transmission which excludes electro-optical drifts, deposits and haze/fog in the sample volume. Basing on the assumption that transmission losses due to gases

other than water vapour will be the same for both the primary and the reference the transmission ratio expresses only the amount of water vapour in the air. The sensitivity of the instrument is dependent on the absorption path length and consequently is modelled through the Beer-Lambert law:

$$T = e^{-\sigma l N}$$

where T is the transmissivity of light through a substance, l the distance the light travels through the material (i.e. the path length), σ is the absorption cross section[2] and N the (number) density of absorbers.

1.2.7 Chilled Mirror Hygrometer

The Chilled Mirror Hygrometer, also known as the optical condensation hygrometer, is a device based on an optical technique for the determination of the dew-point temperature. Up to now it is known to be the most accurate and reliable method providing reference measurements for calibration. The chilled mirror hygrometer is used to provide accuracy as high as $\pm 0.1^{o}C$ demanding though regular maintenance due to contaminants that settle on the mirror surface.

On the following chapters we will extensively analyse the operation and the construction of this kind of sensor.

[2]Absorption cross section is a measure for the probability of an absorption process. More generally, the term cross section is used in physics to quantify the probability of a certain particle-particle interaction.

Chapter 2

Chilled Mirror Hygrometer

2.1 Introduction

The chilled mirror hygrometer, or sometimes called optical condensation hygrometer, is the most accurate, reliable and fundamental hygrometer that is commercially available, even since 1960s. Due to its traceability it is widely used as calibration standard with accuracies as high as 0.1^oC. The main drawback is that it is quite expensive for a single sensor and it requires regular maintenance by skilled personnel.

2.2 Concept of Construction

The chilled mirror hygrometer consists of a small, polished metal mirror that is attached to a cooling module. A thermometer is glued either on or beneath the polished surface of the metal mirror in order to monitor the actual temperature of it. The condition of the mirror surface is continuously checked through a reflective sensor that is situated above the polished side. An LED pours light on the mirror and a photoreceiver (e.g. photodiode, phototransistor or photodarlington) measures the reflectance, recognising the formation of dew/ice. In several implementations there is an extra LED-photoreceiver couple that is used for cancelling the environmental effects like temperature and radiation on the reflectance measurements.

Metal Mirror

The main criteria for choosing between different metal mirrors is thermal conductivity and the reflectance ratio of the polished surface. The main constraint is the need for excellent thermal conductivity and for a flat and polished surface that bears high reflectance at the application's wavelength. Taking into account all the factors above the most appropriate metals are rhodium, stainless steel, platinum or aluminium. Industry usually uses either rhodium or gold-plated mirrors that show

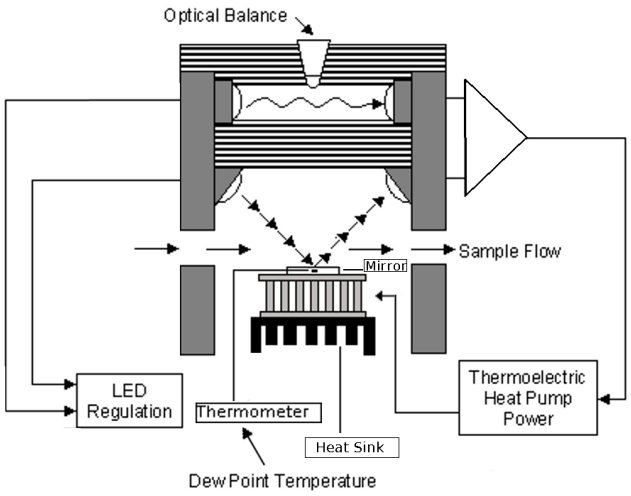

Figure 2.1: Chilled Mirror Hygrometer with differential reflector measurements

excellent chemical stability and robustness to contaminated environments. However, anodized aluminium can be used as a lower budget solution, combining quite good reflectance in the infrared frequencies with very good thermal conductance.

Cooling Module

A typical dew point meter should be able to detect dew points varying from -40^oC to 30^oC. The usual method for implementing this operational range in a chilled mirror hygrometer is through the use of a Thermo-Electric Cooler (TEC) (see appendix B). Commercial CMH are available in single or multiple staged modules achieving measurements even at -85^oC and a dew-point depression[1] above 110^oC. TEC solution also provides easy integration into a compact probe and the possibility of future sensor miniaturization.

Reflective Sensor

The reflective sensor constitutes of a high intensity LED and a photo-detector. While the LED illuminates the mirror, the intensity of the reflected is measured with the optical detector i.e. a photo-transistor. The reflectance ratio is afterwards translated to a description of the mirror state. When there is no dew or frost on the surface, maximum light is received through the detector and the reflectance of the mirror is high. On the other hand when the metal mirror is cooled below the dew-point then moisture condenses on the surface causing light scattering and thereby reducing the amount of light received by the photo-detector.

[1]Dew point depression is a CMH specification that expresses the temperature difference between sensor body and the mirror surface

A separate LED and photo-transistor pair is usually used to compensate for thermally caused effects on the optical components. The two receivers are arranged in an electrical bridge with adjustable balance which controls the current to the TEC and, therefore, the metal mirror temperature.

Thermometer

The thermometer should be a very small, low power component with excellent thermal coupling to the metal mirror. Errors that distort the regional temperature distribution (i.e. self-heating, considerable thermal capacitance) should be minimized. Judging from the above the most appropriate devices are thermistors and RTDs that can be easily inserted within the mirror volume and are very convenient to read through a simple readout circuit.

2.3 Method of Operation

2.3.1 Conventional Chilled Mirror Hygrometer

Operation of the basic optical dew-point hygrometer is described in Figure 2.2. The system is designed to be kept in stable temperature only when a predetermined layer of dew or frost is maintained on the surface of the mirror. Under these equilibrium conditions, the surface temperature is precisely at the dew-point of the gas passing over the mirror. When the mirror is clean a perfect layer of condensed water is maintained on the surface resulting in high accuracy and repeatability.

The main drawbacks of this method are the accuracy distortions that occur from mirror contamination and the lack of surface should be cleaned regularly from the deposited contaminants and that there is no evidence on whether we measure the dew or the frost point of the gas resulting in a systematic error of 3-7^oC.

2.3.2 Automatic Balancing Control (ABC)

The Automatic Balancing Control method automatically interrupts the control loop at prescribed user defined intervals, for example every 12, 24 or 48 hours, depending on the contamination levels of the environment. The mirror is then heated to a temperature above ambient causing the dew to evaporate and leaving only the contaminants on the mirror. The reflectance from the clean but contaminated mirror is then supposed to be the reference value to which we will compare the amount of light received by the photo-detector. The ABC method does not remove any contaminants from the mirror. It only re-standardises the expected reflectance on clean mirror conditions and extends the time period between the required mirror cleanings. However, this method does not take into account the effect of the soluble contaminants to the water vapour pressure resulting in measuring a "fake" dew point.

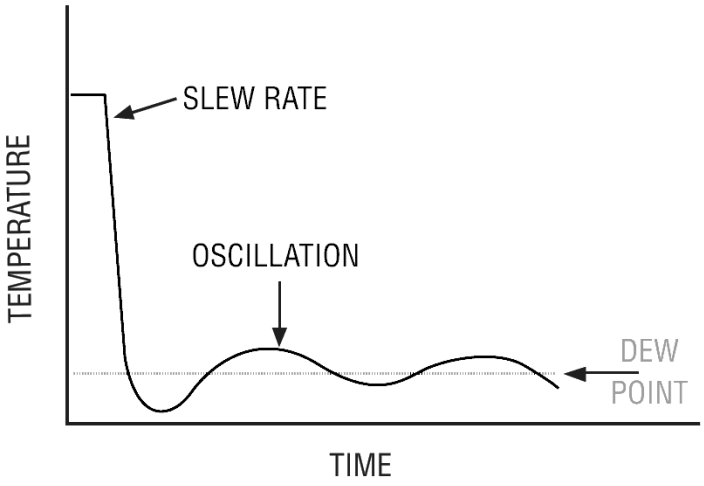

Figure 2.2: Typical response of conventional chilled mirror hygrometers

2.3.3 Programmable Automatic Contaminant Error Reduction (PACER)

The PACER technique is an improvement on the ABC method in order to have a better control on the levels of contamination. The main concept is that through PACER a redistribution of the contaminants is achieved. Unlike the ABC method, it first causes the mirror to cool down below the dew point and thereby increasing the thickness of the layer. A thick layer allows the formation of a "puddle" containing all the contaminants. The PACER method then forces the mirror to rapidly heat up, evaporating the water and breaking the puddle into smaller "puddles" which group the surrounding contaminants. While evaporating the "puddles" shrink in size forming isolated conglomerations of contaminants and leaving bare regions on the mirror surface.

2.3.4 Cycling Chilled Mirror Hygrometer (CCM)

The CCM hygrometer uses a cycling chilled mirror method. The mirror temperature is lowered at a precisely controlled rate until the formation of dew is detected. Before the dew sample is able to form a continuous layer on the surface of the mirror, the mirror is heated up and the formatted dew is evaporated. Hence, the mirror is almost always in the dry state and keeps a water layer only for a short time, during the dew point measurement. This short period of time is not enough for the dew layer to be transformed into frost, even when well below 0^oC. This eliminates the typical problem of conventional chilled mirror hygrometers to detect whether we are measuring dew or frost point when sitting below 0^oC.

Mirror Cycling Procedure

Step 1 : Rapid cooling of the mirror, from a level above ambient temperature, to approxiamtely 1.5^oC above the last known dew point temperature. This reduces the total cycle time, especially when the difference between the measured dew-point and the ambient temperature is large.

Step 2 : Starting at 1.5^oC above the last dew-point measurement the cooling rate is slowed down in order to approach and pass the dew-point as slowly as possible allowing uniform and repeatable formation and detection of the dew layer.

Step 3 : When the dew detection is completed, the TEC current is reversed, causing a rapid rise in temperature rise to few degrees above ambient temperature.

Step 4 : A short period of time between successive cooling loops allows the surface mirror to stabilise thermally and the formed dew layer to evaporate completely.

In this method the time, while a liquid layer on the mirror surface is present, is reduced in almost 5-10% of the whole circle. The advantage of a dry mirror is that particular contaminants do not attach to the mirror surface comparing to the ones that settle in the wet mirror. Moreover it prohibits chemical reactions between constituents and the water droplets in the mirror, a situation that affects the energy exchange with the environment and distorts the measured dew point.

2.4 Deviation in Actual Dew Point Measurements

Chilled mirror dew-point hygrometers are instruments which utilize a thermoelectrically cooled, optically sensed mirror to measure the temperature at which the vapour adjacent to the surface is in equilibrium with the vapour in the sample gas. This is by definition the dew-point temperature of the gas and therefore CMH can be characterized as a fundamental instrument. The errors associated with the dew-point measurement can be divided in two categories :

- Errors which are induced through the assumptions about the quality of the air, the lack of contaminants and water layer phase. Mainly based on the physical effects that affect the ideality of the water layer on the mirror surface.

- Errors which involve the measurement and display of the surface temperature.

2.4.1 Mirror Surface Errors

The Kelvin Effect

When the water distribution on the mirror is uneven we consider the surface as a sum of droplets rather than a uniform layer. The effect of a small droplet is to increase the mirror vapour pressure due to surface tension forces of the droplet and to reduce the mirror temperature required for a given gas vapour sample content. The magnitude of this effect greatly depends on the condition and the treatment of the mirror surface and on the fraction of dry mirror reflectance chosen for the operating point. As thicker the water layer gets, less reflectance we measure and less error is induced due to the Kelvin effect.

The Raoult Effect

The presence of soluble contaminants and especially salts reduces the vapour pressure at the mirror surface for a given temperature. This effect alters the condensation temperature and misleads the system to faulty measurements of the dew point of the contaminant-water mixture instead of the one of the flushed air. The magnitude of the effect is depended on both the concentration and the kind of the contaminants and can reach even 5^oC. For a given amount of contaminants on the mirror surface, a thicker operating layer can help to reduce this effect and the resulting errors.

Dew/Frost Interpretation Errors

In the region between 0^oC and -30^oC, a condensation layer can exist either in water phase or in ice. Water may be preserved for an undetermined period of time (even permanently), thereby introducing a significant error, on the condition that the instrument cannot recognise the phase (supecooled dew or frost) it is referring to. This is particularly true if the mirror is completely clean or if it is contaminated with salty deposits. There is no automatic way to determine the nature of the layer and there is a strong research effort for this. The most usual way is to inspect the mirror surface with a microscope and visually determine the phase of the deposit. As it has been discussed, the CCM hygrometer offers the advantage of always measuring dew point, because of the very short time the water layer exists on the mirror surface. For conventional hygrometers there is another procedure that can be used to eliminate this error. This involves forced cooling of the mirror to well below the frost point by overriding the automatic control system. The mirror must be kept to this temperature for a significant period of time, until the deposited dew is frozen. With this method we ensure that the measurements below 0^oC are, in fact, determining the frost point of the air sample.

Errors from Other Vapour Constituents

Though the condensation hygrometer is a fundamental instrument it cannot distinguish between water vapour and other gaseous vapours. When the mirror is

cooled it is assumed that the first vapour to condense is coming from water, as it is usually the first to saturate. In case that the sample contains gases which condense in higher temperature than water, the instrument will measure other vapours than water. Relying on this some condensation hygrometers are used to control gases such as carbon tetrachloride, freon and ethers.

2.4.2 Mirror Temperature Measurement Errors

Common sources of errors in measuring the precise measurements of the water layer temperature:

- Temperature gradient from water to mirror surface.
- Temperature gradient from mirror surface to the thermometer
- Measurement error due to thermometer self-heating
- Measurement error occurring from thermal conductance of thermometer leads and the connecting cables
- Measurement error due to readout circuit

In order to avoid the complexity of taking in mind all the possible combinations of these error factors we will rely on the worst case estimation of the error induced due to temperature measurement.

2.4.3 Summary

The following table is a rough estimation of the errors induced in the dew-point measurements. We can observe that the main error is inserted through the "Raoult Effect" and the accuracy limitation of the thermometer. Even using one of the most reliable and precise thermometers i.e. a platinum RTD, we cannot expect the accuracy to be better than 0.1^oC.

Phenomenon	Typical Error
Kelvin effect	-0.005^oC to -0.01^oC
Raoult effect	+0.05^oC to +0.5^oC
Gradient from water surface to mirror	+0.002^oC
Gradient from mirror to thermometer	+0.001^oC
Dew/Frost-point interpretation	1^oC to 6^oC
Self heating	+0.04^oC
Thermal conduction of thermometer leads	+0.005^oC
Thermometer limitations	+0.05^oC
Temperature readout calibration limitation	+0.03^oC

Table 2.1: Typical errors inserted in the dew point temperature measurements

2.5 Method Evaluation - Proposal

Taking into account the advantages and the disadvantages of all the methods mentioned above, the CCM method is proved to be the most reliable, although losing some of its fundamental characteristics. The main advantages are

- Lower levels of contamination
- Dew/Frost point interpretation

On microcontroller based system the sensor's operating algorithm is fully controlled by the software of the microcontroller and can be altered easily. The current implementation will be based on the conventional chilled mirror hygrometer algorithm (see chapter 5). In particular, it will be a variation of what is described by Jackowicz[13] as optimal procedures.

Chapter 3

Sensor Description

3.1 Introduction

As mentioned before the sensor will be constructed with a metal mirror, a thermometer, a cooling module, a reflective sensor and a couple of LED and a phototransistor like the ones used in the reflective sensors. For the control and the readout of the circuit we will have to implement a circuit based on a microcontroller that will synchronize the individual devices, process the received data and send the final measurement to a computer through an RS-232 interface.

The layout of the implemented sensor and the control/readout system is presented in Figure 3.1

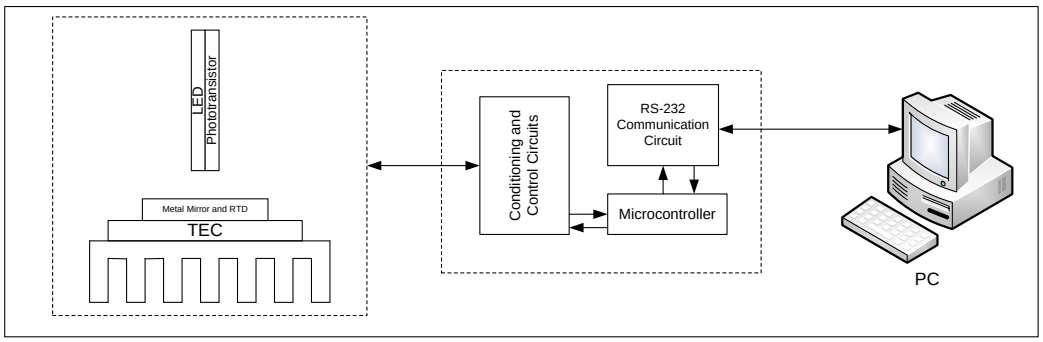

Figure 3.1: Description of the system used to measure the dew-point

3.2 Metal Mirror

The metal that will be used should combine excellent thermal conductivity, good reflectivity and small price. Furthermore it should be easily treated, as we need to open a small hole inside the metal for the thermometer and polish the upper surface of the mirror. Hence one of the best choices, that combines the previous

properties, is aluminium. The thermal conductivity of aluminium is $237W \cdot m^{-1} \cdot K^{-1}$ and the reflectance spectrum is presented in Figure 3.2b.

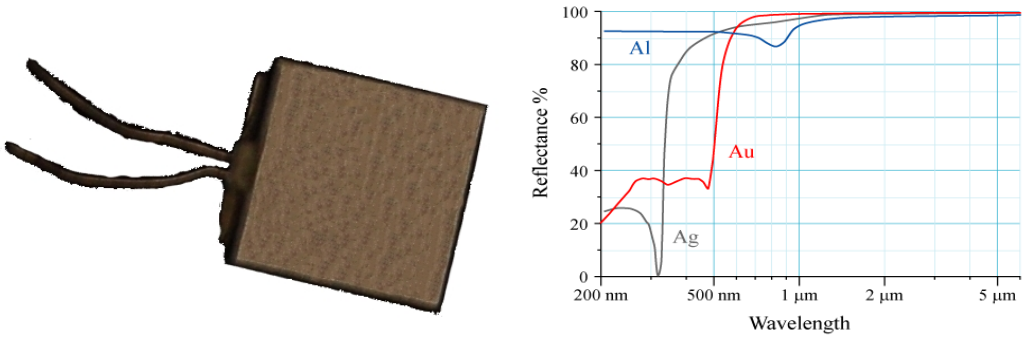

(a) (b)

Figure 3.2: a. A photo from the constructed aluminium metal mirror with the RTD thermometer inside b. Presentation of the metal reflectance as a function of varying wavelengths

As presented aluminium is a quite good metal mirror and its reflectance is always greater than 85% for wavelengths between $200nm$ and $5\mu m$. Although the better response of Au and Ag in the "near infrared" region we will use Al as the cost is apparently lower and the treatment undoubtedly easier. However aluminium mirror lacks in reliability, as aluminium surfaces react with atmospheric O_2 forming aluminium oxides, which have a reduced reflectance ratio. In this direction, a future implementation should replace aluminium with gold (Au) or rhodium (Rd) that are much more stable and reliable.

3.3 Thermometer

The main sensors that are used for temperature measurements are three; the industry standard RTDs, the cheap thermistors and the thermocouples. In this implementation a thin film platinum Resistance Temperature Detector (PCA 1.2005.10S, Class DIN B), supplied by Jumo [14], will be used as an accurate, fast, small and linear thermometer.

The dimensions (see Fig. 3.3b) of the specific RTD that we will use are $B = 2.0mm$, $L = 5mm$, $H = 1.3mm$, $0.64mm$, $L1 = 10mm$ and $D1 = 0.20mm$. The temperature coefficient is $\alpha = 3.850 \cdot 10^{-3}\ ^oC^{-1}$ for temperatures between 0^oC and 100^oC. Finally the response time of the RTD attached in the solid volume of aluminium should be smaller than what it is in the case of water $t_{90\%} < 0.3s$.

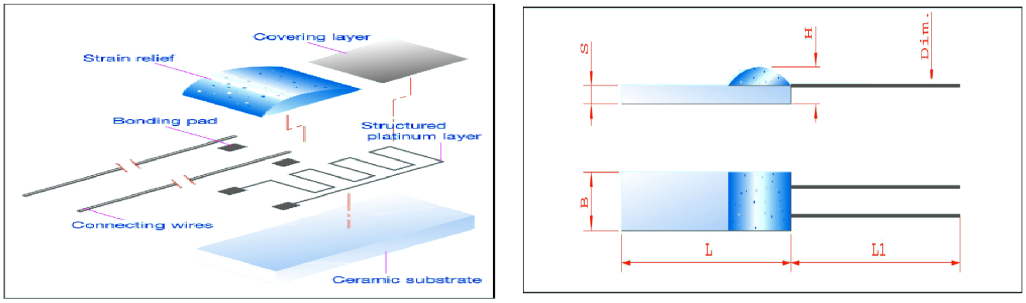

(a) (b)

Figure 3.3: a. Drawing describing the RTD thermometer b. The definitions of the RTD dimensions [14]

3.4 Cooling Module

As it is referred before the most practical and effective solution for cooling and heating the metal mirror is the Thermoelectric Cooler (TEC) which is based on the Peltier effect (for a more detailed explanation of the Seebeck-Peltier effect refer to Appendix B).

In order to specify the exact characteristics of the TEC we have to specify two parameters the maximum differential temperature between the hot and the cold side and the power rating that expresses the amount of heat a TEC can pump from the cold side to the hot.

The first step is to calculate the thermal energy that is needed in order to lower the mirror temperature. In this point we should make a working assumption that the metal mirror is a compact volume of aluminium neglecting the RTD thermometer inside the mirror volume. Therefore we can make a rough thermal model of the mirror using the simple heat transfer equation.

$$Q = m \cdot c \cdot (T_{final} - T_{start}) \tag{3.1}$$

The specific heat capacitance of aluminium is $c = 0.897J \cdot g^{-1} \cdot K^{-1}$ and the mass of the mirror $m = 0.6g$. Assuming that the operating temperature of the system is 25^oC and the detected dew-point temperature should be as low as -25^oC we deduce that $T_{final} - T_{start} = 50^oC$. Therefore the thermal energy needed to cool down the mirror for 50^oC is

$$Q = 0.6 \cdot 0.897 \cdot 50 = 26.91J \tag{3.2}$$

The temperature difference in question depicts the transition from ambient temperature to the threshold where the mirror will get wet and represents the maximum temperature change that will occur to the metal mirror. This procedure will be repeated every time the sensor is re-initialized and should last around 5 seconds. Hence the anticipated thermal power is :

$$P_Q = 5.382 \simeq 5.4W \tag{3.3}$$

The metal mirror is attached to the thermoelectrical module by a thin deposition of the thermal conductive and adhesive glue E-SOLDER provided by Epoxy Produkte Gmbh. Assuming the thermal resistance of such a thin layer of glue as negligible, we could assume that the thermal load of the TEC module (P_c) equals P_Q. Nevertheless, both the metal mirror and the cold side of the TEC are not perfectly sealed and there will be thermal interaction (although less than the one previously described) that is not taken into account on the current calculations. In order to incorporate these interactions we should assume that the total power the TEC can pump from its cold side to its hot is raised by 20%, resulting in

$$P_c = 1.2 * P_Q = 6.48W \simeq 6.5W \tag{3.4}$$

This quantity represents the worst case scenario for the thermal power that the TEC should pump. Therefore In order to make the appropriate thermal study of our system we will base our calculations on the handnote provided by the manufacturer [15]. The amount of heat(P_h) that will be rejected on the hot side of the thermoelectrical cooler (neglecting the heat exchange through radiation) is the sum of the energy supplied py the power source and the heat absorbed from the cold side.

$$P_h = P_c + P \tag{3.5}$$

Assuming that the TEC will operate with $P = 10W$ the heat that will be released on the hot side is almost $P_h = 16.5W$.

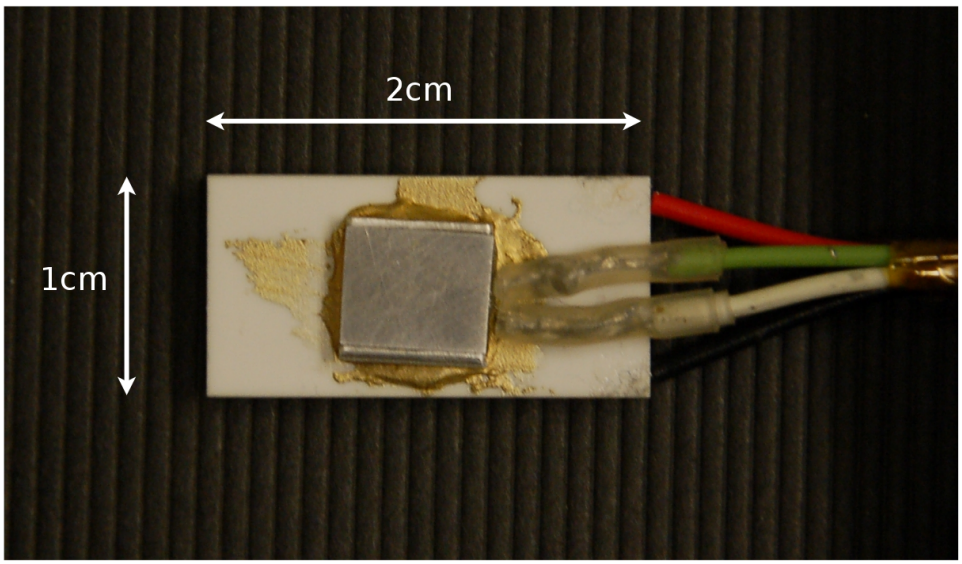

Figure 3.4: The TEC module with the metal mirror attached on it.

Heatsink

The overheating of the hot side of the thermoelectric module will increase the minimum operating temperature and can lead to inefficiency in reaching the dew-point. In order to avoid this case we have to use a proper heatsink, with the properties displayed in the following thermal circuit :

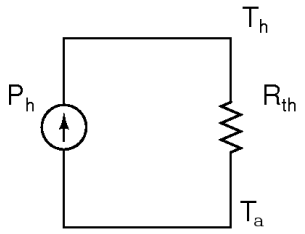

Figure 3.5: Thermal circuit that describes the thermal response of the heatsink

The circuit analysis leads to :

$$T_h - T_a = P_h \cdot R_{th} \Rightarrow T_h = T_a + P_h \cdot R_{th} \tag{3.6}$$

The commercial heatsinks have a thermal resistance of the order of $10 - 20^oC/W$. The best affordable but not very compact heatsink had a thermal resistance of $1.5^oC/W$. Hence from Eq. 3.6 the expected temperature on the hot side when the TEC is working at full power is:

$$T_h = 49.75^oC \simeq 50^oC \tag{3.7}$$

The hot side temperature $T_h = 50^oC$ and the target temperature for the mirror (-25^oC) determine the maximum differential temperature between the two sides of the TEC to $\Delta T = 75^oC$.

Concluding the main characteristics of the used TEC module will be:

$$P_c = 6.5W \text{ and } \Delta T = 75^oC$$

3.5 Reflective Sensor

The reflective sensor is a way to understand whether there is condensed water on the mirror surface or not. For this reason we have to study the absorption properties of water and decide the most appropriate operation wavelength for our reflective sensor. According to [16] and [17] for liquid water the spectrum is shifted to longer wavelengths for 60nm comparing to what is depicted in Figure 3.6. While it is obvious that water absorbs greatly the ultraviolet and far IR waves, these frequencies are not commercially available for a reflective sensor. The usual operating frequencies for this kind of device are on the near IR spectrum ($800nm < \lambda < 1000nm$). Hence the most suitable wavelength in this frequency span is 970nm as there is a peak in absorption.

Figure 3.6: Water vapor absorption spectrum

The LED and the phototransistor of the reflective sensor are sensible to the temperature variations and to radiation effects. It has been already mentioned in Chapter 2 that the most indicated solution for this is to use a differential circuit instead of the regular emitter-receiver circuit. Through this circuit the parasitic effects will be self-cancelled and the final signal will get derived only from the unbalance that the condensed water will cause. There are two ways to subtract the two signals; the analog and the digital. Although the analogue solution is more accurate and robust, it lacks in flexibility. The main advantage of the digital solution is that it provides an easy way of resetting the balance and even leave the differential mode of operation in case something gets damaged.

Despite all the reasons mentioned above the final implementation will be using only one LED-phototransistor couple. This selection is done for simplicity reasons, because this prototype is targeted for experimental use in temperature controlled environments. Furthermore the algorithm forces a system re-initialization each time there is a considerable humidity -and therefore temperature- change, re-standardizing also the expected clean mirror reflective sensor response.

The reflective sensor that will be used is HOA0708-011 [18] provided by Honeywell and is presented in Figure 3.7.

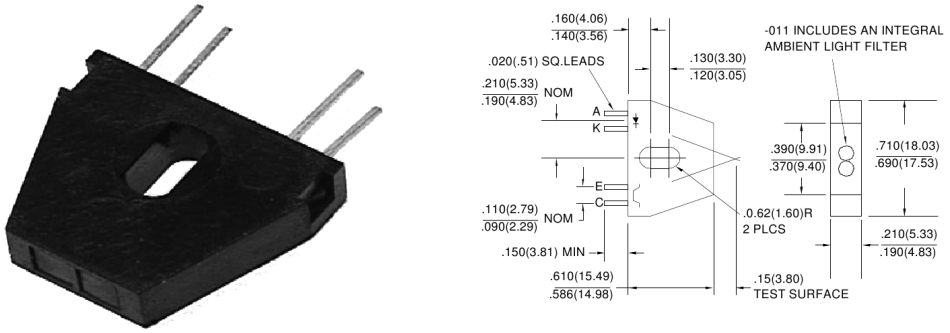

(a) (b)

Figure 3.7: a. Photo of the HOA0708-011 reflective sensor b. The dimensions and the focal length of the sensor

3.6 The Assembled Sensor

In the figure below (Fig. 3.8) the final assembly of the dew-point sensor is presented. In order to reduce energy losses and achieve more stable mirror temperature extra insulation is added around it.

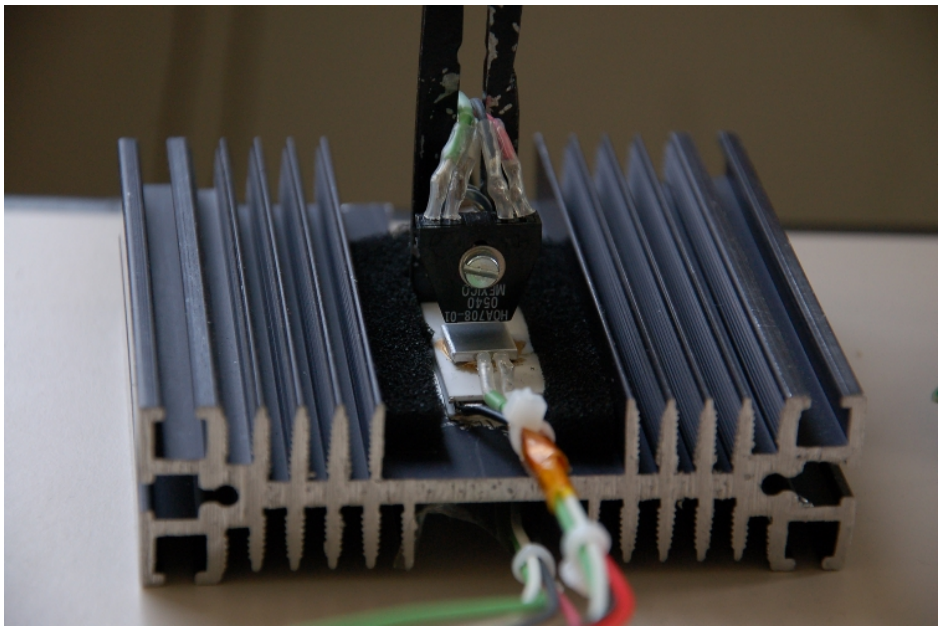

Figure 3.8: The final assembly of the dew-point sensor. The metal mirror, the TEC, the reflective sensor, the heatsink and the cabling are consisting the presented structure.

Chapter 4

Control and Readout Circuit Description

4.1 Introduction

As mentioned many times before the chilled mirror dew point sensor consists of a temperature sensor, a reflective sensor and a thermoelectric module that is needed for cooling and heating the metal mirror. These devices need to be synchronized and read through a custom-made circuit that will interface between the sensors and the output device (a computer or an LCD monitor). This is exactly what will be described in the current chapter.

For this kind of work the ideal combination of efficiency and cost is a microcontroller based solution that includes:

- a multiple channel Analog-to-Digital Converter (ADC)
- a Pulse Width Modulation (PWM) device
- a serial communication port (RS-232)
- a ability for in-system programming

A quite common, commercial and handful microcontroller that corresponds to the above specifications is ATmega32 an AVR type microcontroller from ATMEL. This microcontroller will play a key role in our readout as it will be the brain for all the control, conditioning and communication sub-circuits will be connected on it. The particular circuits mentioned and analysed below are:

- The RTD conditioning circuit which will be connected to an ADC port
- The reflector control and conditioning circuit which will also be connected to another ADC port.
- The TEC control circuit which will be connected to the pulse generator of the microcontroller.
- The serial communication that will be connected to the UART module of the microcontroller

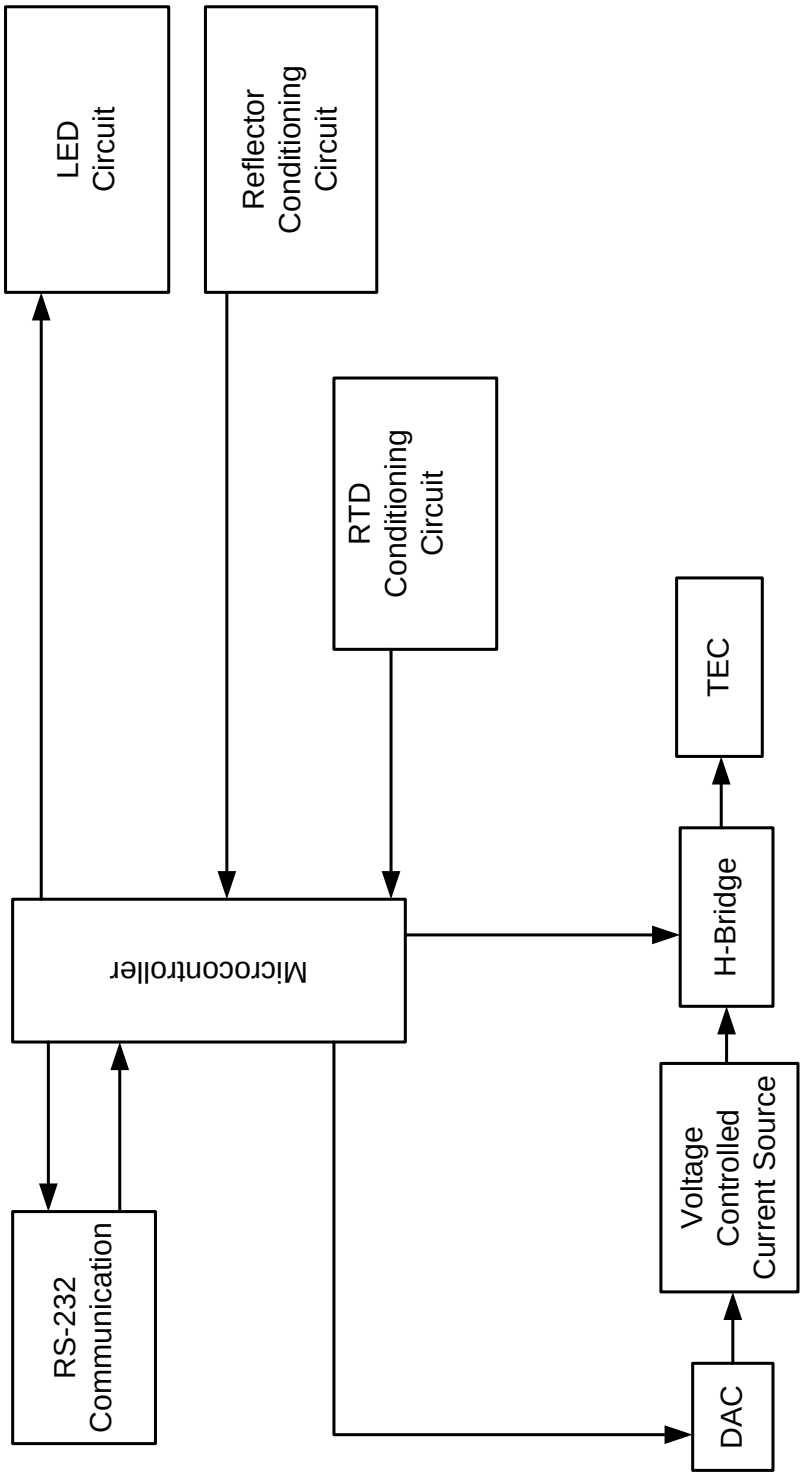

Figure 4.1: A description of the readout circuit interconnections

4.2 Microcontroller

ATmega32 is a microcontroller based on the RISC architecture with a set of 131 instructions, most of them executed in single-clock cycle. ATmega32 achieves throughputs approaching 1 MIPS per MHz allowing the optimization of power consumption versus processing speed. The main features of ATmega32 that we will use in our implementation are : the Analog to Digital Converter (ADC), the Timer/Counter for generating PWM signals and the Serial Communication port (USART). For programming the device we will use the In-System Programming (ISP) configuration connected to STK-500, a development kit provided by ATMEL.

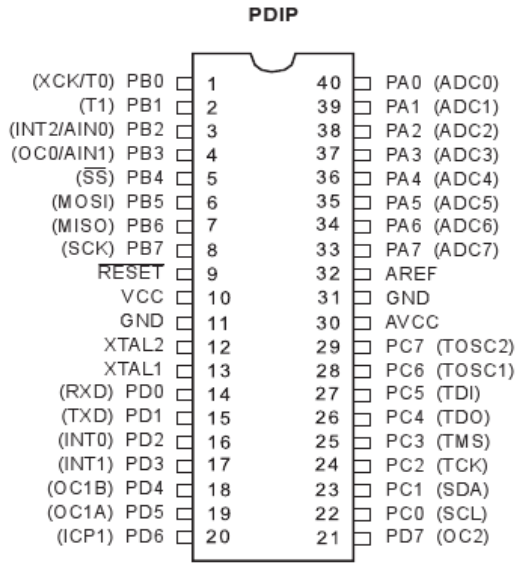

Figure 4.2: The pin configuration of ATmega32

A brief description of the microcontroller peripherals is necessary in order to provide an understandable description of the implemented sub-circuits and the developed software. Further information on the microcontroller can be retrieved through the datasheet of the device[19].

4.2.1 Analog to Digital Converter

The ATmega32 features a 10-bit successive approximation ADC that is connected to an 8-channel Analog Multiplexer. It allows 8 single-ended voltage inputs (referenced to GND and having a 10bit resolution) constructed from the pins of PORT A and 16 differential voltage input combinations. Two are equipped with a programmable amplification stage. The provided steps of gain are 0 dB (1x), 20

dB (10x) or 46 dB (200x) on the differential input voltage before the A/D conversion. Seven differential analog input channels share a common negative terminal (ADC1), while any other ADC input can be selected as positive input terminal. If 1x or 10x gain is used, 8-bit resolution can be expected whereas for 200x gain a 7-bit resolution can be achieved.

The ADC is powered through an individual supply voltage pin (AVCC), which must not defer more than $\pm 0.3V$ from the VCC. The internal reference voltages for the ADC are 2.56V or AVCC. An external reference (AREF) can also be connected. Furthermore the ADC contains a Sample and Hold circuit that ensures that the input voltage is held to a constant level during conversion.

The analogue input circuitry of the ADC is presented in Figure 4.2.1. The analog signal that will be applied to the ADCn pin will be subject to the capacitance and the leakage current of the pin. When the channel is selected as input the source must drive the $C_{S/H}$ capacitor and a resistor in series, that depicts the combined resistance of the input path. The ADC is optimized for analog signals of $10K\Omega$ or less output impedance. If a source with higher impedance is applied then the sampling time will depend on the time the source needs to charge the $C_{S/H}$ capacitor. In the case of differential gain channels the circuitry is a bit different, although source impedances of the magnitude of hundreds $K\Omega$ should be used.

Signal components higher than the Nyquist frequency ($f_{ADC}/2$) should not be present for either kind of channels, to avoid distortion from unpredictable signal convolution. For this reason a low-pass filter, before applying the signals as inputs to the ADC, will be used.

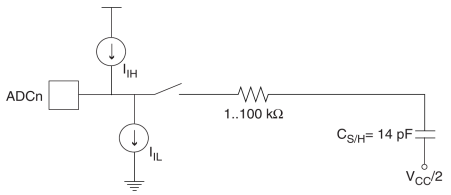

Figure 4.3: Analogue input circuitry for single-ended channels

Analogue Noise Cancelling Techniques

Digital circuitry inside and outside the device generates EMI which might affect the accuracy of analogue measurements. If conversion accuracy is critical, the noise level can be reduced by applying the following techniques:

1. Keep analogue signal paths as short as possible. Make sure analogue tracks run over the analogue ground plane, and keep them well away from high-speed switching digital tracks.
2. The AVCC pin on the device should be connected to the digital VCC supply voltage via an LC network.
3. Use the ADC noise canceller function to reduce induced noise from the CPU.
4. If any ADC port pins are used as digital outputs, it is essential that these do not switch while a conversion is in progress.

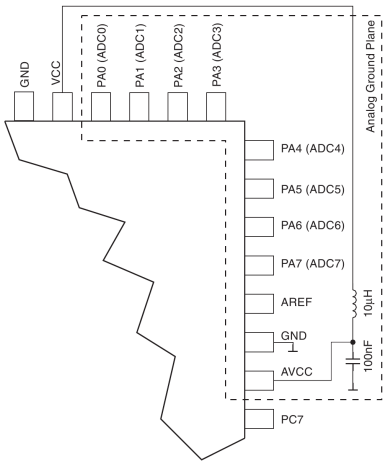

Figure 4.4: Configuration used for noise cancelling in the AVCC pin through a simple LC filter

4.2.2 Pulse Width Modulation

PWM is a signal modulation technique where the duty cycle of a pulse wave signal is modified. It is an easy and efficient way of converting digital signals to analogue. Varying the signal's duty cycle one can create intermediate power levels between the two state digital logic voltages.

ATmega32 features three fully operating independent timers that can be used to generate PWM waveforms in three possible ways. We will analyse these modes through describing briefly the typical AVR ATmega 16bit timer, as it is the most complicated of the three. In the datasheet of the microcontroller this device is referred as Timer1.[1]

Before the detailed description, some definitions (registers, power levels) are necessary to be done. However we will omit the features that are not used in our implementation.

Timer: it is a programmable bi-directional counter unit, that can be clocked externally or internally, via a prescaler. Access to this unit is achieved through the Timer/Counter (TCNT1) 16-bit register. Depending on the mode of operation the counter is cleared, incremented or decremented at every timer clock. The counting sequence is determined by the Waveform Generation Mode (WGM13:0) bits located in the Timer/Counter Control Registers A and B (TCCR1A and TCCR1B).

Output Compare: the Output Compare Register (OCR1x) is continuously compared with TCNT1. If these two registers become equal, a flag is set. The

[1]This is the reason why on the following pages number 1 will be displayed on the registers' names. It can be replaced with 0 or 2 for the other two 8bit timers, Timer0 and Timer2 respectively. Letters A and B are used to distinguish HIGH and LOW 8bit registers that map the 16bit registers.

flag is used to generate an output according to the selected operation mode (see WGM register).

Output: OC1x is referring to the corresponding output register of Timer1.

Prescaler: the prescaler is a way to clock the timer by fractions of the systems clock. The divisors of f_{clock} can be 1, 8, 64, 256 or 1024.

Control Registers: TCCR1x is a 16bit register(TCCR1A/TCCR1B) that controls the operation of the Timer1. The waveform generation mode, the clock value and the output compare mode are the main features that can be mastered through this.

BOTTOM: the counter reaches BOTTOM when it is 0x0000.

MAX: the counter reaches MAX when it becomes 0xFFFF.

TOP: the counter reaches TOP when it equals the highest value in the count sequence. The TOP value in ATmega can be assigned to be one of the fixed values : 0x00FF, 0x01FF or 0x03FF or to the value stored in OCR1A or ICR1 register. This assignment is depended on the operating mode.

The modes of operation for the PWM generator of ATmega32 are: Fast PWM, Phase Correct PWM and Phase-Frequency Correct PWM.

Fast PWM

This mode can provide a high frequency PWM waveform. "Fast PWM" differs from the other modes by its single slope operation. The counter follows a sawtooth waveform, counting from BOTTOM to TOP and restarts to BOTTOM. During this period when the Output Compare register (OCR1x) matches the TCNT1 counter the output is unset until the next BOTTOM-TOP cycle. Fast PWM gives the ability to change the duty cycle rapidly, in applications where the phase change does not matter.

If OCR1x is set to BOTTOM the output will be a quick and narrow spike for each TOP+1 timer clock cycle, while if it is set to TOP it will be a narrow deep on the TOP+1 timer clock cycle. The "Fast PWM" resolution and frequency can be displayed through the following formulas:

$$R_{FPWM} = \frac{log(TOP+1)}{log2}$$

$$f_{OC1x} = \frac{f_{clkI/O}}{N \cdot (1+TOP)}$$

where N is the prescaler divider.

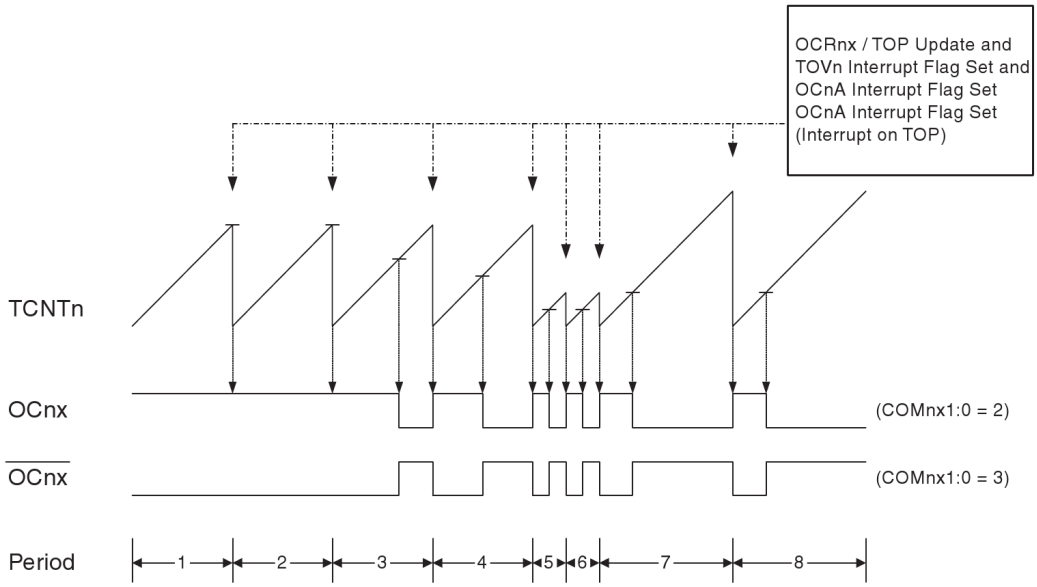

Figure 4.5: The Fast PWM generation mode

Phase Correct PWM

The "Phase Correct PWM" mode provides a high resolution waveform that is more accurate than "Fast PWM", lacking, though, in speed. It is based on a dual-slope operation where the counter TCNT1 counts continuously from BOTTOM(0x0000) to TOP and backward. The register OC1x is cleared on compare match between TCNT1 and OCR1x while upcounting and set on compare match while downcounting. The dual-slope mode has lower maximum frequency operation than single-slope, providing, however, phase correctness due to its symmetry. This feature is very useful in motor driving applications where avoiding spikes and deeps during operations plays a vital role.

If OCR1x is set to BOTTOM (TOP) the output will be continuously low (high), in contrast with the "Fast PWM" mode where we would have a spike (deep).

The "Phase Correct PWM" resolution and frequency can be displayed through the following formulas:

$$R_{PCPWM} = \frac{log(TOP+1)}{log2}$$

$$f_{OC1x} = \frac{f_{clkI/O}}{2N \cdot TOP}$$

, where N is the prescaler divider.

Phase and Frequency Correct PWM

The "Phase and Frequency Correct PWM" operates similarly to the "Phase-Correct PWM" but not identically. The main difference is in the time that the

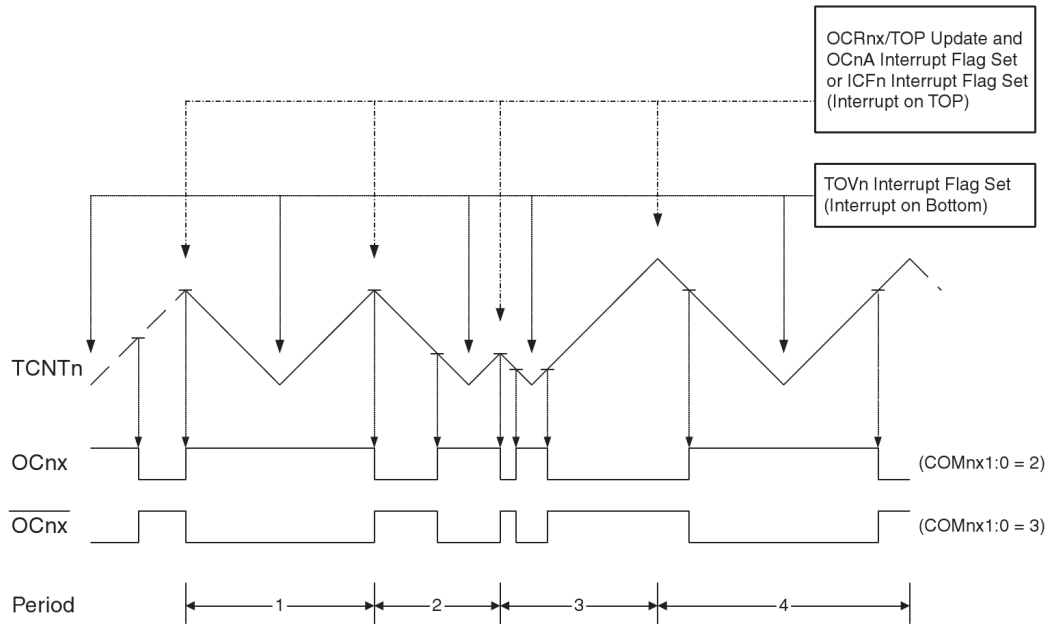

Figure 4.6: The Phase Correct PWM generation mode

OCR1x register is updated by the OCR1x Buffer Register (comparing Figures 4.6 and 4.7 we can spot that difference). As it is illustrated in the 3^{rd} triangle of Figure 4.6, an asymmetry is produced when changing the TOP while the Timer/Counter is running. The reason for this can be found in the time that an update occurs to OCR1x register. Since the OCR1x is updated at TOP, the PWM period starts and ends at TOP. This implies that the length of the falling slope is determined by the previous TOP value, while the length of the rising slope is determined by the new TOP value. When these two values differ the two slopes of the period will differ in length. In "Phase and Frequency Correct PWM" (see Figure 4.7) OCR1x are updated at BOTTOM resulting, in any case, in equal length of the rising and the falling slopes.

The resolution and the frequency of the "Phase and Frequency Correct PWM" are described through the same equations with "Phase Correct PWM".

$$R_{PFCPWM} = \frac{log(TOP+1)}{log2}$$

$$f_{OC1x} = \frac{f_{clkI/O}}{2N \cdot TOP}$$

, where N is the prescaler divider.

4.2.3 Serial Communication

ATmega32 features a serial port communication system named "Universal Synchronous and Asynchronous Receiver and Transmitter". It supports full duplex op-

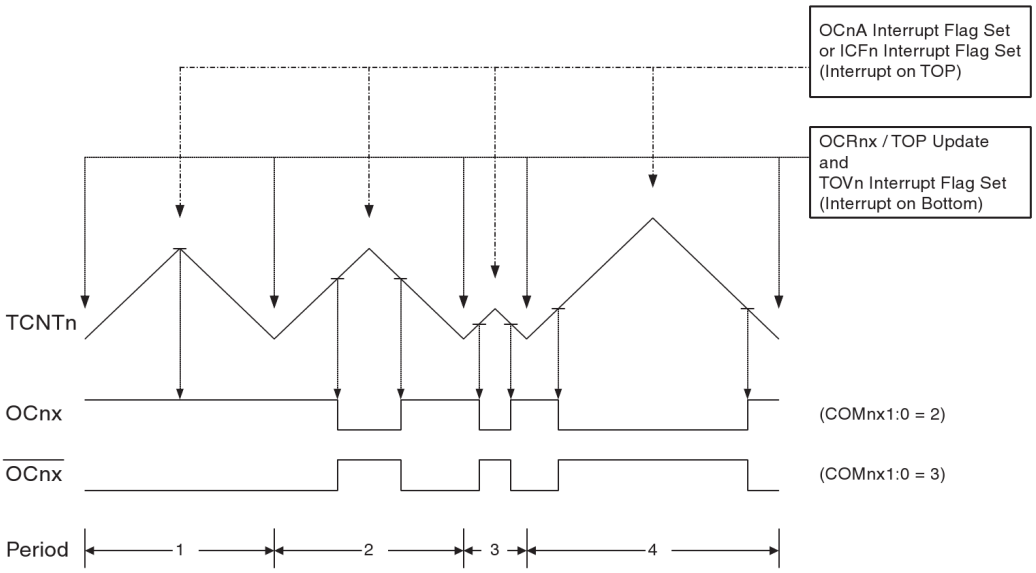

Figure 4.7: The Phase and Frequency Correct PWM generation mode

eration with independent receive and transmit registers. It can follow asynchronous and synchronous (either master or slave clocked) communication through a high resolution baud rate generator. The data frames can be either 5, 6, 7, 8 or 9 bits with 1 or 2 Stop Bits. The system also includes some data correction modules.

In order to use the serial communication, USART should be initialized before any packet exchange takes place. The initialization process normally consists of setting the baud rate, setting frame format and enabling the Transmitter or the Receiver. It can be also driven through interrupts, though clearing the Global Interrupt Flag when doing the initialization. On the following chapter (see Chapter 5.2.3) concerning the developed software there will be a more detailed description of the specific initialization actions to be taken.

For the communication between USART and a computer a special voltage-level converter circuit (based on chip MAX-232) is employed.

4.3 The RTD measurements

4.3.1 The RTD conditioning circuit

The RTD thermometer that we will use is a thin film Class B RTD sensor manufactured by JUMO. The accuracy(D_T) of a Class B RTD is given by:

$$D_T(^oC) = \pm(0.30 + 0.005\,|T|)$$

where: T is the operating temperature in ^oC

According to the table of values provided in DIN IEC 60 751 the function that describes the relationship between temperature and resistance for Pt-1000 RTDs

is :
For the range $\underline{-200^oC < T < 0^oC}$

$$R_T = R_0 \left[1 + A \cdot T + B \cdot T^2 + C(T - 100) \cdot T^3\right]$$

For the range $\underline{0^oC < T < 850^oC}$

$$R_T = R_0 \left[1 + A \cdot T + B \cdot T^2\right]$$

, where

T the temperature in ^oC
R_T the RTD resistance in Ω
R_0 the resistance of the RTD on 0^oC. In this occasion it is 1000Ω.
$A = 3.9083x10^{-3}\ ^oC^{-1}$
$B = -5.775x10^{-7}\ ^oC^{-2}$
$C = -4.183x10^{-12}\ ^oC^{-4}$

In order to simplify the equations model we can simply rely on a linear approximation of the function as it is specified in the datasheet of the device:

$$R_T = 1000 + a \cdot T \tag{4.1}$$

where $a = 3.850^oC^{-1}$
Taking under consideration the sensor specifications and a safety margin of 15^oC, the temperature range that the sensor will be operating is :

$$-40^oC < T < 60^oC$$

Therefore from 4.1

$$-40 \cdot 3.85 + 1000 < R_T < 60 \cdot 3.85 + 1000 \Rightarrow$$

$$846\Omega < R_T < 1231\Omega \tag{4.2}$$

In order to achieve as good accuracy as possible, an appropriate conditioning circuit must be designed. This conditioning circuit should translate the linearly varying resistance of the RTD (R_T) to a voltage that can be read from the microcontroller's ADC.

A key issue in the temperature measurements is the self-heating that is caused from the thermometer itself. According to the devices specification the maximum current that should pass from the RTD should not be over $1mA$ whereas the ideal is $0.1mA$, keeping the heat dissipation well below $1mW$.

In Figure 4.8 a basic RTD conditioning circuit is described, while it is kept as simple as possible. The value of the resistor R_1 is chosen so as

$$I_{R1} \simeq \frac{5V}{10K\Omega + R_T} < \frac{5V}{10K\Omega + 846\Omega} \Rightarrow I_{R1} < 0.46mA$$

The self heating of the RTD therefore is

$$P_{RTD} = I_{RTD}^2 \cdot R_T < 0.22 \cdot 1.3K\Omega = 0.286mW$$

It is worth mentioning that the above calculation is based on the fact that ATmega32 ADC is a high impedance port. Hence the current flowing to the ADC is negligible and $I_{R1} = I_{RTD}$. For further details on this subject refer to chapter 4.2.

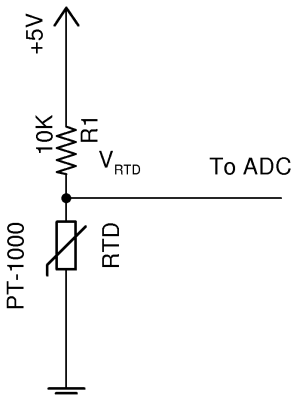

Figure 4.8: The conditioning circuit for reading the Pt-1000 RTD sensor

In Figure 4.8 it can be easily calculated that :

$$V_{RTD} = \frac{R_T}{R_T + 10K\Omega} \cdot 5V \tag{4.3}$$

Taking in mind both eq.4.2 and the above equation it is derived that :

$$0.390V < V_{RTD} < 0.548V \tag{4.4}$$

$$\Delta V_{RTD} = 158mV \tag{4.5}$$

As described in chapter 4.2, the single-ended ADC samples with 10bit resolution while the conversion uncertainty is 2LSB. This makes it possible to distinguish between a voltage difference of $4.90mV$ when the voltage reference is at $5V$. If we directly connect the ADC to V_{RTD} the voltage difference between -40^oC and 60^oC is $\Delta V_{ADC} = \Delta V_{RTD} = 548mV - 390mV = 158mV$. This means that the maximum accuracy achieved can be

$$Max.TemperatureAccuracy = \Delta T \cdot \frac{4.90}{158} = 3.1^oC$$

Of course this value not satisfactory and we should amplify the signal to increase the achieved accuracy. If we use only one amplification stage then the maximum gain will be constrained by the maximum voltage the ADC can handle. This means that G is :

$$G = 5V/0.548V = 9.1 \simeq 9$$

Using an amplifier with $G = 9$ after V_{RTD} (see Figure 4.9) we increase the voltage range that the ADC can measure to $\Delta V_{ADC} = 9 \cdot \Delta V_{RTD} = 1422mV$. Hence the improved maximum temperature accuracy is :

$$\text{Max. Temperature Accuracy} = \Delta T \cdot \frac{4.90}{1422} = 0.35^{o}C$$

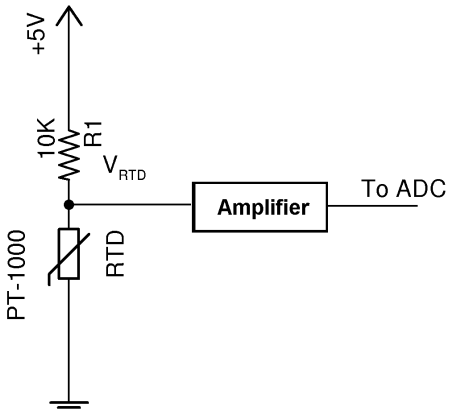

Figure 4.9: The conditioning circuit for reading the Pt-1000 RTD sensor with amplification

The amplifier described above is an easy circuit to implement if we base our design on a typical operational amplifier. The layout is described in Figure 4.10. In order to have a gain of $G = 9$ we should have a resistance ratio of :

$$R_3/R_2 = 8$$

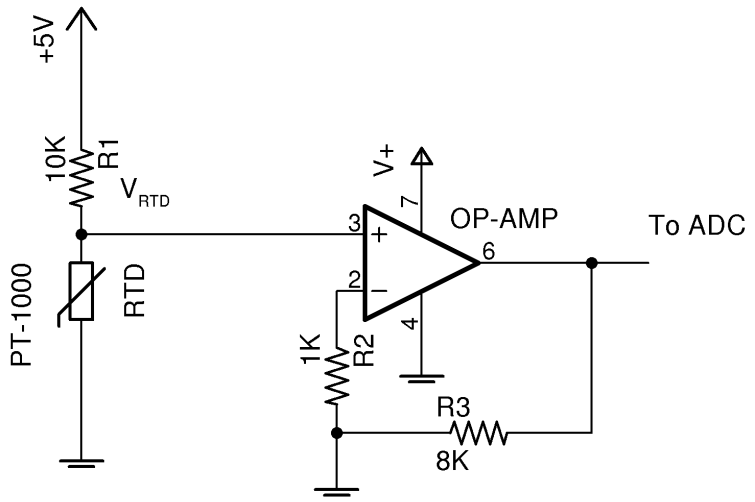

Figure 4.10: The implementation of the RTD conditioning circuit with 9x signal amplification.

However, further improvement of the measurement accuracy is possible if we use a rail-to-rail amplifier to amplify the signal up to 12V[2]. A subtractor will follow the amplified signal removing the voltage offset that represents temperatures below -40^oC. This method allows a higher amplification of the signal resulting in an increased accuracy.

The schematic of the above circuit can be seen in Figure 4.11. The maximum allowed amplification will be determined by the maximum output voltage of OP_AMP1 and the maximum input voltage of OP_AMP2. The nominal operating voltage for low-end commercial amplifiers is from GND to $V_{cc} - 1.5V$, where V_{cc} is the voltage supplied to the op-amps. In order to avoid distortions we should use a safety margin of $2V$. Therefore working for maximum R_T we derive :

$$G = \frac{12V - 2V}{0.548V} \simeq 18$$

After amplification the signal is processed through a differential amplifier that is working without gain and is removing the offset that corresponds to temperature below -40^oC. At -40^oC , $R_T = 846\Omega$ and $V_{RTD} = 0.390$. This means that the amplified signal will be:

$$18 \cdot 0.390V < V_{out,op\_amp1} < 18 \cdot 0.548V \Rightarrow$$

$$7.02V < V_{out,op\_amp1} < 9.86V$$

The operational amplifier that we are using is working quite well near GND. Therefore we can subtract a constant 7V voltage from the signal that comes from

[2]12V is the primary voltage source that will the system be operating on. Afterwards a voltage regulator is used to produce a stable 5V power supply

OP_AMP1. Now the signal is varying between:

$$0.02V < V_{out,op\_amp1} < 2.86V$$

The fluctuation of V_{out,op_amp1} for only $2.84V$ leads to an extra system moodification that will increase the accuracy. Instead of the 5V ADC reference we can use the internal 2.56V and double the quantization accuracy while reducing the quantization error to the half. If we choose to subtract 5V in the stage of OP_AMP2. The final gain will derive from the following equation :

$$\frac{5V}{0.390} < G < \frac{2.56V + 5V}{0.548V}$$

$$12.82 < G < 13.8 \Rightarrow G \simeq 13 \tag{4.6}$$

The final system has a response of :

$$V_{out,op\_amp2} = 13 \cdot V_{RTD} - 5V \tag{4.7}$$

and varies between

$$0.070 < V_{out,op\_amp2} < 2.124V$$

for temperatures $-40^oC < T < 60^0C$ respectively.

In the following circuit the OP_AMP1 amplifier is used as an active, single-stage low-pass filter with cut-off frequency $f_{-3dB} = 1/R3 \cdot C1 = 1/(12K\Omega \cdot 3\mu F) \simeq 27.7Hz$ that is used to remove high frequency noise and parasitic effects.

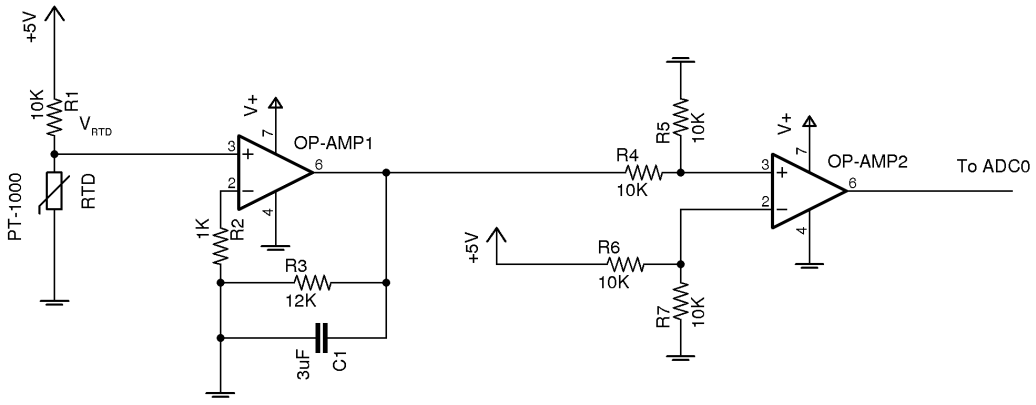

Figure 4.11: The implementation of an amplifier with G=13 and a subtractor of a 5V offset. Th final signal varies between $0.070V < V_{out,op\_amp2} < 2.124V$ and is suitable to be read from an ADC with 2.56V voltage reference.

The measurement accuracy that is achieved through this circuit is doubled, comparing to the previous circuit. It is calculated to be:

$$\delta T = \Delta T \cdot \frac{V_{ref}}{2^n \cdot \Delta V_T} = 100^oC \cdot \frac{2.56V}{1024 \cdot 2054mV} = 0.12^oC \tag{4.8}$$

4.3.2 Resolution Enhancement by ADC Oversampling

Oversampling is the process of sampling a signal with a sampling frequency (f_s) significantly higher than the Nyquist frequency (f_N).[3] The oversampling factor is defined as

$$\beta = \frac{f_s}{f_N}$$

and is meter of the excessive sampling frequency.

In practice, oversampling is implemented in order to achieve cheaper higher-resolution A/D conversion. For instance, to implement a 12-bit converter, it is sufficient to use a 10-bit ADC that can run at 16 times the target sampling rate. Averaging a group of 16 consecutive 10-bit samples adds 2 bits to the resolution of the average, producing a single sample with 12-bit resolution. The number of samples required to get n additional bits is:

$$samples = 2^{2n}$$

These samples are summed and divided by 2^n to get the final result.

At this point it is important to notice that this averaging is possible only if the signal contains perfect equally distributed noise with an amplitude that is greater than the value of the quantization error (0.5 LSB). If the ADC is perfect and the signal's deviation from an A/D result step lies below the 0.5 LSB, the conversion result will be as inaccurate as if it had been measured by the low-resolution core ADC and the oversampling benefits will not take effect. Noise amplitude of 1-2 LSB is even better because this will ensure that several samples do not end up getting the same value.

In our case the quantization error without oversampling is 0.5 LSB or 0.06^oC and the amplitude of the Gaussian noise is affecting 3 LSB (in measurements with 10bit resolution) or 0.96^oC as it can be seen in Figure 4.12a. After oversampling the quantization error has dropped to 0.015^oC while the effect of the Gaussian noise in the temperature measurement drops at 0.36^oC (in measurements with 12bit resolution).

[3] $f_N = 2 \cdot f_{max}$, where f_{max} is the bandwidth of the signal or the highest important frequency.

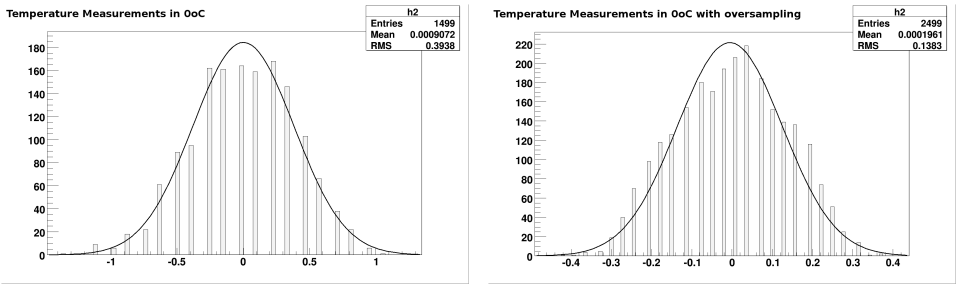

(a) (b)

Figure 4.12: The nominal temperature in both figures is 0^oC. In figure a. we can observe that the measurement resolution is 0.12^oC while in figure b. the signal is oversampled (12bit), achieving a resolution of 0.03^oC

4.4 The Reflective Sensor conditioning circuit

As described in chapter 3 the reflective sensor is a device that is used to measure the percentage of reflected light from a specific surface. The device that we will use is a combination of a Light Emitting Diode (LED) and a phototransistor and it will be able to detect the condensed water on the metal mirror. This device is Honeywell HOA0708-011 and the detailed specifications can be found in the manufacturers datasheet [18]. Therefore this subcircuit can be divided in two smaller individual parts:

- The LED driving circuit
- The phototransistor readout circuit

that will interact with each other through the reflection of the light emitted by the LED on the metal mirror.

4.4.1 The LED driving circuit

The driving circuit will mainly consist of a switch that will be able to drive a maximum of 50mA to the LED, as this is the manufacturer's allowed forward current (I_f). The switch will enable the software control on the state of the LED (ON or OFF) and improve the power consumption of the device. The most cheap, easy and reliable way to implement this is through a single low-power transistor, either a BJT or a FET.

In our implementation(see fig. 4.13) we will use a 2N3904 BJT transistor, supplied by ST-microelectronics. Switch use necessitates that the transistor will be operating in saturation mode. For this reason R_8 will be used to regulate the minimum base current ($min\ I_B$) in order to allow as much current as needed to flow through the collector.

$$minimum\ I_B = \frac{I_f}{min\ h_{FE}} = \frac{50mA}{75} = 0.66mA$$

Relying on this value is not always feasible and operating. Therefore we will use a current three times more in order to take in mind the voltage drop across the transistor when it will be in saturation.

$$R_8 = \frac{5V}{3 \cdot min\, I_B} = \frac{5V}{3 \cdot 0.66mA} = 2.53K\Omega$$

R_9 is not necessary but is used to eliminate the possibilities of a backward conduction. It's value is usually chosen to be $R_8 = 5 \cdot R_9 \simeq 12.5K\Omega$

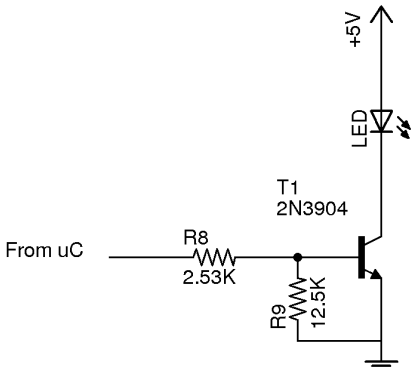

Figure 4.13: The driving circuit of the LED on the reflective sensor

4.4.2 The phototransistor readout

According to the specifications, the phototransistor will feel the 20% of the LED's I_f, when it is biased with $V_{CE} = 5V$ and the optical coupling is perfect. Assuming that the LED will be operating with $I_f \simeq 50mA$ the anticipated collector current, in clean mirror conditions, is $I_c \simeq 10mA$ followed by a dark current about $100nA$ (at 60^oC) that can be neglected.

Moreover HOA0708-011 employs an IR transmissive filter to minimize the effects of visible light and provide a smooth optical interface which prevents the accumulation of airborne contaminants in the optical path. The latter makes redundant the use of an extra filter to remove the constant voltage offset, as it is negligible.

The implemented circuit is presented in Figure 4.14. In order to overpass the delay induced by the capacitive operation of the resistor we will try to keep it as low as possible without decreasing the measurement resolution ($R_{10} \simeq 2.5K\Omega$). The voltage range in the ADC input is expected to be from $0 - 2.5V$.

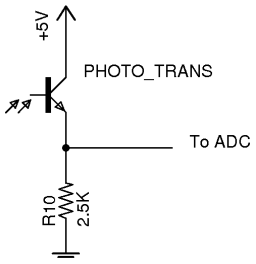

Figure 4.14: The readout circuit for the phototransistor

4.5 The TEC control circuit

This was the most challenging analog part of the readout because it is a combination of low and high current circuitry. The supporting circuit should give to the microcontroller the ability to control the amplitude and the direction of the current flowing through the TEC module. The solution to this is given by the control sequence described in Figure 4.15

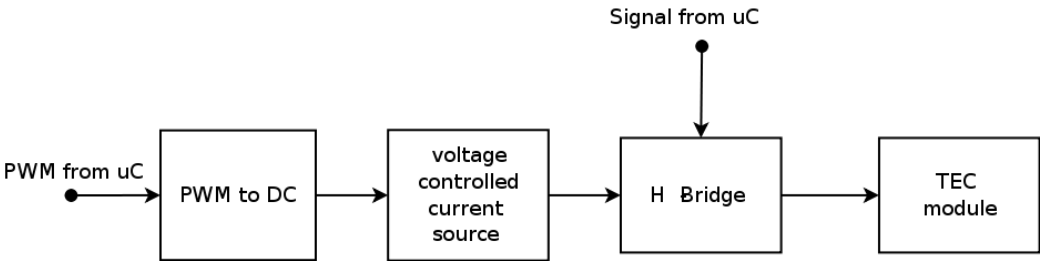

Figure 4.15: The control concept of the TEC module

4.5.1 PWM to DC filter

As referred in section 4.2 the microcontroller is able to generate a 16bit PWM signal with a frequency equal to that of the microcontroller's central clock. This means that we will be able to control the duty cycle of the PWM signal with an accuracy of $100\%/(2^{16}-1) = 0.00015\%$. This accuracy is more than enough and thus we can sufficiently restrain the resolution to 10bit or $\sim 0.1\%$ step in the duty-cycle percentage scale.

PWM is the most common way to generate an analogue signal through a microcontroller. With the use of ATmega32 PWM it is possible to generate various analogue functions with different frequencies and forms. The PWM signal requires a frequency (F_{PWM}) that is equivalent to the update rate of the DAC, because each change in PWM duty cycle is the equivalent of one DAC sample. The frequency of the PWM timer depends on F_{PWM} and on the desired resolution (n) through the following equation:

$$F_{CLOCK} = F_{PWM} \cdot 2^n$$

Judging from the application and the desired signal there is a variety of different filters that can be applied on the PWM pulse. The complexity of these filter and the number of stages is dependent on the use of the produced analogue waveform. The current implementation needs a filter that will keep the voltage as stable as possible through the pulse wave discontinuities, allowing though smooth transitions during the duty cycle variations.

As mentioned before the frequency of the PWM signal can be controlled from the microcontroller and in particular the currently used frequency will be $f_{PWM} = F_{CLOCK}$. As it can be clearly seen in Figure 4.16a the PWM spectrum has parasitic peaks in

$$f_n = n \cdot f_{PWM}, n = 0,\ 1,\ 2,\ ...$$

that we should exclude through the use of the low-pass filter. Therefore the filter's f_{-3dB} is chosen to be smaller than f_{PWM}. Arbitrarily we choose

$$f_{-3dB} < \frac{f_{PWM}}{5} \Rightarrow \frac{1}{2\pi R_{11} C_2} < \frac{f_{PWM}}{5} \Rightarrow R_{11}C_2 > \frac{5}{2\pi f_{PWM}} \Rightarrow$$

$$R_{11}C_2 > \frac{5}{2\pi f_{CLOCK}}$$

In the worst case that $f_{CLOCK} = 1MHz$ we conclude that

$$R_{11}C_2 > 0.049 \cdot 10^{-6}\Omega \cdot F$$

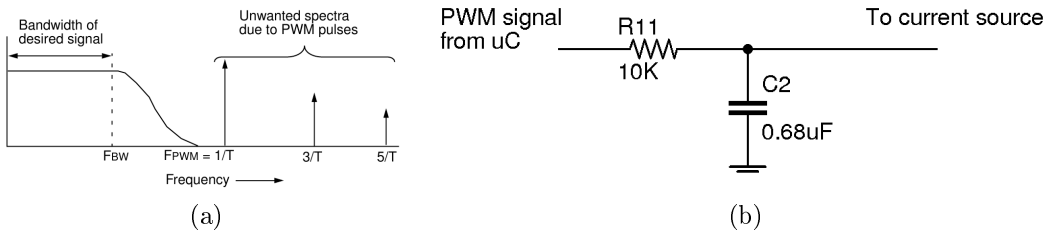

(a) (b)

Figure 4.16: a. The spectrum of the PWM superimposed with the low-pass filter response b. The filter applied to convert the PWM to DC

4.5.2 Voltage Controlled Current Source

During the sensor operation and the dew-point detection there is a need of regulating the amount of heat that will provided to or absorbed from the mirror. This is achieved by controlling the current flow in the TEC; thus adjusting the heat transfer rate. A simple implementation consists of a circuit that varies the voltage across a known resistor, connected in series with the load. In order to overcome the power limits of most of the IC we will use a Power-MOSFET (BUZ73L by Infineon) as a switch between the load and the ground, safely allowing 4A to run

through the TEC device. Considering that a feedback loop is always helpful to provide self-adjustment and better control, we will use an operational amplifier as described in Figure 4.17. Through this specific build it is possible to control the voltage (0-5V) across the sense resistor R_{SENSE} resulting in a controlled current (I_{TEC}) through the resistor and the load.

$$0 \text{ to } \frac{5V}{R_{SENSE}}$$

The current allowed in the TEC that we will use is 0-4A therefore $R_{SENSE} \simeq 1.25\Omega$. The power rating of this resistance should be

$$P_{R_{SENSE}} = I_{TEC}^2 \cdot R_{SENSE} = 20Watt$$

Taking in mind the above calculation we choose BUZ73L by Infineon as it can draw a maximum current of 7A.

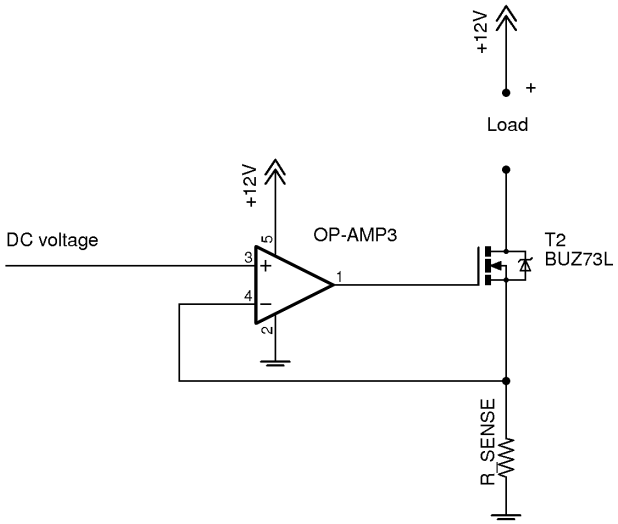

Figure 4.17: The implementation of the voltage regulated current source

4.5.3 H-Bridge

An H-bridge is an electronic circuit which enables a voltage to be applied across a load in either direction. These circuits are often used in robotics and other applications to allow DC motors to run forwards and backwards. The H-Bridge arrangement is generally used to reverse the polarity of the motor, but can also be used to 'brake' the motor, where the motor comes to a sudden stop, as the motor's terminals are shorted, or to let the motor operate in 'free run' until it stops, as the motor is effectively disconnected from the circuit(fig. 4.18).

H-bridges can either be built by discrete components (transistors, relays) or found as integrated circuits. A solid-state H-bridge is typically constructed using

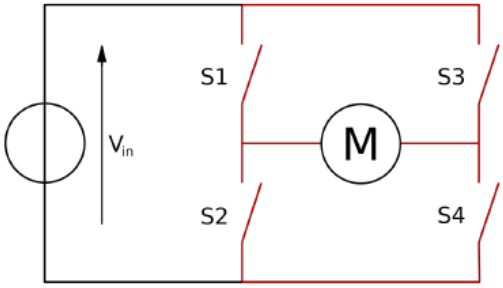

S1	S2	S3	S4	Result
1	0	0	1	Forward
0	1	1	0	Backward
0	0	0	0	Free run
0	1	0	1	Brake
1	0	1	0	Brake

Figure 4.18: The configuration of an H-bridge

reverse polarity devices (i.e. PNP BJTs or P-channel MOSFETs connected to the high voltage bus and NPN BJTs or N-channel MOSFETs connected to the low voltage bus). The most efficient MOSFET designs use N-channel MOSFETs on both the high side and low side because they typically have a third of the ON resistance of P-channel MOSFETs. This requires a more complex design since the gates of the high side MOSFETs must be driven positive with respect to the DC supply rail. In this direction many integrated circuit MOSFET drivers include a charge pump within the device.

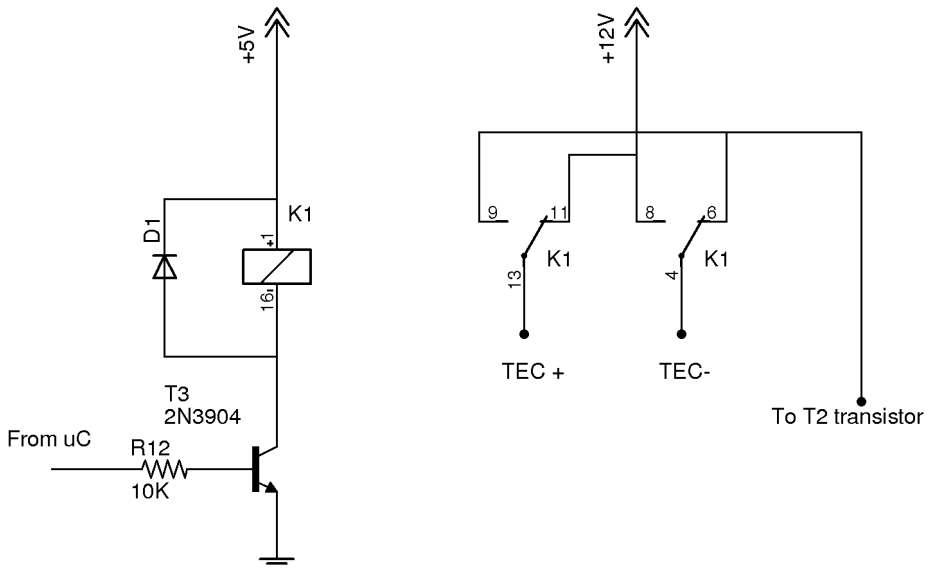

Figure 4.19: H-bridge implementation with a DPDT relay

Alternatively, a switch-mode DC-DC converter can be used to provide isolated ('floating') supplies to the gate drive circuitry. A multiple-output flyback converter is well-suited to this application. Another method for driving MOSFET-bridges is

the use of a specialised transformer known as a GDT (Gate Drive Transformer), which gives the isolated outputs for driving the upper FETs gates. The transformer core is usually a ferrite toroid, with 1:1 or 4:9 winding ratio. However, this method can only be used with high frequency signals. The design of the transformer is also very important, as the leakage inductance should be minimized, or cross conduction may occur. The outputs of the transformer also need to be usually clamped by zener diodes, because high voltage spikes could destroy the MOSFET gates.

Our implementation is based on a DPDT relay configured as described in Figure 4.19. In order to drive the relay through the microcontroller we will use a BJT transistor switch. Due to the inductive operation of the mechanical relay that we are using we will have to use a protection diode in order to take care of the inverse EMF that is induced according to Lenz's law. With the use of this diode we force the energy that is stored in the relay coil to be consumed through a current inside the coil.

4.6 Serial Communication circuit

As described in section 4.2 a serial communication device is embedded in ATmega32. We will follow the asynchronous type of communication between the microcontroller and the connected computer. For this link we should use a voltage-level converter to convert the transmitted signal from the TTL level of the μC to RS-232 voltages (approx. $\pm 7.5V$). This level shift is achieved through a very commonly used IC, MAX232, that is provided by several manufacturers. It is a dual driver/receiver circuit to convert the R_x/T_x signals and is powered through a single 5V source, not exceeding the standard TTL voltage. The circuit implementation is described in Figure 4.20 and based on MAX232I, provided by Texas Instruments. In this schematic, $1\mu F$ capacitors are used in order to raise the voltage level from 5V to RS-232 level (charge-pump operation).

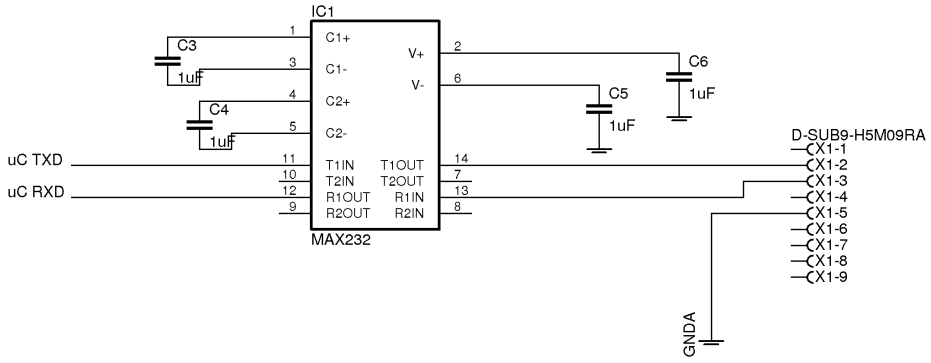

Figure 4.20: The serial communication circuit based on chip MAX232N by Texas Instruments

4.7 Final Schematics and Photos of the Hardware

The final schematic and the photos of the constructed system can be seen in the pictures that follow.

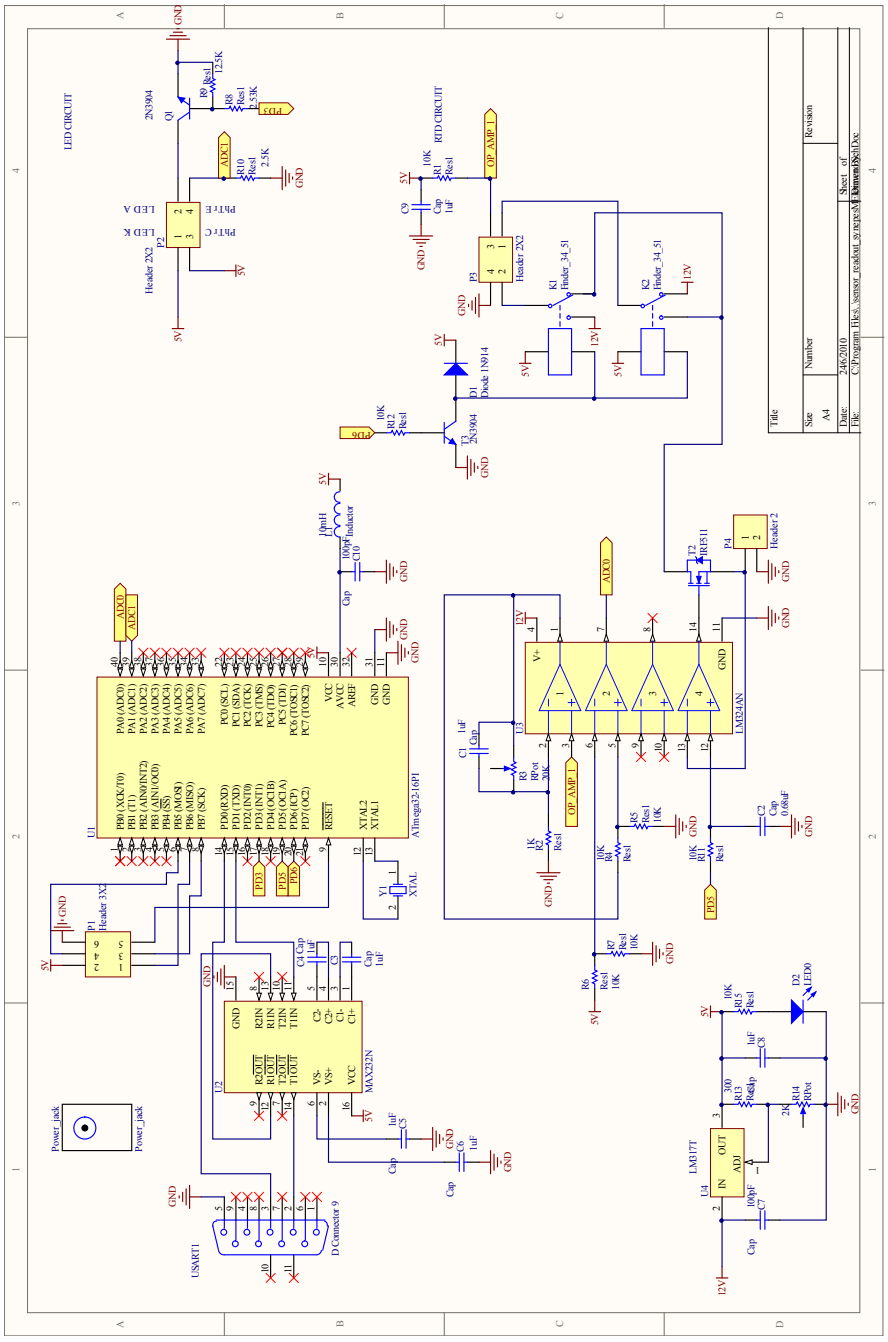

Figure 4.21: The final schematic of the readout/control system.

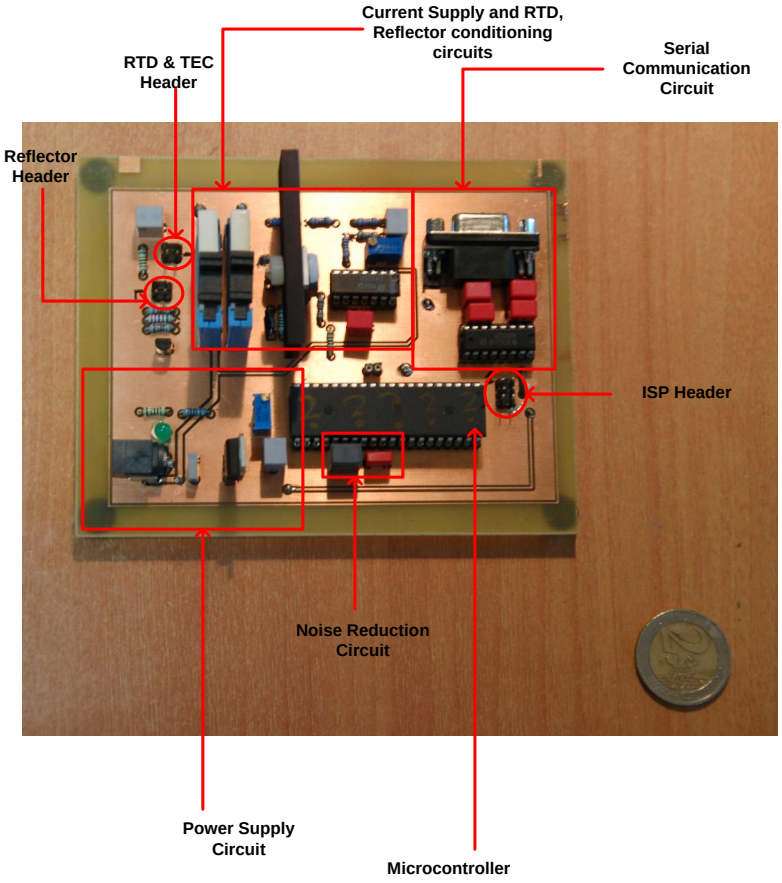

(a)

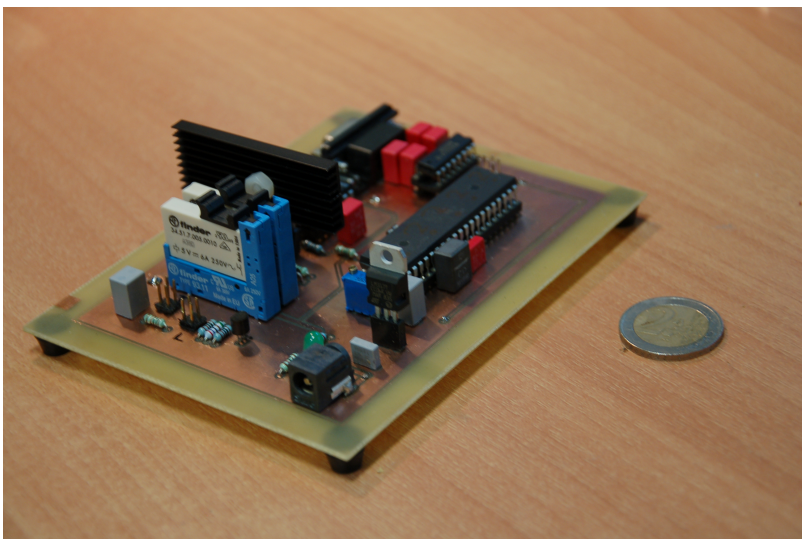

(b)

Figure 4.22: a.Top-view of the developed board compared to a coin of 2€. b.Side view of the board.

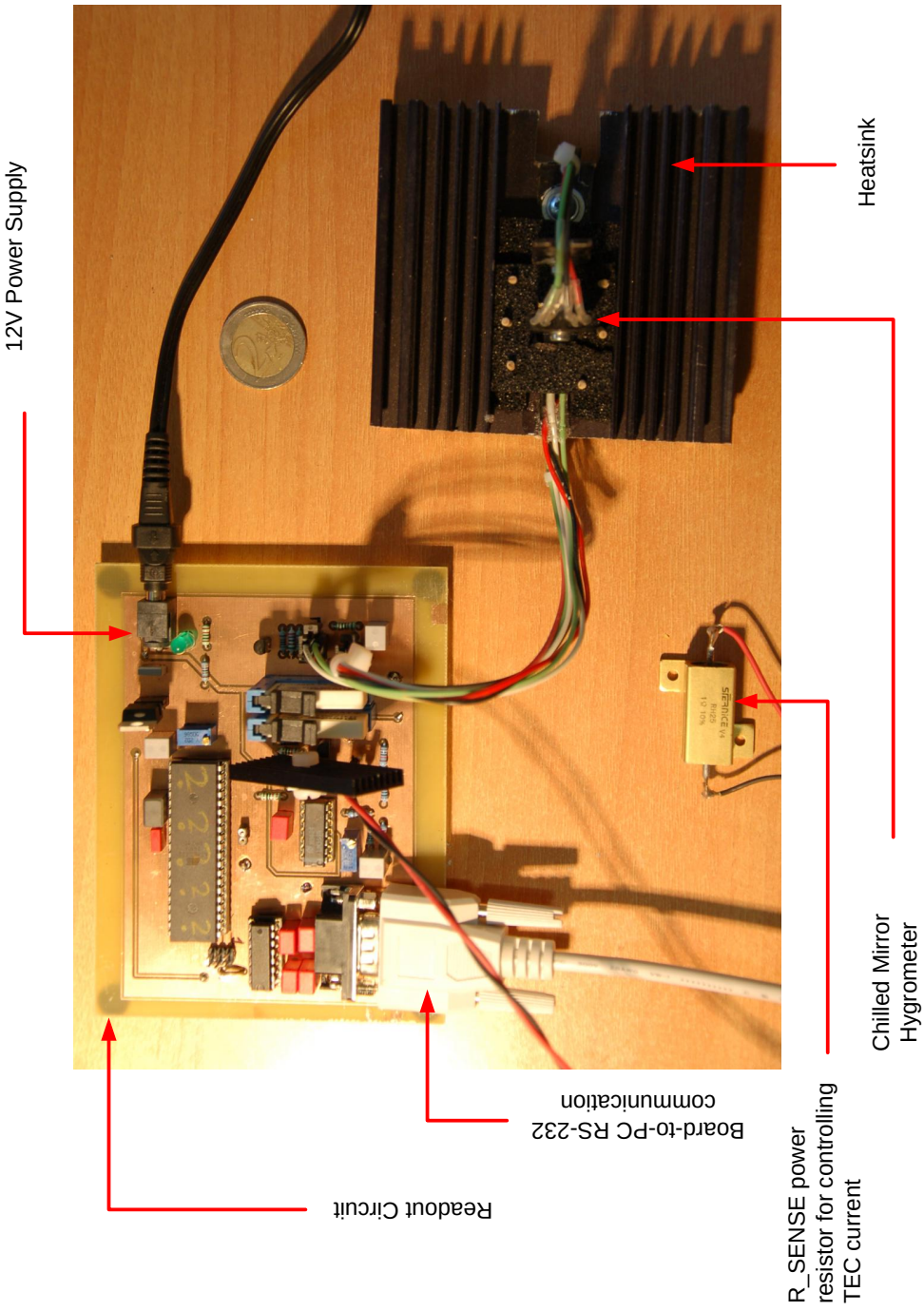

Figure 4.23: Photo of the whole system, including the readout circuit, the Chilled Mirror Hygrometer, the power resistor for the TEC supply, the 12V power supply and the RS-232 communications cable.

Chapter 5

Programming the Control and the Readout Procedures

As it is described in the previous chapters the central unit of the control and readout system is the ATmega32 microprocessor. All the individual sub-circuits are connected either to the microcontroller's inputs or outputs, allowing the device to handle the analogue control and the communication interface. The developed software should perform the following tasks:

1. Measure the temperature of the surface of the metal mirror.
2. Measure the reflectance of the surface of the metal mirror.
3. Decide whether the mirror is wet or not.
4. Stabilize the mirror temperature and preserve a fixed water layer on the mirror surface by controlling the cooling intensity of the TEC.
5. Send the results to a computer via RS-232 communication.

The tasks described in 1, 2 and 5 are simple implementations of standard procedures concerning the initialization and the readout of two channels of the ADC (embedded in the microcontroller) and the use of the USART module. Regarding the 3^{rd} task the decision on whether the mirror surface is clean or wet is equivalent to the selection of the water layer thickness. According to [13] the accuracy of the dew-point measurements is determined by the water layer selection and is dependent on the partial pressure of water in the gas under test. As the research on this exceeds the target of this thesis, we will have to make a simplification and choose a standard percentage of the clean mirror reflectivity in order to define the threshold between "clean" and "wet" mirror. This ratio is set to 99% and consequently,

$$\rho_{wet} < 0.99 \cdot \rho_{clean} \tag{5.1}$$

The 4^{th} task can be achieved through a control procedure that will be analysed in detail in the following section (5.1).

5.1 Algorithmic Optimization

According to what is described in chapter 2 the operation of the conventional CMH is based on a temperature oscillation around the actual dew-point. The accuracy of the measurement is strongly dependent on the scheme and the amplitude of this oscillation. One first approach is displayed in Figure 5.1 where the dew-point is located between T_{max} and T_{min}.

The optimal control and measurement procedures can be simplified to the actions that minimize the difference $T_{max} - T_{min}$. This minimization necessitates the recognition of all the aspects of the physical phenomena on which the operation of the chilled mirror hygrometer is based.

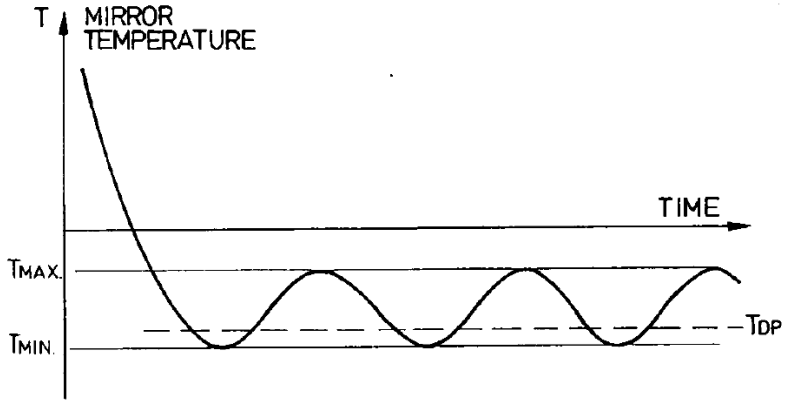

Figure 5.1: Ideal representation of the mirror temperature variation around the dew-point region. The actual dew-point (T_{dp}) is located between T_{max} and T_{min}

5.1.1 Heat Transport, Temperature Control and Molecular Thermokinetics of Water Vapour

A simplified, one dimensional, thermodynamic model of the hygrometer head is shown in Figure 5.2a. Due to the thermoisolator around the block the heat dissipation of the sides can be neglected resulting in the thermal transfers that are marked with the arrows. In order to control the mirror temperature T_x some online measurements are obligatory. This forces the measurement of the gas temperature T_G and flow velocity as well as the ability of the radiator to keep a constant temperature on the hot side of the TEC (T_h) through measuring the temperature and the flow velocity on the cold side of the radiator (T_{sg} and V_s respectively). However the direct approach for setting T_x is not only expensive but also can be unreliable and unsafe as unexpected environmental changes can happen affecting T_g, V_g, T_{gs} and V_s.

As it can be seen the system is thermally inertial because of the relatively low TEC efficiency and the relatively high TEC mass comparing to the metal mirror. Therefore it is difficult to change the temperature rapidly enough to avoid

overcondensation during the cooling cycle, resulting in an unavoidable temperature overregulation (see Fig. 5.2b). The asymmetric oscillation that is produced between the cooling and the heating phase is due to the external heat contribution of the environment that retards cooling and accelerates heating. These procedures can be separated in three regions; the water condensation (region 1), the water evaporation (region 3) and the temperature overregulation (ΔT_e - region 2). The latter expresses the energy required to evaporate the overcondensed water layer, which is caused by a prolonged condensation time (long region 1) due to cooling inertia.

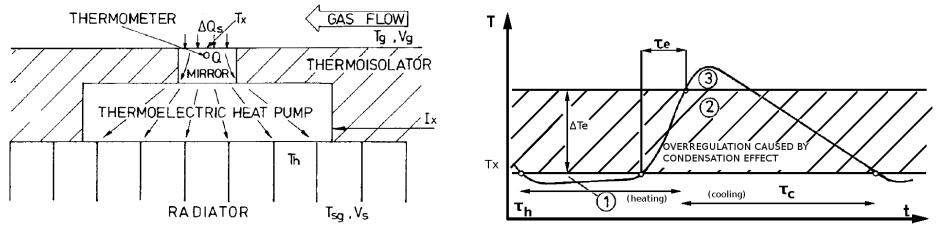

(a) (b)

Figure 5.2: a. 1D thermodynamic model of the hygrometer head b. Illustration of significant mirror temperature overregulation (region 2) caused by water overcondensation (region 1). Regions 1 and 3 are typical and unavoidable of a inertial cooling system

During water condensation, some additional heat is supplied to the mirror from the molecules, and during evaporation some heat is picked up from the mirror by the evaporating molecules. The complexity of the thermokinetic problems does not allow the construction of a simple physical phenomena model.

To surpass the previous difficulties an effective adaptive algorithm is employed that is based on the feedback of the final control results such as the range of mirror temperature and the time needed for the cooling and heating procedures. The target of this algorithm will be the minimization of ΔT_e through the accurate control and stabilization of the condensed water layer. However, the system parameters should be determined and several tests have been performed to obtain them.

5.1.2 Algorithmic Description

The main task of the dew-point temperature measurement system is to keep the condensed water layer as stable in thickness as possible. As mentioned before the binary signal, whether the metal mirror is "wet" or "clean", is used for this regulation. It should be noticed that an overcondensation is proportional to both the depth and the duration of the overcooling. This is shown in Figure 5.2b where the time τ_e, and the temperature rise ΔT_e, are necessary for overcondensed water molecules to evaporate. Both of these two factors influence the length of cooling τ_c as well. When the dew thickness is too low, the measurement error can increase

considerably. However different supply current I_{TEC} do not affect the temperature of condensation but only the evaporation temperature ($T_x + \Delta T_e$) and the condensation/evaporation time constants.

The evaluation of the condensation/evaporation process provides important information for designing optimal control and measurement procedures for the operation of dew point hygrometers.

- Temperature stabilization of the mirror is provided by regulation of the electrical heat pump. The pump together with the mirror, as an inertial system, causes considerable temperature overregulation, in spite of the negligible reflector signal delay.

- The measurement of the mirror temperature at the moment of dew condensation gives the most accurate results.

- The dew layer thickness for dew-point determination appears to be quite important for accurate humidity measurements and depends on the partial pressure of water in the gas being tested.

- Mirror overcooling below the dew point temperature T_{DP} is responsible for overregulation above T_{DP} (see Fig 5.2b). Overcooling is very critical and should be carefully avoided.

In the dew-point hygrometry and, generally on processes that measure critical points, it is practical to use different procedures; one that will run during the initialization or in notable changes of environmental conditions (Rapidly Changing Conditions Procedure - RCCP) and another that will be activated for stable working points (Stable Conditions Procedure - SCP). Particularly on our sensor RCCP is a quick way to reach the actual T_{DP} and enter the more accurate SCP where temperature will be oscillating around T_{DP} allowing though small dew-point variations without quitting this process.

Initialization

Once the device is switched on there is a short time gap where the microcontroller peripherals are initialized. During this period both the reflector and the thermometer conditioning circuits are stabilizing and initialized. The main target of this step is to define the reflectance of the clean mirror, according to which the dew formation decision will be made. In order to achieve this the temperature of the metal mirror (T_x) should remain safely above dew-point -at least 10^oC- and as stable as possible. The average of the set of reflectance measurements taken in the conditions mentioned above is the "clean mirror reflectance", while the "wet mirror reflectance" is the 99% of this value.

This procedure will be called each time a restandardization is needed. This can happen either from an external demand or as a regular process to enhance stability and accuracy over long term operation.

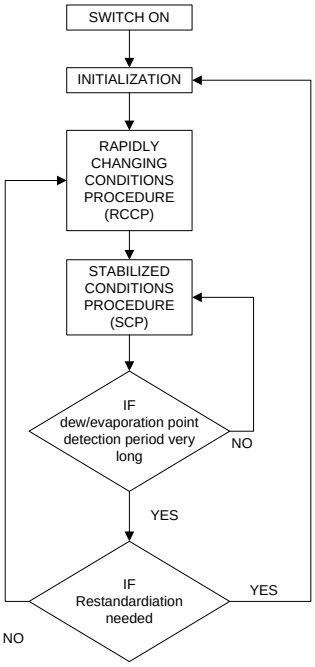

Figure 5.3: The concept of sensor operation. The combination of the individual procedures forms a well responding sensor in totally varying environments.

Rapidly Changing Conditions Procedure - RCCP

This procedure is referring to the operation point where the dew-point temperature region is not yet found. This can happen either after the initialization phase, during the first attempt to find dew-point, or after rapid and considerable changes in the environmental conditions -temperature or RH-, as it is described in 5.3. This procedure is working with maximum current through the TEC (I_{TEC}) in order to reach as quickly as possible the new dew-point region and find a first approximation of the actual T_{DP}. Thereafter the sensor enters the SCP mode where the more accurate measurements allow better a estimation on T_{DP}. The RCCP mode is enabled again when there is no dew/evaporation point detection for a long time.

Stabilized Conditions Procedure - SCP

The most important process for hygrometer operation is the control procedure for a quasi-stable work point (i.e. constant or smoothly changing humidity). On the basis of the analysis described in section 5.1.1 an algorithm to determine T_{DP} in a dynamic way is developed. As it was mentioned before, the goal of this algorithm is to minimize the overcondensation phenomenon and the consequent temperature overregulation.

The flowchart displayed in Figure 5.6 is describing the control loop in the SCP mode. The procedure is based on two identical sub-processes; the cooling procedure

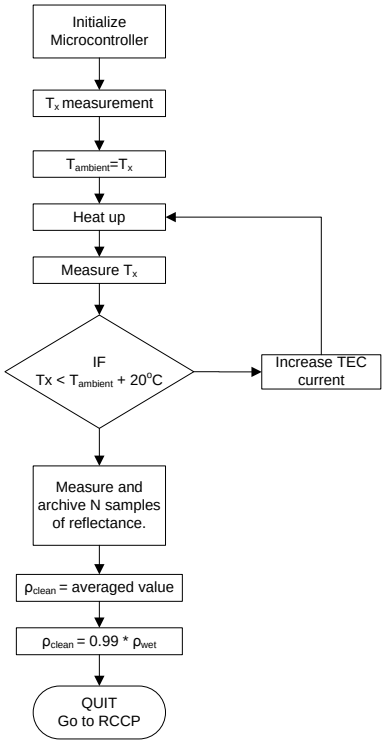

Figure 5.4: Initialization procedure which is executed each time sensor is powered on. It can also be called on demand for more stabilized long-term operation.

that aims to detect the condensation point and the heating procedure that detects the evaporation point. The fundamental concept of these algorithms is that the mirror should be kept in thermal equilibrium at any moment. This criterion solves two main problems in the control design, though lengthening the time between two successive detections. Firstly the temperature gradient between the surface of the mirror and the thermometer is minimized. Secondly the temperature transitions during cooling/heating phase become smoother, resulting in the minimization of the water overcondensation and the temperature overregulation.

The condition mentioned above means that I_{TEC} will be changing, by a minimum quantity ΔI_{LOOP} only when there is no detection and the temperature fluctuation of the last measurements is quite small. This can be evaluated by the following equation :

$$\sigma_T < \sqrt{\delta T} \tag{5.2}$$

where σ_T is the standard deviation of the last temperature measurements and δT is the accuracy of temperature measurements as expected by the thermometer readout circuit.

Depending on the operating phase -cooling or heating- the quantity of ΔI_{LOOP} will be added or deducted to I_{TEC} in order to get colder or hotter respectively.

The previous describe the cooling/heating phase while there is no dew-point/evaporation-point detection. Once the reflector signal flags a detection the system exits the loop

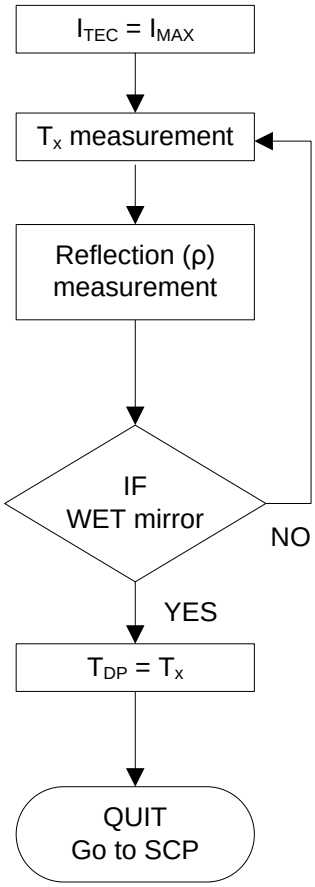

Figure 5.5: The Rapidly Changing Conditions Procedure (RCCP) that is executed when the environmental conditions are changing quickly.

and calculates the critical point.

Cooling Phase: If the active phase is the cooling, then dew-point T_{DP} is defined as the temperature T_x that the mirror has at the moment of dew detection. I_{TEC} is reduced by ΔI_{STEP} in order to warm up the mirror and evaporate the water layer.

Heating Phase: If the active phase is the heating, then evaporation-point T_{DP} is defined as the temperature T_x that the mirror has at the moment of clean mirror detection. I_{TEC} is increased by ΔI_{STEP} in order to cool down the mirror and form a dew layer.

The values of ΔI_{LOOP} and ΔI_{STEP} are subject to the specific structure of the device. Therefore it was crucial to study and investigate on the way that these variables affect the temperature overregulation. Through the experiments we have used several values and reached the following results :

$$\Delta I_{STEP} = 2 \cdot \Delta I_{LOOP}$$

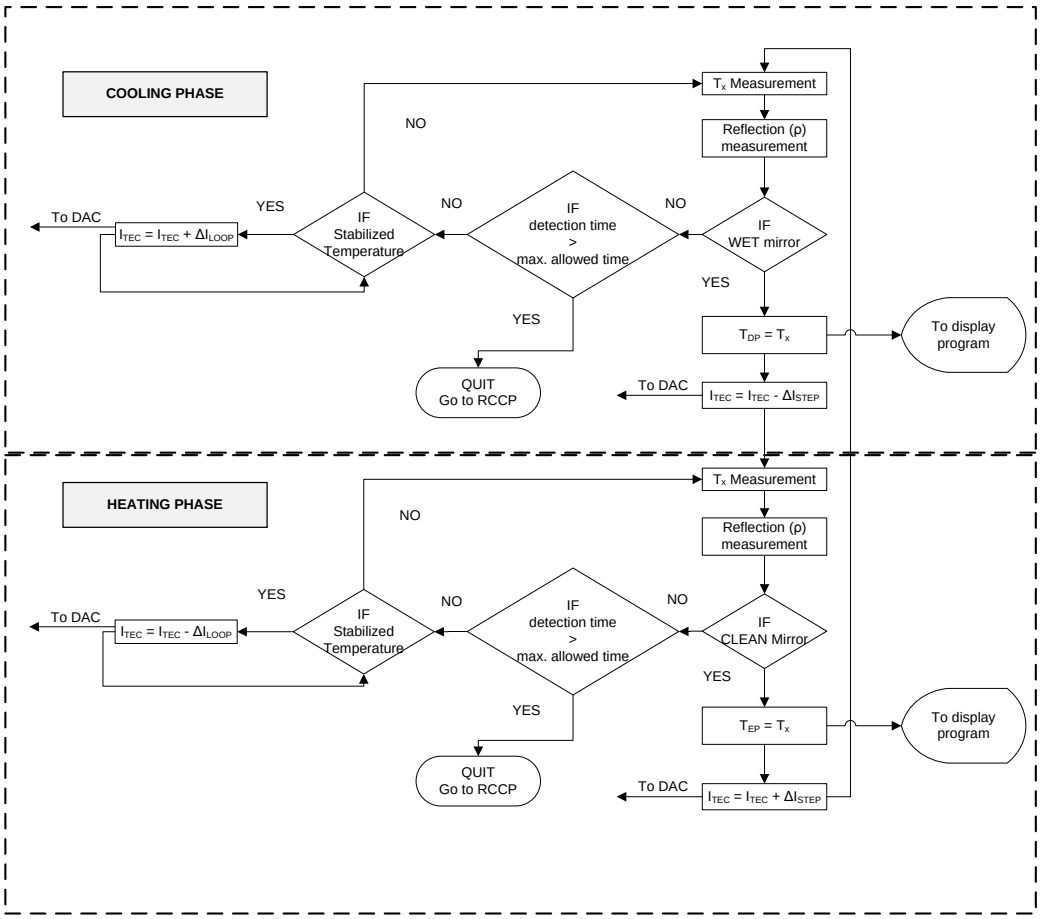

Figure 5.6: The Stable Conditions Procedure (SCP) that is executed when the sensor runs in stable conditions.

$$\Delta I_{LOOP} = 0.1\% \cdot I_{TEC,MAX}$$

5.2 Software

Whatever is described in the previous sections should be implemented in the microcontroller software. The source code that is presented below is designed to operate for the microcontroller ATmega32. It was developed in programming language C and compiled through AVR Studio ver. 4.15 that is provided by ATMEL and is based on the GCC - AVR Libc project. The files that were developed are :

- DPsensor.c
- scp.h
- rccp.h
- helpingFunctions.h
- readout.h
- adc.h

- pwm.h
- usart.h
- define.h
- Makefile

The files above will be presented in the following paragraphs starting from the most high-level procedures and proceeding with an in-depth description of the low-level register handling.

5.2.1 The Main Program

The files 1. DPsensor.c 2. scp.h 3. rccp.h 4. helpingFunctions.h are describing the main procedures of the sensor operation. They are implementing the algorithms that are described in section 5.1.2, providing the ability of switching ON/OFF the sensor and formatting the transmitted output. For the relevant C code refer to Appendix C.1

5.2.2 Measurement Functions

ATmega32 is featuring an 8-channel ADC. In order to change between the channels and translate the ADC measurements in temperature or reflectance we should implement a function that is expressing the transfer function of the circuit and is based on the real properties of it. Unfortunately even with accurate measurement of the discrete devices, a system calibration was needed, especially for the temperature conditioning circuit (see section 6.1.2). These details are taken into account in the functions described in Appendix C.2.

5.2.3 USART/ADC/PWM Functions

These functions are used for communication between the microcontroller ATmega32 and the serial port of the computer, the ADC initialization and reading and the PWM settings. For more details refer to Appendix C.5, Appendix C.3, Appendix C.4 respectively.

5.2.4 Circuit Constants

All the values and the properties of the readout/control circuit are included in define.h. For more details look into Appendix C.6.

5.3 The Microcontroller Programming Procedure

Programming ATmega32 is easily achieved through the ISP configuration. In this layout the microcontroller device that is embedded on the constructed board is connected to a programming device through a 6-pin header. The device that was used for this goal was STK-500 by ATMEL (see photo 5.7)

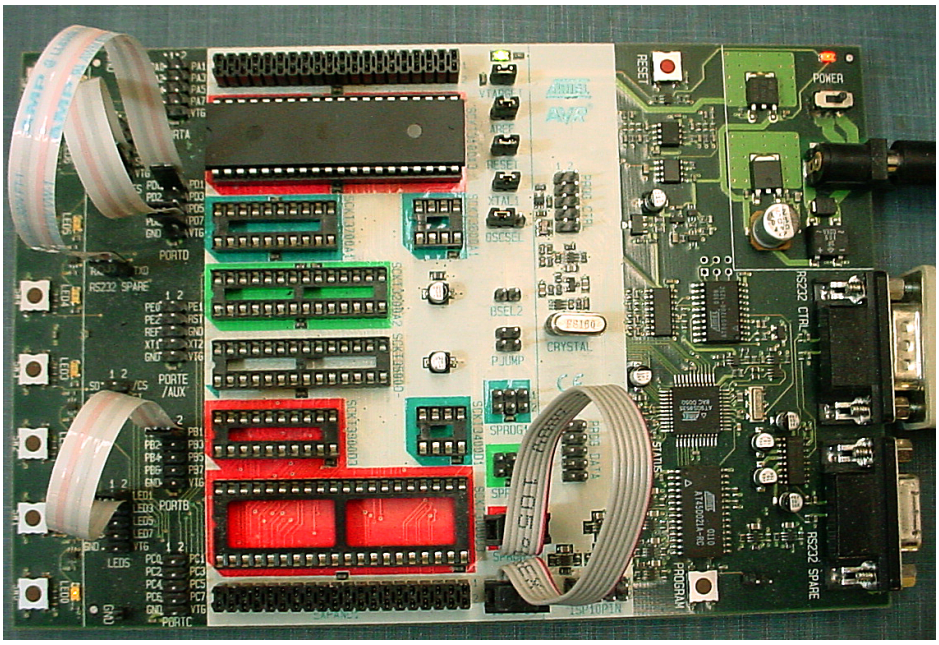

Figure 5.7: The board STK-500 produced by ATMEL was the device that we used to program the microcontroller.

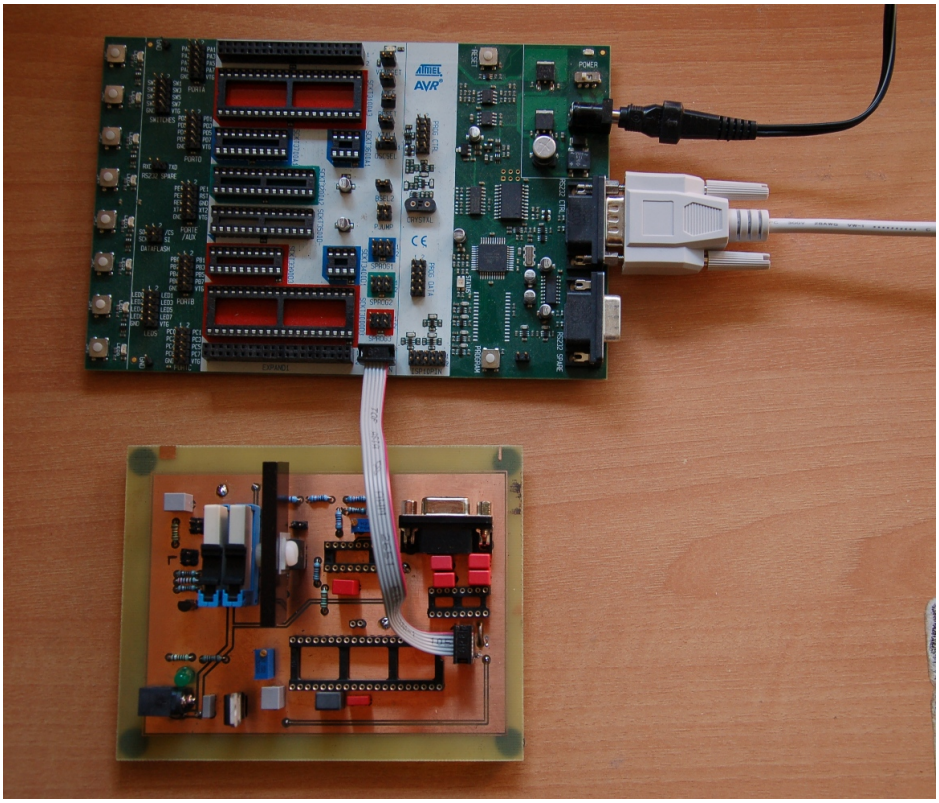

Figure 5.8: ISP configuration used for programming the readout board.

Chapter 6

Data Processing and Experimental Procedure

Once the sensor and the control/readout system is constructed and programmed the main target is to read the output through a PC. Several programs for receiving/transmitting data through the serial port are available either for Microsoft Windows or GNU/Linux platforms (HyperTerminal, Terminal, gtkTerm, minicom etc.). The data will be archived in a form that is easy to analyse through data-analysis programs as Matlab or ROOT.

In our analysis we will use ROOT(`http://root.cern.ch/`) and all the following plots are produced through this software. ROOT is a powerful data-analysis program targeted for High Energy Physics where the analysis of large amounts of data is necessary. It is a free, open-source program that is distributed in GNU/GPL license.

At this final step we should evaluate the sensor's accuracy and response.

6.1 Temperature Measurements

6.1.1 Noise Reduction

In the measurements that are presented in Figure 4.12b, it can be clearly seen that thermal noise is inducing a major signal fluctuation that is measured through the ADC and is producing misleading results regarding the actual temperature. As mentioned many times before, the fact that the measurements follow the Gaussian distribution proves that the induced noise is white and that the measurement error is random.

The basic properties of the white noise is that its mean ($\mu_w(t)$, $t \in \mathbb{R}$) and the autocorrelation ($R_{ww}(t_1, t_2)$) function satisfy the following:

$$\mu_w(t) = \mathbb{E}\{w(t)\} = 0$$

$$R_{ww}(t_1, t_2) = \mathbb{E}\{w(t_1)w(t_2)\} = (N_0/2)\delta(t_1 - t_2)$$

In other words the white noise signal is a zero mean process and has infinite power at zero time since its autocorrelation function is the Dirac delta function.

The double assumption that the frequency of the noise signal (f_{noise}) is greater than the sampling frequency of the ADC (f_s) which, in turn, is greater than the Nyquist frequency of the signal (f_N) forms the basis of reducing the fluctuation of our measurements improving the accuracy of the device. From the relationship $f_{noise} >> f_{ADC}$ one can deduct that the ADC samples will have random noise amplitude. The sum of that noise ideally tends to 0 eliminating the effect of white noise. However the second inequality secures that the signal will not be changing a lot during the conversion, a condition that is necessary to fulfil in order to be able to use average values.

In the current implementation f_N is very small[1], $f_{ADC} = 125KHz$ and the white noise frequency is greater enough to meet the previous points. Therefore we can use an average of n measurements (as many as the microcontroller can handle without algorithm violation and significant signal change) to reduce the effect of the noise (see Eq. 6.1) and to implement a software lowpass filter that will smooth the effect of the high frequency noise.

$$\sum_{i=1}^{n}(x_i - \tilde{x_i}) = \sum_{i=1}^{n} e_i \simeq 0 \Rightarrow \tilde{x_i} \simeq \bar{x_i} \tag{6.1}$$

In our implementation $n = 16$ which means that the current temperature value is calculated as the average of 16 successive oversampled ADC measurements. The results can be observed in Figure 6.1c. The delay that is induced through this procedure is expressed by the following equation:

$$f_{Total} = \frac{\text{1 oversample}}{\text{16 ADC samples}} * \frac{\text{1 averaged sample}}{\text{16 oversamples}} * \frac{\text{1 ADC sample}}{\text{13 ADC cycles}} * f_{ADC} \Rightarrow$$

$$f_{Total} = 37 \text{ samples/sec} \tag{6.2}$$

6.1.2 Calibration

As it is well described above the temperature sensor that is used is a Pt-1000 RTD thermometer. A very useful property of this sensor is that its nominal resistance at 0^oC is $1K\Omega$, and this property is well guaranteed by all the manufacturers. Therefore the replacement of the RTD with a simple $1K\Omega$ resistor can be a quite simple and effective method of calibrating the readout system. Through this, the circuit is isolated from ambient temperature variations and measures accurately the offset and the noise that are induced into the signal from the rest of the electronics.[2]

[1] The response time of the Pt-1000 that we are using is 0.3s. Hence a sampling frequency of $f_s = f_N = 2 \cdot 1/0.3Hz \simeq 7Hz$ is enough. However we will remain in the region $50KHz < f_s < 200KHz$ where our ADC operates optimally.

[2] At this point it should be made clear that the system is analysed and modelized through a linear approximation although there are always non-linearities in op-amp circuits.

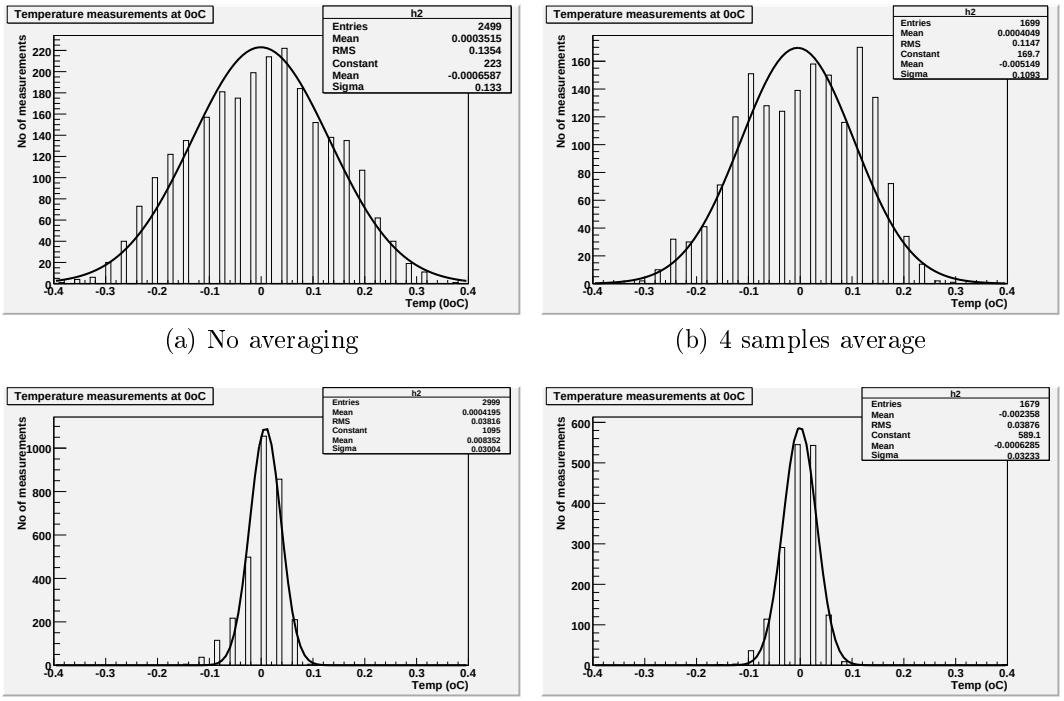

(a) No averaging

(b) 4 samples average

(c) 16 samples average

(d) 32 samples average

Figure 6.1: Temperature measurements with the 12bit oversampling ADC at 0^oC conditions. In a. is the unprocessed signal, in b, c, d there is a 4, 16, 32 samples averaging respectively. It is obvious that in c, d the measurements' error is smaller.

6.2 Reflector Measurements

As described in Chapter 4 the conditioning circuit of the reflective sensor is quite simpler than the configuration used for temperature measurements. Hence the electronic noise on the measurements will be much less. Furthermore a light filter is embedded in the HOA0708 reflector which blocks the visible frequencies and reduces to minimum the noise originating from ambient lights.

The main difference between the reflector measurements and the temperature ones, is that reflectance (ρ) is not measured absolutely but relatively to clean mirror reflectance (ρ_{clean}) as it is measured in the "Initialization" procedure (see section 5.1.2). The reflectance values that will be of great concern will be the ones that will be in the region of ρ_{clean} ($\sim 1-3\%$) as the existence of water layer is directly affecting the mirror.

6.2.1 Resolution Enhancement and Noise Reduction

This field of analysis was well described in the previous section for the temperature measurements (see 6.1). The same improvements have been implemented for

the reflectance measurements increasing the ADC resolution to 12bit and constraining the white noise effect. In the reflectance measurements there is no meaning in translating the ADC counts in reflectance as

$$\frac{\rho}{\rho_{clean}} = \frac{\text{ADC result}}{\text{ADC result for clean mirror}}$$

It is important to highlight the clean mirror result is the outcome of the reflectance measurement during the initialization phase when the metal mirror is still free of moisture, containing though contaminants, especially after a long period of operation. However a periodic re-initialization of the sensor can solve this problem as the contaminants effect will be reckoned in the wet-mirror threshold calculations.

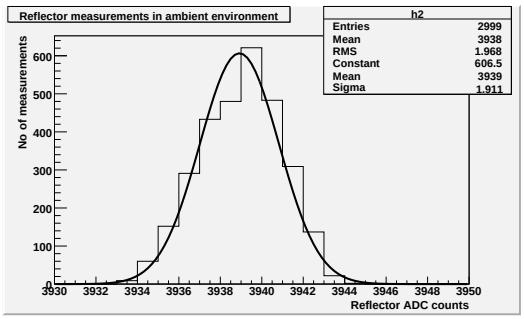

(a) No averaging

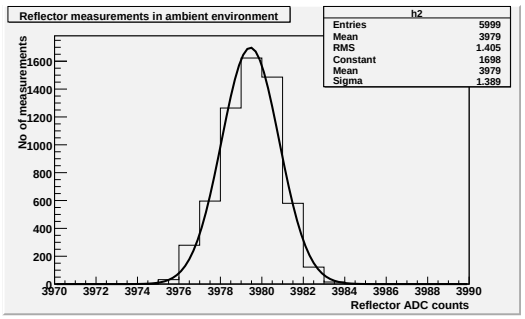

(b) 4 samples average

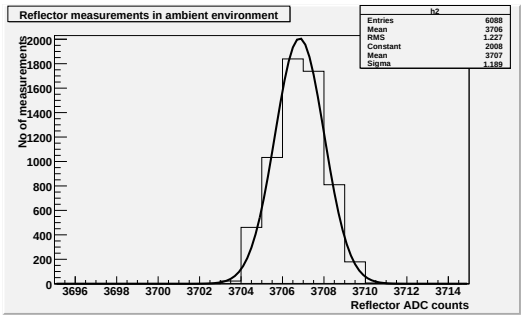

(c) 16 samples average

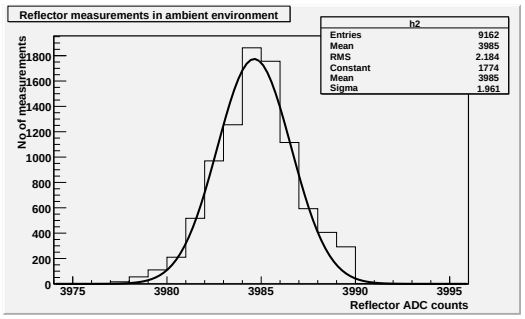

(d) 32 samples average

Figure 6.2: Reflectance measurements with the 12bit oversampling ADC at stable illumination conditions. In a. is the unprocessed signal, in b, c, d there is a 4, 16, 32 samples averaging respectively. It is obvious that in b, c the measurements' error is smaller.

6.2.2 Calibration

This step determines the water layer thickness that we use as "wet mirror" definition. The relation between water-layer thickness and reflectance is continuous, encumbering the establishment of an obvious threshold. There have been done

several experiments to determine the best thickness of the water layer. However this investigation exceeds the scope of this thesis as the conclusion is totally dependent on each specific implementation of the TEC-mirror complex. Therefore a generic conclusion could not be achieved. As a representative thickness of water layer we will use the reduction of ρ by 1% of the ρ_{clean} or

$$\rho_{wet} = 0.99 \cdot \rho_{clean}$$

At this thickness we achieved that the measured dew-point was the same between our sensor and a combined temperature/humidity/dew-point reference sensor, when both were put in the same conditions. The reference sensor was SHT71[20] by Sensirion and its readout was accomplished by the company's evaluation kit EK-H4[21].

6.3 Dew-Point Measurements in Changing Environmental Conditions

In the following pages some plots that describe the sensor's operation will be presented.

In Figure 6.3 we can see that the temperature overregulation is not very high and varies from below 0.1^oC to a maximum of 0.3^oC. The regular temperature fluctuation is below $\pm 0.2^oC$ from average value ($\sim 20^oC$) proving that the system has a quite good accuracy for stabilied conditions.

In Figures 6.4b and 6.4a a comparison between the two tested operation modes is done. In the first picture the CMH operates only with the SCP and achieves first detection after 2000 counter cycles whereas this time is reduced to 400 counts when the RCCP procedure is used.

In Figures 6.5a and 6.5b the transitions between RCCP and SCP operation can be seen. It should be noted that when operating in RCCP temperature fluctuation is greater and therefore the T_{dp} measurement accuracy is not so good.

Finally Figures 6.6a and 6.6b show the measurements that have taken place during a whole day. In Figure the close-up proves that the temperature variation during long runs, remains at $\sim \pm 2^oC$.

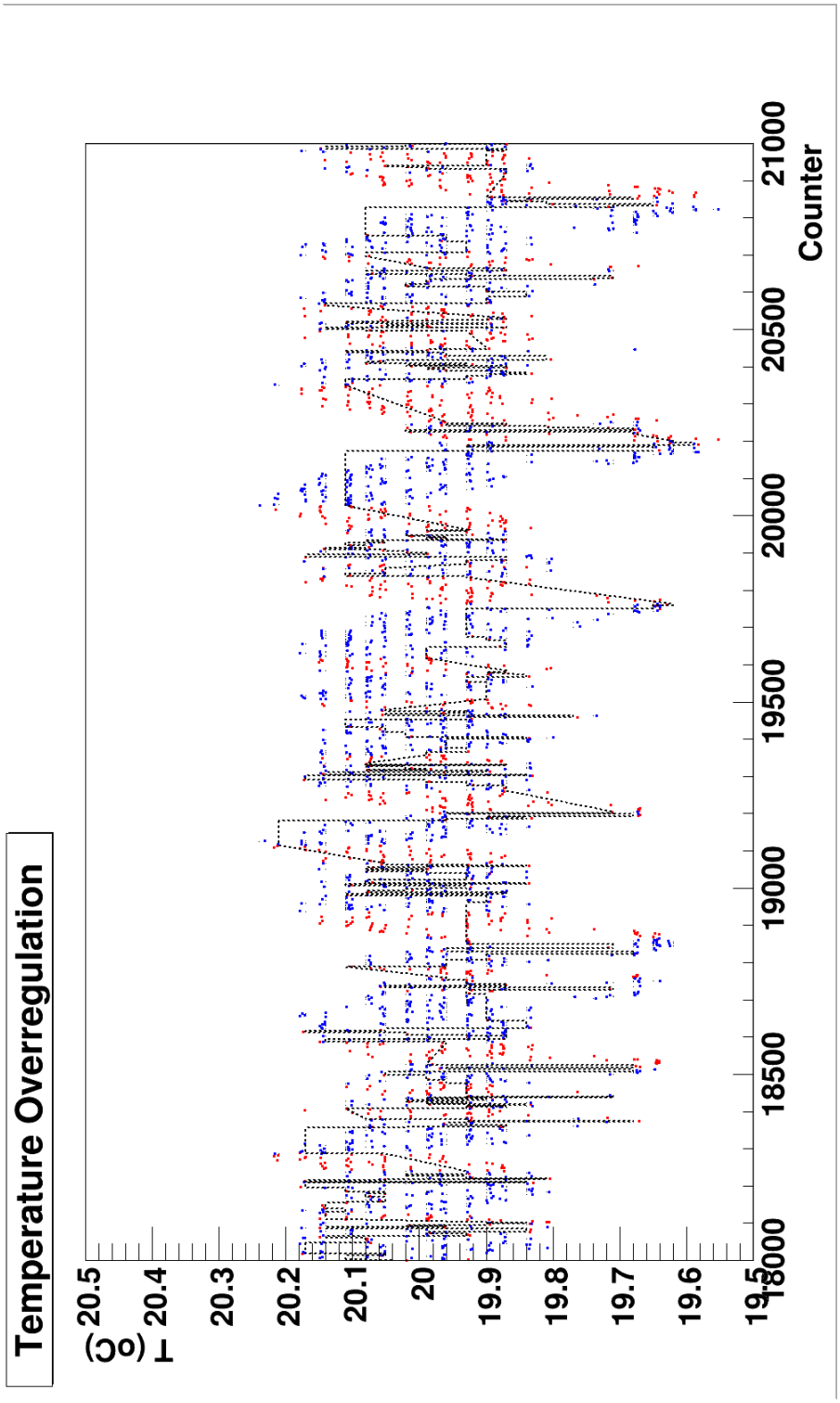

Figure 6.3: The temperature fluctuation in almost stable dew point conditions. The red dots depict the heating cycle while the blue depict the cooling one. The dotted line shows the measured T_{dp}. The time period corresponds to 50min.

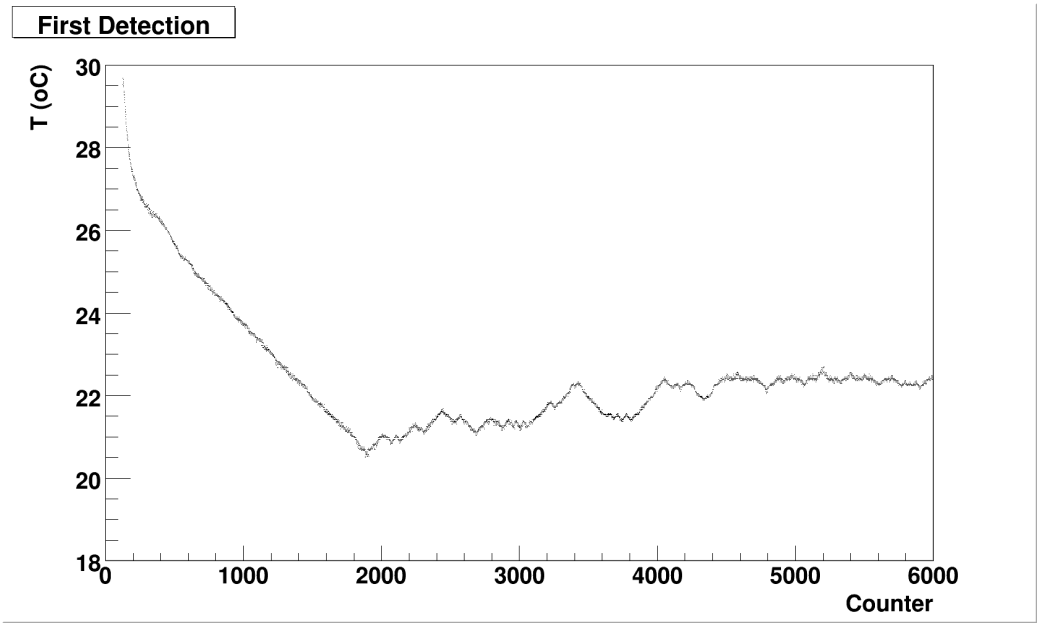

(a) SCP operation

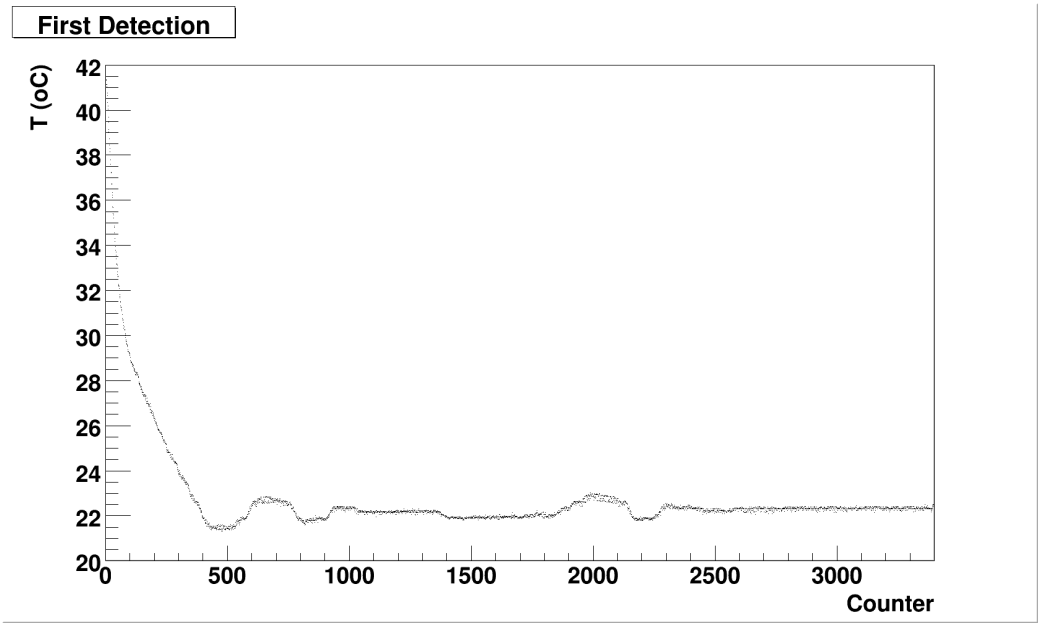

(b) RCCP operation

Figure 6.4: Two graphs showing the time needed for the first detection after initialiation. The Y-axis shows the mirror temperature and the X-axis the synchronized counter cycles. Graph (a) describes SCP operation while graph (b) RCCP. It is obvious that RCCP detection time is much smaller than the one of SCP.

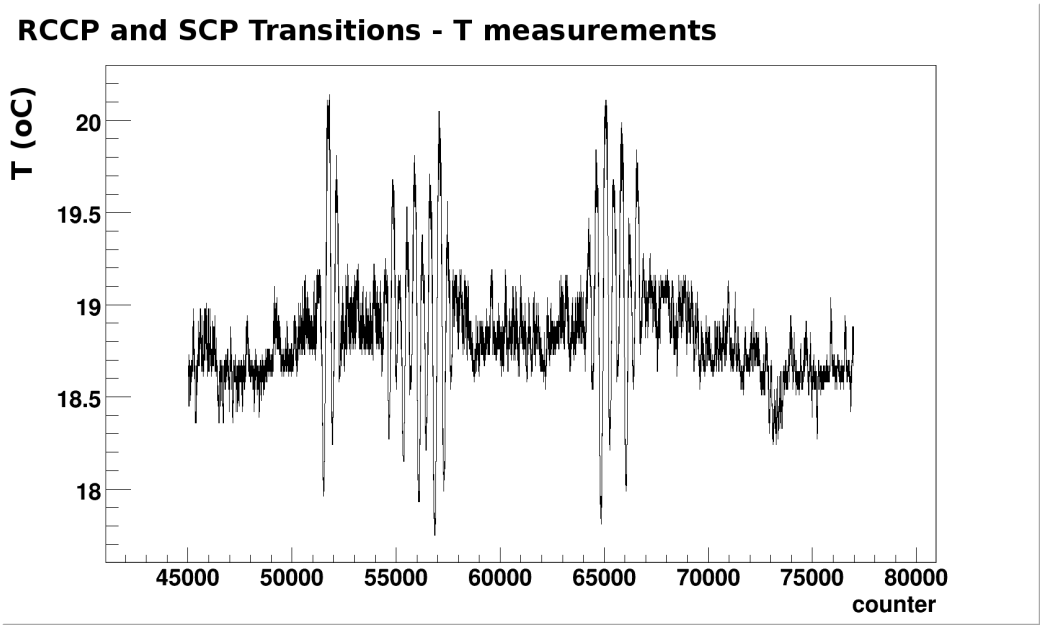

(a) Mirror T measurement

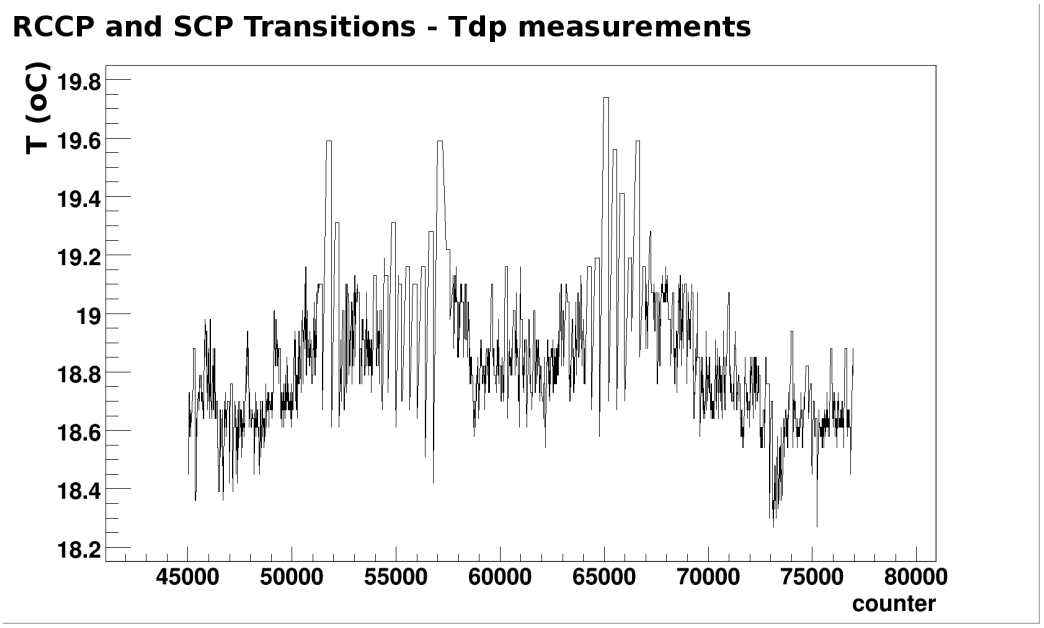

(b) T_{dp} measurement

Figure 6.5: Two graphs showing the transitions between RCCP and SCP operation. It should be noted that during RCCP operation the detection time is increased due to considerable dew point fluctuation.

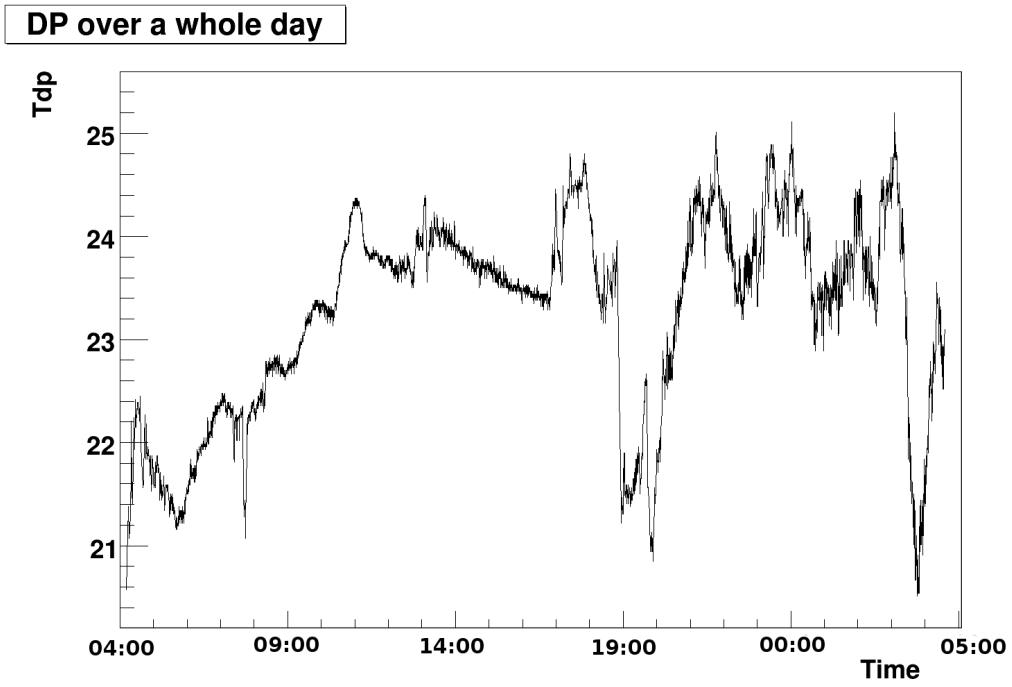

(a) T_{dp} measurement

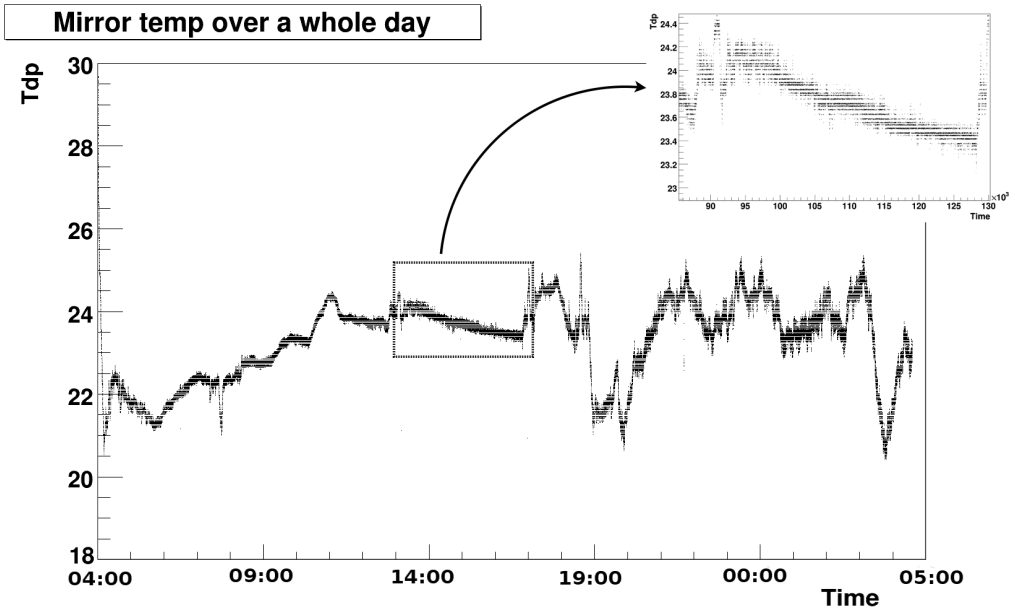

(b) Mirror T measurement

Figure 6.6: a. The dew point measurements over a day b. The temperature variation over the same day.

Chapter 7

Applications

As it was mentioned in the beginning of this thesis (see Chapter 1) humidity measurements are important in a wide range of applications. In most of the cases bulk polymer RH sensors are adequate for monitoring necessities. However there are applications where accuracy, reliability and long-term stability are crucial; for these the use of the CMH is the best available solution.

Part of the research for this thesis was conducted as a part of the CERN Technical Student Program in CMS [1] experiment at CERN, Geneva. For this reason the current chapter will include an asymmetric description of the possible CMH applications, emphasizing on the particle detectors. The complexity of these devices makes a brief description necessary for understanding the humidity problem that arises.

7.1 Elementary Particles Detectors

The idea of developing a dew point sensor was partially motivated by the possible use of such a sensor in the climatic control of High Energy Physics experiments and particularly in particle detectors. Particle detectors are large scale machines that are designed to measure the properties of sub-atomic particles. The main mechanisms are based on defining the energy and the routes that they follow in excellently controlled electromagnetic environment. Modern detectors are tracking the path of the particles through a large scale positioning system based on silicon diodes. However silicon is sensitive to radiation in two main ways; bulk (crystal) damage due to Non Ionizing Energy Loss (NIEL) and surface damage due to Ionizing Energy Loss (IEL). These can lead to changes in the effective doping concentration, increase of the leakage current, increase of charge carrier trapping, changes in interstrip capacitance and probable electrical breakdown. The only way of limiting this effect is by lowering the operating temperature. If operating temperature is below dew point, then formation of dew and ice is unavoidable. However, condensation on the detector electronics is a situation that should at any

[1] CMS or "Compact Muon Solenoid" is one of the two big experiments that take place in the Large Hadron Collider (LHC) at CERN.

cost be avoided. This is the main reason that the environment inside detectors should be dry and the necessity of T_{DP} measurements is prominent.

7.1.1 Brief Description of CMS particle detector

Quick View of CMS

CMS is comprised of a series of detectors, built in concentric radial layers around the axis of the beampipe. In the geometric center of the detector, proton-proton collisions occur producing a shower of elementary particles, which, due to the strong magnetic field ($4T$), follow radial trajectories and cross the following layers:

- the silicon Tracker
- the crystal Electromagnetic Calorimeter (ECAL)
- the Hadronic Calorimeter (HCAL)
- the solenoid magnet
- the four station muon detection system

The innermost part of the CMS dcetector is occupied by a silicon microstrip Tracker which precisely identifies and measures the momentum of muons, electrons and photons over a large energy range. The Tracker is also used to identify photons and leptons.

Around the Tracker lays the ECAL that has been designed for high precision measurement of photons, which is crucial in the discovery of low-mass Higgs. The calorimeter is constructed with homogeneous scintillating $PbWO_4$ crystals, whose density ensures that the system is highly compact.

In the next layer sits the HCAL which measures the energy and the direction of all hadronic showers, while also enhancing the detection of photons, electrons and muons. HCAL is fully hermetic, a feature that is necessary for the search of new particles where their signatures include missing transverse energy in the form of netrinos and anti-netrinos.

The muon system of the CMS is located in the outermost layer of the detector. Its target is to discover the crossing muons and measure their momentum, as well as trigger the archiving of the data for the whole system. Muon identification is achieved with accurate positional determination as a result of using drift tubes and cathode strip chamber detectors. The momentum measurements are performed in conjunction with the information of the Tracker.

Detailed descriptions of each system can be found in the related Technical Design Reports of the CMS experiment [22].

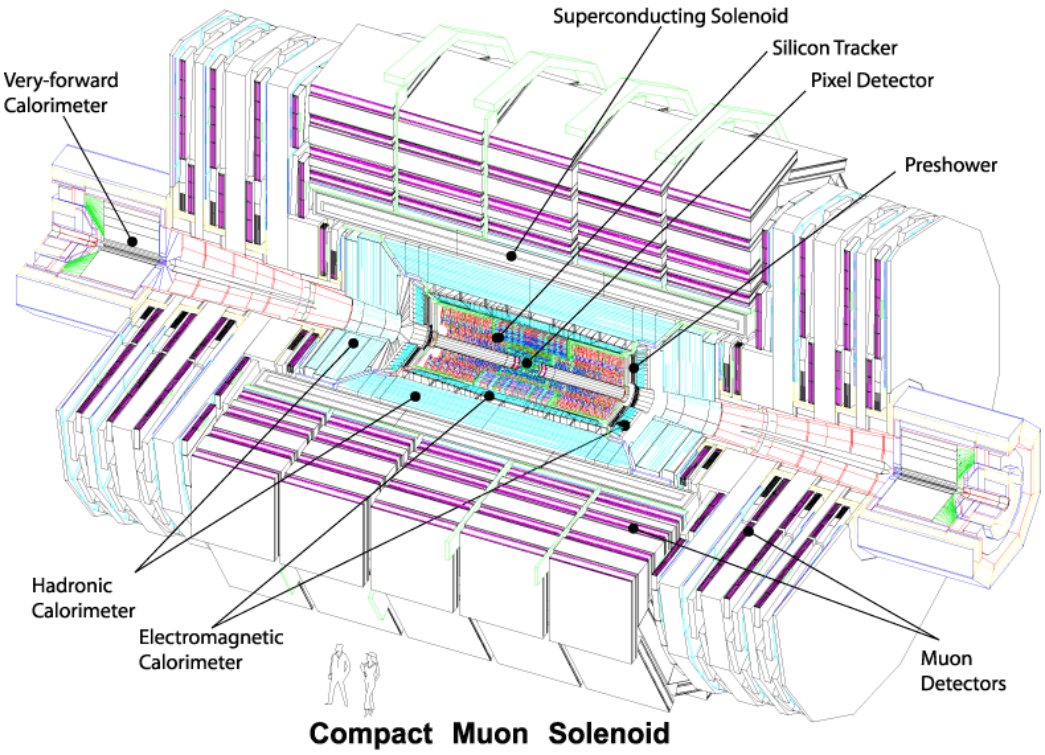

(a)

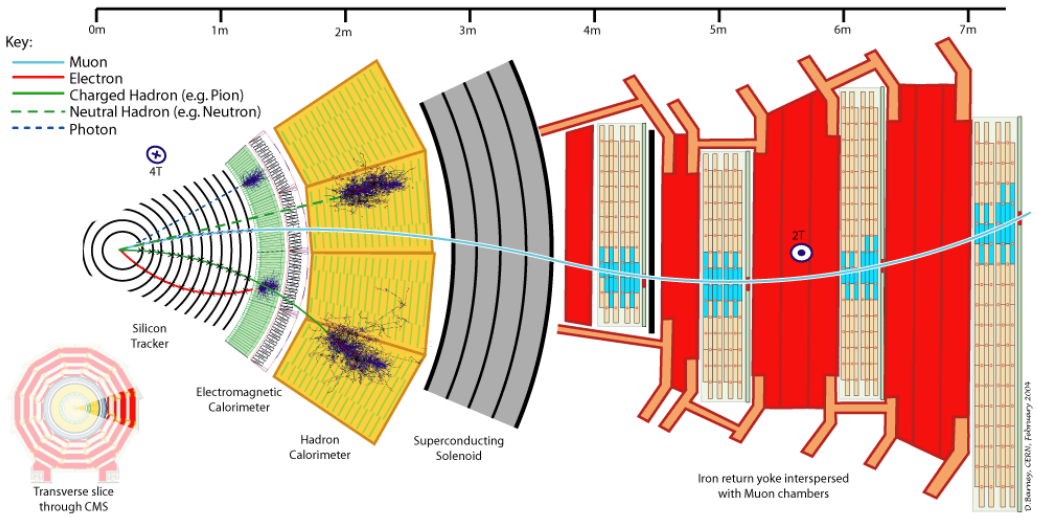

(b)

Figure 7.1: a. Drawing describing the structure of the CMS experiment b. A cross-section view of the CMS detector describing the path of an elementary particle [23]

CMS Silicon Tracker

The CMS Tracker (see Figure 7.2) is the largest semiconductor-based position sensing system existing nowadays. It is divided in the pixel detector and in the silicon strip part. The basis of this device is a huge matrix of p-n diode structures that are reverse biased to full depletion. When a charged particle crosses this junction electron-hole pairs are produced and a current signal is generated.

The pixel detector is placed very close to the beampipe in order to measure vertices accurately. Pixels are arranged in a 3-layer barrel with a 2-layer endcap per side. The silicon strips cover a quite larger volume ensuring that adequate bending will occur to the particles' track while inside the detector. The latter allows accurate momentum measurements of very high energy charged particles.

The Tracker strips can be divided in 4 regions :

TIB: Tracker Inner Barrel is the innermost part and contains 4 barrels.
TID: The inner part of the endcap system which consists of 3 inner endcap disks.
TOB: Tracker Outer Barrel is surrounding TIB and TID part and contains 6 barrels.
TEC: Tracker End Cap is the 9 outer disks of the endcap system.

The reason for dividing the Tracker in smaller regions is not simply topological but is based on the radiation dose of each. Silicon modules with low resistivity are more radiation tolerant, though this increases the nominal depletion voltage. Therefore the sensors that sit in the TIB/TID are low-resistivity sensors with a thickness of $320\mu m$ while in the outer regions sensors have a thickness of $500\mu m$. In order to limit the effect of radiation on the silicon sensors the Tracker should be operated in low temperatures, highlighting the need of climatic control inside its volume.

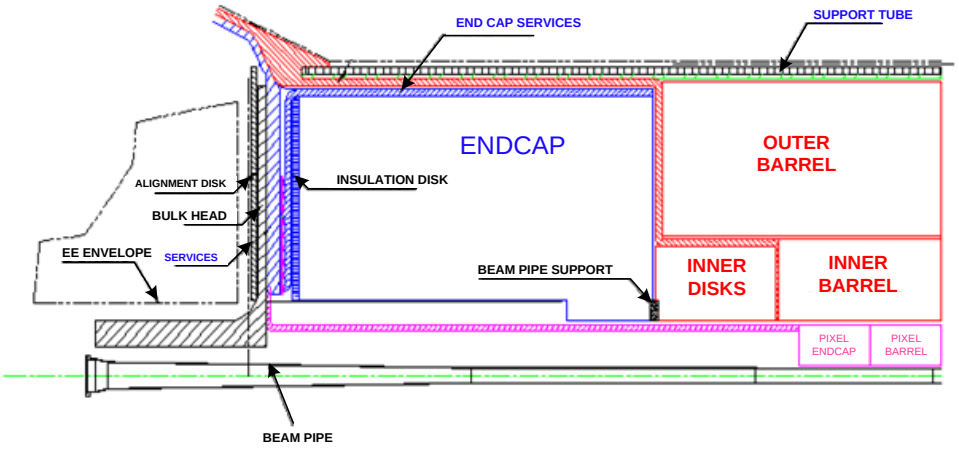

Figure 7.2: Symmetric quarter section of the CMS Silicon Tracker

7.1.2 Environmental measurements in the CMS Silicon Tracker

The conditions for safe Tracker operation have been known since the consolidation of the final design, in 2000. The accumulated expected dose over 10 years of operation for the Tracker is 10 Mrad (100 kGy) ionizing radiation and a fluence of $10^{14} n_{eq}/cm^2$ in terms of equivalent 1 MeV neutron flux. To limit the effect of radiation damage to the silicon and to keep the leakage current in low levels the Tracker must be operated at temperatures between -10^oC and -20^oC, achieving the full lifetime and performance of the initial plan. Accurate measurements of the temperature with high granularity are needed in order to ensure the successful control of the temperature throughout the detector volume.

A side benefit of this is the efficient monitoring of the temperature of the readout and control part of the Tracker as it is an integral part of the detector structure itself, thus being able to control the always risky overheating in the power-dense and restricted environment of the detector. To this end, thousands of temperature sensors are installed in the Tracker volume measuring the local temperature with a precision of 0.5^oC (this is a conservative error estimate on the measurement).

Given the fact that the Tracker has to be permanently cooled, the second environmental variable that is a point of major concern is relative humidity. This can be well explained in the case of temperature decreasing below the dew point of the Tracker environment, where water condenses on the detector modules and electronics causing destructive effects; going below the frost point even in the service parts would translate into ice forming around the cooling pipes severely reducing the heat transfer efficiency, or even inside the Tracker support structures with the possibility of mechanical damage. Humidity is removed from the Tracker by flushing with inert gas (N_2) during operations and with dry air during the maintenance periods via an extended network of pipes. The possible sources of humidity inside the Tracker are three; the external environment, the inert gas itself and the continuous outgassing of the different materials used in the Tracker that will free water molecules inside the Tracker volume.

The presence of some water is therefore unavoidable, and this will be a critical risk factor for the Tracker operations. The Tracker is protected from the cavern environment by a special "envelope". However, this envelope is not meant to, and cannot, ensure that the Tracker will be airtight and completely isolated from the external environment. Hence, there is an obvious need for well distributed network of humidity sensors to prevent any condensation of water vapour. Thus environmental conditions inside the Tracker are monitored through thermometers (NTC-thermistors, RTDs) and humidity sensors (HS-2000, HIH-3610, HMX-2000) and play a vital role in the security system. The measured values are used to calculate the critical point (dew/frost point) and detect the risk of condensation.

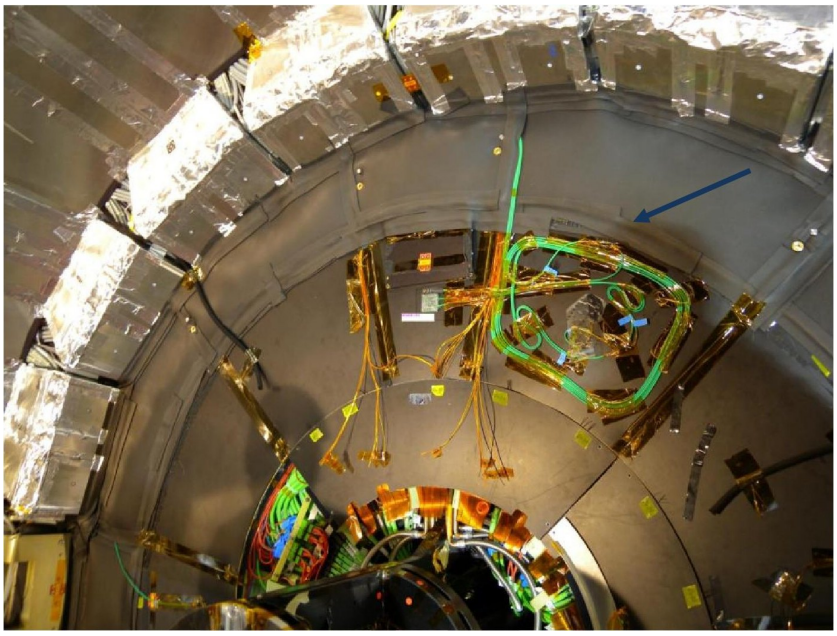

Figure 7.3: The Bulkhead of the CMS Silicon Tracker. The blue arrow points to the temperature & humidity sensor (PT-1000 and HMX-2000 respectively).

7.1.3 Chilled Mirror Hygrometer Suitability

Up to now the sensor that has been qualified for use inside the CMS Tracker was HMX-2000, a RH sensor that is produced by Hygrometrix. This device has undertaken several tests that proved its radiation tolerance, although some of its characteristics changed with radiation dose. The final result was that although the device was in need of re-calibration, it remained capable of measuring RH.

However HMX-2000 is at this point a deprecated sensor, forcing the research in new technologies of humidity measurement. A good humidity sensor for the CMS Tracker should combine the following properties :

1. Good response in the region of $-40^oC < T_{DP} < 10^oC$ or equivalently 0-20% RH at $T_{ambient} \sim -20^oC$.
2. Resistant to ionizing radiation up to 10 Mrad (100 KGy) and fluence of $10^{15} n_{eq}/cm^2$ (in 1 MeV equivalent neutron flux doses).
3. Not affected by strong magnetic field.
4. Small size (should not exceed cm scale).
5. No conditioning circuits "close" to the sensor.
6. Minimum cabling.
7. Minimal power consumption.

The Chilled Mirror Hygrometer is one of the main solutions as it combines accurate dew point measurements even at very low humidity (of the order of ppm) without the presence or the necessity of high complexity electronics near the sensor. However it lacks in the fields of size and power consumption. Radiation tolerance and strong magnetic field insensitivity are subject of further investigation that is

currently performed at CERN.

7.2 Environmental Test Chambers

Environmental test chambers rely on various types of sensors for control and monitoring. Most of the chambers require fast sensors that can drive the machine to a stable conditions. However when calibration and validation are required the usual scheme is that a sensor is used to control the chamber and a reference sensor (i.e. the Chilled Mirror Hygrometer) to verify the environmental conditions. Although the control sensor should be fast and stable, it is not always accurate and is in need of regular re-calibration.

Concerning the environmental chambers one should always keep in mind that water vapour concentration and prevailing pressure will equalize. Due to the fact that the actual dew point depends only on water vapour pressure, this variable will be uniform in the chamber's volume and only one measurement is representative of the conditions. On the other hand there will always be a gradient in temperature resulting in diverse RH conditions[2], which leads to the usage of several RH sensors in order to average the results. Taking in mind that the sensor constructed in this thesis is quite cheaper (1/10 of the CMH commercial value) than the usual CMH, the dew point measurements are advantageous to RH ones in both fields of price and accuracy.

7.3 Pharmaceuticals and Medicine

Because of the accuracy, the reliability and the NIST traceability, the chilled mirror hygrometers are usually the most practical solution for the pharmaceutical industry. Many medical applications, ranging from the manufacturing of medicines to the preparation of oxygen bottles, require that humidity levels during production are closely controlled.

In the field of medicine, over the last years, there has been an increasing interest in studying the humidity of the human body (e.g. water loss of human skin, nose and throat study). As it has been recently presented in [24], miniaturized CMH can have an important role in the accurate and traceable measurements that are needed.

[2]Remember that RH is a function of both temperature and saturation vapour pressure.

Chapter 8

Conclusions and Further Improvement

8.1 Conclusions

Humidity is the 2^{nd} most important variable in environmental monitoring and can be measured through a wide variety of sensors. However the most accurate, reliable and fundamental method, up to now, is the detection of the temperature at which a water condenses. This is the basis of the Chilled Mirror Hygrometer, the kind of sensor that this thesis is tampering with. The results prove that the final implementation has quite good characteristics

- Accuracy of $\pm 0.2^oC$
- Independency between sensor and readout system for distanced sensing.
- Wide range of operation $-25^oC < T_{DP} < 60^oC$
- Reproducibility
- Low-cost ($\sim$ 100\$) comparing to the expensive commercial Chilled Mirror Hygrometers ($\sim$ 2000\$)

The algorithm that is used is allowing the system to stabilize thermally before changing the target temperature. This procedure minimizes temperature overregulation and assures that the RTD thermometer, which is placed inside the metal mirror, is following the actual temperature of the surface.

8.2 Proposals for Further Development

The developed system works quite well on typical environmental conditions. In the case of operation in extreme conditions (i.e. $T_{DP} < -30^oC$, highly contaminated environments, radioactive environment) there should be a more detailed research on the materials that are used.

8.2.1 Radiation Hardness

The main incentive to CMH development was the development of a sensor that can be converted to a radiation hard device. The current implementation was not tested under radioactive conditions and it is believed not to survive in these

environments. However research is being carried out at CERN on the radiation hardness of the TEC module, the construction of a radiation hard reflective sensor -keeping the LED-Phototransistor pair in a radiation safe region and propagating the light through optical fibres can be one solution although it requires at least one optical fibre per sensor- or possible development of a totally new dew point detection concept.

8.2.2 Operating Range - Differential Reflector

The use of multi-stage TEC modules can improve the range of dew point temperatures that can be detected. The use of a differential reflective sensor can improve the system stability to environmental variations as both the reflectors will be affected and the inverse effects will get compensated in the final measurement.

8.2.3 Miniaturization

MEMS (Micro Electro-Mechanical Structures) is quite new technology that uses the standard industrial techniques of silicon treatment to construct miniaturized devices and sensors. The miniaturization of the sensor will definitely minimize the power consumption and probably improve its accuracy. There are great possibilities of enhancing sensor's response to harsh and radioactive environments.

There have been several attempts to construct MEMS dew point sensors [24] based on variations of the classic CMH. However a lot of research is still needed to prove that these techniques can produce reproducible and commercialized sensors.

Appendices

Appendix A

Hygrometry Terminology

A.1 Dalton's Law

In 1807 John Dalton, considered what would happen if a volume contained not just one type of gas, but a mixture of gases (suppose a, b and c). If we consider this question in terms of an ideal gas following the equations $PV = nRT$ or $P = \frac{nRT}{V}$ we can calculate the individual contribution of each gas to the total pressure in the volume as:

$$P_a = \frac{n_a RT}{V}, P_b = \frac{n_b RT}{V}, P_c = \frac{n_c RT}{V}$$

These pressures are known as "partial pressures" due to the fact that they contribute "partially" to the total pressure inside the volume. Dalton proposed that the total pressure should be the sum of all the partial pressures constituents. Hence

$$P_{total} = P_a + P_b + P_c \tag{A.1}$$

The Dalton's law can be expressed as follows:

> "The total pressure of a mixture of gases is equal to the sum of the pressures of the constituent gases, if each were individually to occupy that same volume, at that same temperature."

A.2 Water vapour Pressure

The water vapour pressure is that part of the total pressure that is contributed by the water vapour. It is expressed in units of pressure, i.e. in Pascals (Pa), millibars(mbar), millimeters of Hg (mm Hg) or psi (gage or absolute).

The saturation vapour pressure expresses the water vapour pressure when there is a dynamic equilibrium between the liquid/solid and the gaseous form of water. It is a function of temperature only, although it depends on the phase we are referring to liquid water or ice.

Saturation vapour pressure over liquid water (according to CIMO[25]) is described as

$$e_{water,s} = 6.112 \cdot e^{\frac{17.62T}{243.12+T}} \tag{A.2}$$

and ice :

$$e_{ice,s} = 6.112 \cdot e^{\frac{22.46T}{272.62+T}} \tag{A.3}$$

These functions help us redefine the actual water vapour pressure as

$$e_a = e_w - p_{sta}(T - T_w)0.00066\,[1 + 0.00115 \cdot T_w] \tag{A.4}$$

,where e_w is the saturation vapour pressure for Wet Bulb Temperature (T_w), p_{sta} is the station pressure in $milibar$ and usually equals $1atm \approx 10^5 mbar$. The factor $(1 + 0.00115 \cdot T_w \simeq 1)$ for temperatures between -100^oC and $+100^oC$.

A.3 Humidity Parameters

A.3.1 Wet Bulb Temperature (T_w)

The wet-bulb temperature is a type of temperature measurement that reflects the physical properties of a system with a mixture of a gas and a vapour, usually air and water vapour. Wet bulb temperature is the lowest temperature that can be reached by the evaporation of water only. It is the temperature you feel when your skin is wet and is exposed to moving air. Unlike dry bulb temperature, wet bulb temperature is an indication of the amount of moisture in the air.

The thermodynamic wet-bulb temperature is the minimum temperature which may be achieved by purely evaporative cooling of a water-wetted (or ice-covered), ventilated surface.

For a given parcel air at a known pressure and dry-bulb temperature, the thermodynamic wet-bulb temperature corresponds to unique values of relative humidity, dew point temperature, and other properties. The relationships between these values are illustrated in a psychrometric chart.

A.3.2 Dew Point

The dew point is the temperature to which a given parcel of air must be cooled, at constant barometric pressure, for water vapour to condense into water. The condensed water is called dew. The dew point is a saturation point where

$$e = e_{water,s}$$

The dew point is associated with relative humidity (see below). A high relative humidity indicates that the dew point is closer to the current air temperature. Relative humidity of 100% indicates the dew point is equal to the current temperature and the air is maximally saturated with water. When the dew point remains constant and temperature increases, relative humidity will decrease.

At a given barometric pressure, independent of temperature, the dew point indicates the mole fraction of water vapour in the air, and therefore determines the specific humidity of the air. The dew point is an important statistic for general aviation pilots, as it is used to calculate the likelihood of carburettor icing and fog, and estimate the height of the cloud base.

The dew point is calculated by the following equation :

$$T_d = 243.5 \frac{\ln(e/6.112)}{17.67 - \ln(e/6.112)} \tag{A.5}$$

A.3.3 Frost Point

The dew point is the temperature to which a given parcel of air must be cooled, at constant barometric pressure, for water vapour to condense into ice. The condensed ice is called frost. The dew point is a saturation point where

$$e = e_{ice,s}$$

A.3.4 Relative Humidity

Relative Humidity (RH) is the percentage of the actual partial vapour pressure to the saturation vapour pressure of the gas, at the prevailing ambient temperature. Therefore for actual vapour pressure e and saturation vapour pressure e_s, RH is :

$$\%RH = \frac{e}{e_s} \cdot 100\% \tag{A.6}$$

A.3.5 Absolute Humidity

Absolute Humidity (AH) is defined as water vapour density and it expresses the mass of water vapour per unit of volume of dry air. It can be formulated as follows :

$$AH = \frac{m_w}{V_a} \tag{A.7}$$

where m_w is the water vapour mass and V_a is the reference volume.

From its definition it is deducted that for temperatures above the dew-point it is independent of temperature. Due to the latter, this variable is used when the mass (or the molecules) of vapour inside as volume is needed.

A.3.6 Psychrometric Chart

A psychrometric chart is a graph of the thermodynamic properties of moist air at a constant pressure (often equated to an elevation relative to sea level). The ASHRAE-style psychrometric chart, shown here, was pioneered by Willis Carrier in 1904. It depicts these properties and is thus a graphical equation of state. The properties are:

- Dry-Bulb Temperature T_{DB} which is actually the temperature of the air.
- Wet-Bulb Temperature as described before.

- Dew Point Temperature
- Relative Humidity
- Humidity Ratio
- Specific Enthalpy
- Specific Volume

The versatility of the psychrometric chart lies in the fact that by knowing three independent properties of some moist air (one of which is the pressure), the other properties can be determined.

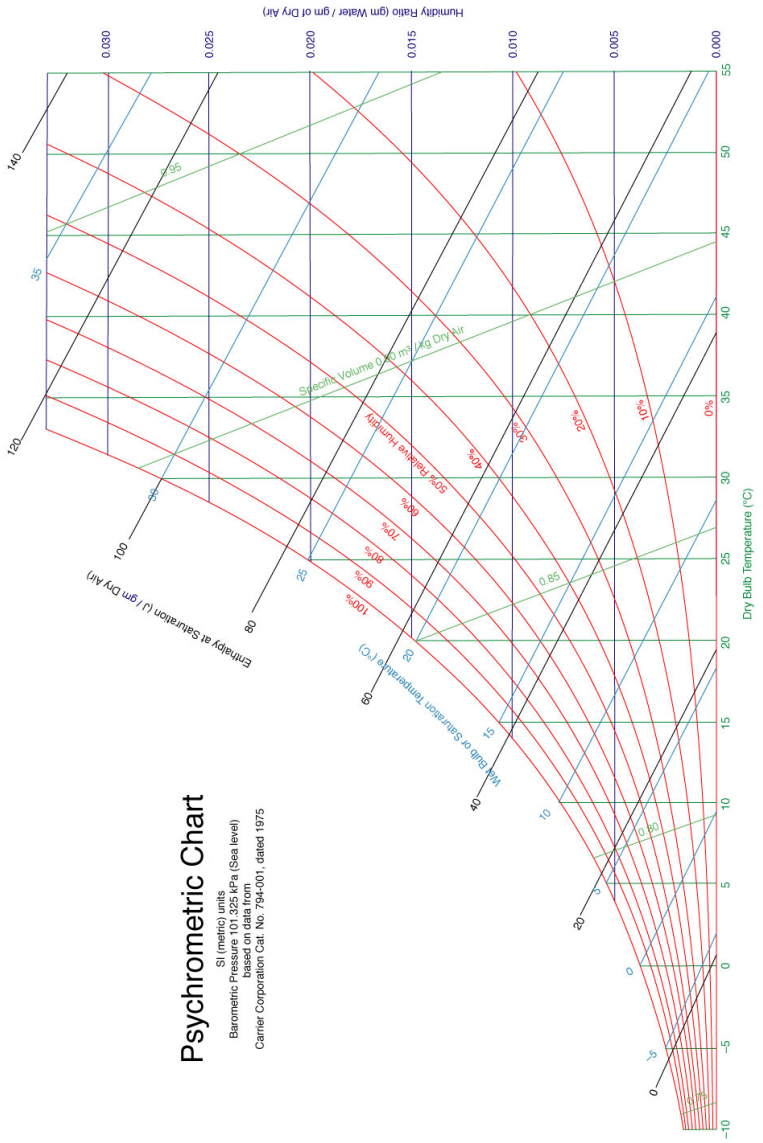

Figure A.1: A psychrometric chart referring to sea-level and using SI units

Appendix B

The Thermoelectric Effect and the Thermoelectrical Modules

The term "Thermoelectric Effect" refers to a class of phenomena in which a temperature difference creates an electrical potential or, vice-versa, an electrical potential creates a temperature difference.

B.1 The Seebeck Effect

Definition : A temperature difference between two points in a conductor or semiconductor results in a voltage difference between these two points. Stated differently, a temperature gradient in a conductor or a semiconductor gives rise to a built-in electric field. This phenomenon is called Seebeck effect or Thermoelectric effect. The Seebeck coefficient is a measure of the magnitude of this effect. The thermoelectric voltage developed per unit temperature difference in a conductor is called the Seebeck coefficient. Only the net Seebeck voltage difference between different metals can be measured. The principle of the thermocouple is based on the Seebeck effect.

B.1.1 Macroscopic Description

The Seebeck effect describes the macroscopic laws of a combination of two microscopic effects; charge carrier diffusion and phonon drag which will be both explained below. In order to describe the Seebeck effect macroscopically we introduce a special coefficient which is defined as the potential difference developed per unit temperature difference.

$$S = \frac{dV}{dT} \tag{B.1}$$

By convention, the sign of S represents the potential of the cold side with respect to the hot side. If carriers diffuse from hot to cold end, then the cold side is negative with respect to the hot side and the Seebeck coefficient is negative. In a p-type semiconductor, on the other hand, holes would diffuse from the hot to the cold end.

The cold side would be positive with respect to the hot side which would make S a positive quantity. $S = S(T)$ is a material property that depends on temperature and it is tabulated for many materials as a function of temperature. Given the Seebeck coefficient S(T) for a material, the voltage difference between two points with temperatures T_A and T_B, is given by :

$$\Delta V = \int_{T_A}^{T_B} S(T)\, dT$$

A typical circuit that describes the Seebeck effect is presented in B.1. The accompanying equation that calculates the thermoelectrical EMF (Electro Motive Force) is :

$$V = \int_{T_1}^{T_2} \left(S_{\mathrm{B}}(T) - S_{\mathrm{A}}(T)\right)\, dT$$

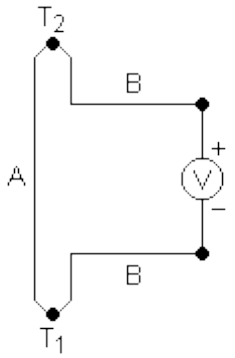

Figure B.1: Seebeck Effect Circuit

B.1.2 Microscopic Description

The previous section was intended to illustrate the macroscopic model that describes the Seebeck effect. However it is helpful to understand the mechanisms underlying in order to explain the differences that arise in the materials response.

Charge Carriers Diffusion

Charge carriers in the materials (electrons in metals, electrons and holes in semiconductors, ions in ionic conductors) will diffuse when one end of a conductor is at a different temperature than the other. Hot carriers diffuse from the hot end to the cold end resulting in the formation of a potential difference between the bare ions on the hot side and the carriers in the cold side.

The electrical field, that is formed inside the material, forces the cold carriers to move towards the hot side, resulting in a continuous loop. In a system where both ends are kept in constant temperature, the diffusion inside the material will

reach a thermodynamic equilibrium. Due to the fact that the hot and cold carriers have different energy and thus different mobility, a voltage across the two sides of the material is produced.

The subject of the mobility is a key to explain the different voltage polarity in various materials or in other words the different sign of the Seebeck coefficient. When the carriers are electrons S is expected to be negative, whereas when the carrier is holes the coefficient is expected to be positive. That describes well the response of the semiconductor material, nonetheless is inaccurate with the metals. In order to explain the response of the metals we should overpass the "free electron theory of metals" and look on the interactions of the conduction electrons with the metal ions and the lattice vibrations, resulting on the scattering of electrons.

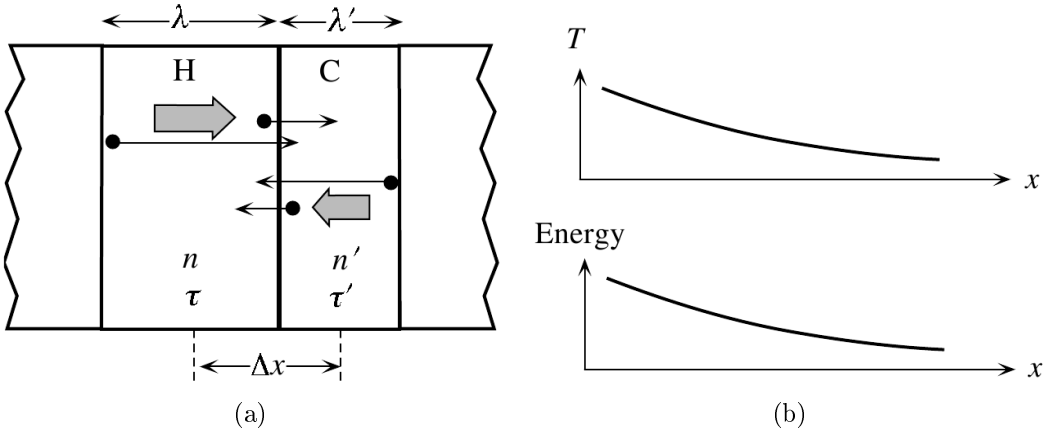

Figure B.2: Two neighboring regions. H is hot and C is cold

Consider two neighboring regions H (hot) and C (cold) with widths corresponding to the Mean Free Paths (MFP) λ and λ' in H and C. Half the electrons in H would be moving towards $+x$ direction and the other half towards $-x$. Half of the electrons in H therefore cross into C, and half in C cross into H. The electron concentration is n and n' and the mean scattering time is τ and τ' for H and C respectively. The total electron flux Γ is

$$\Gamma = \Gamma_{HC} - \Gamma_{CH} = \frac{n\lambda}{2\tau} - \frac{n\lambda'}{2\tau'} \tag{B.2}$$

We can write $n' \approx n + (dn/dx)\Delta x, \lambda' \approx \lambda + (d\lambda/dx)\Delta x, \tau' \approx \tau + (d\tau/dx)\Delta x$ and assuming $\Delta x = (\lambda + \lambda')/2 \approx \lambda$ then Eq. B.2 is

$$\Gamma \approx -\frac{\lambda^2}{2\tau}\left(\frac{\partial n}{\partial x}\right) - \frac{n\lambda}{2\tau}\left(\frac{\partial \lambda}{\partial x}\right) + \frac{n\lambda^2}{2\tau^2}\left(\frac{\partial \tau}{\partial x}\right) \tag{B.3}$$

It is clear that the net electron migration is determined by n, λ and τ. Usually n and τ increase with temperature. What is greatly affected is λ because higher T means higher energy and bigger oscillations of the net atoms and hence higher possibility of electrons-net interactions which affect the expected free path. This is the reason why we observe some metals with negative S and others with positive.

Phonon Drag

Phonon drag is an increase in the effective mass of conduction electrons or valence holes due to interactions with the crystal lattice in which the electron moves. As an electron moves through atoms in the lattice its charge distorts or polarizes the nearby lattice formations. This effect leads to a decrease in the electronic (or hole, as may be the case) mobility, which results in a decreased conductivity. The magnitude of this effect is typically appreciable only at low temperatures (<200 K).

Phonons are not always in local thermal equilibrium; they move against the thermal gradient. They lose momentum both by electron (or other carriers) interaction and by crystal displacements. If the phonon-electron interaction is predominant, the phonons will tend to push the electrons to one end of the material, losing momentum in the process. This contributes to the thermoelectric field that is already present and become most important in the temperature region where phonon-electron scattering is predominant.

$$T \approx \frac{1}{5}\theta_{\mathrm{D}}$$

where θ_D is the Debye temperature.

At lower temperatures there are fewer phonons available for drag, and at higher temperatures they tend to lose momentum in phonon-phonon scattering instead of phonon-electron scattering.

B.2 The Peltier Effect

The Peltier effect is the reverse Seebeck effect and describes the transfer of heat across a junction when a current is present. When a current I is made to flow through the circuit, heat is produced in the one side and absorbed in the other. In order to quantitate this effect we can define the Peltier coefficient of a material A (Π_A) as a measure of the energy carried per unit charge. It is important to emphasize that the Peltier effect is measurable only on the junction of two different materials. Since charge current must be continuous across a junction, the associated heat flow will develop a discontinuity if Π_A and Π_B are different. This causes a non-zero divergence at the junction where heat must accumulate or deplete, depending on the sign of the current.

The heat power absorbed by the cold junction of materials A and B is

$$P_Q = \Pi_{AB} I = (\Pi_B - \Pi_A)\, I \tag{B.4}$$

,where Π_{AB} is the Peltier coefficient of the entire system.

The Peltier effect between two metals is quite small , due to the fact that the conduction electrons in a metal have energies very close to the Fermi energy, E_F, which is the highest energy level occupied by an the electrons, at 0K. On the other hand semiconductors tend to have larger Peltier coefficients and therefore better efficiency in energy transfer. Figure B.3 shows an arrangement utilizing p-

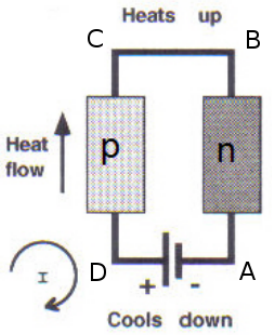

Figure B.3: Two neighboring regions. H is hot and C is cold

and n- doped semiconductors that shows how heat can be extracted from one side and transferred onto the other side. The electrons are excited to higher energy at point A of the n-semiconductor, absorbing energy. Then they move towards lower energy regions, depositing heat at B. The same logic applies for the holes of the p-semiconductor which jump to a higher energy state at point D and deposit heat at C.

The most commonly used semiconductors for Peltier effect devices are Bi_2Te_3 and $PbTe$

B.3 Thermoelectrical Modules

The Thermoelectrical Cooling (TEC) modules are devices that are based on the Peltier effect in order to cool down or heat up a surface. They can be described as solid-state active heat pump which transfers heat from one side of the device to the other side against the temperature gradient (from cold to hot), with consumption of electrical energy. Other commercial names are "Peltier device", "Peltier diode", "cooling diode", "Peltier heat pump" and "solid state refrigerator".

An assortment of n- and p-doped semiconductors in series (see Fig. B.4a) can increase the temperature difference that is achieved between the two sides of the module (ΔT). Moreover the placement of TEC modules in a stack, can be even more effective. Achieving $\Delta T \sim 110^oC$ is rational and well performed in a wide range of applications.

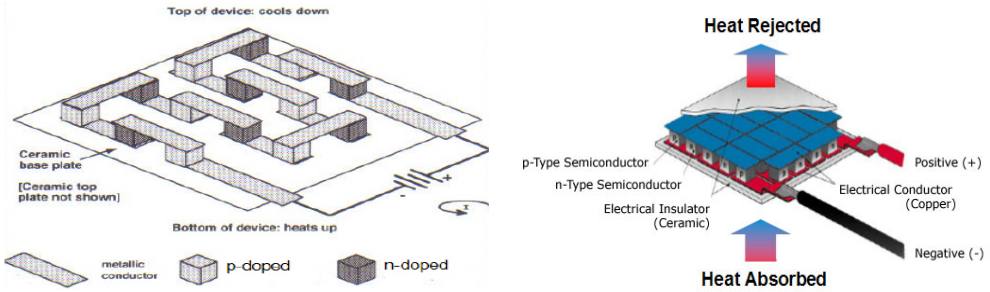

(a) (b)

Figure B.4: Thermoelectric Cooler a.Principle of construction b. Commercial TEC implementation

Appendix C

Microcontroller Software

C.1 Main Programs

For clarity reasons it is necessary to point out that constants written in capital letters (e.g. WATER_LAYER_ADC, INIT_COOLING_DC, CLEAN, WET etc.) are describing circuit/system variables that are defined in the file define.h and are not changing throughout the program execution. These definitions are common for all the files listed below.

C.1.1 DPsensor.c

```
#include <stdio.h>
#include <math.h>

#include <util/delay.h>

#include <avr/interrupt.h>
#include <avr/io.h>

#include "pwm.h"
#include "usart.h"
#include "adc.h"
#include "readout.h"
#include "define.h"
#include "helpingFunctions.h"
#include "scp.h"
#include "rccp.h"


// ================================
// GLOBAL VARIABLES
// ================================
// The current Dew Point
float G_current_dp = 0;
// The current Evaporation Point
float G_current_ep = 0;
// The current difference of Dewpoint - Evaporation point.
float G_current_dp_ep = 0;
// The current Duty Cycle.
int G_pwm_dc_set = INIT_COOLING_DC;
// The Global counter
```

```
int32_t G_counter = 0;
//Counter of the DP detections. Increased in the end of the cooling loop.
int32_t G_DP_counter;
// Operation mode definition. 0=initialize, 1=RCCPcooling, 2=RCCPheating,
// 3=SCPcooling, 4=SCPheating
int G_mode = 0;
//Counter of the time that last EP detection lasted.
int G_last_detection_time_H = 30;
//Counter of the time that last DP detection lasted.
int G_last_detection_time_C = 30;


// ================================
// MAIN PROGRAM
// ================================
int main()
{
        // ******************
        // Starting
        // ******************

        // Initialize devices
        usart_init(12);
        pwm_init();
        adc_init_sc();
        // Setting sleep mode to "ADC Noise Reduction"
        MCUCR |= (1 << SM0);
        sei();

        //Set PORTC2 as ouput
        DDRC  |= 0b00000100;

        // Initialize constants
        char job;
        int wet_threshold =0;
        int free_reflex = 0;

        while(1) {
                usart_puts("Enter m for start measuring \n");
                job = usart_receive();

                // ************************
                // Initialization
                // ************************
                //Measure the reflectivity of a clean mirror
                if (job == 'm'){
                        free_reflex = free_reflex_avg(50);
                        wet_threshold = free_reflex - WATER_LAYER_ADC *
                                free_reflex;

                        usart_puts(" *** Free mirror ADC are : ");
                        usart_putint(free_reflex);
                        usart_put(0x0D);
                        usart_puts(" *** Wet Threshold is : ");
                        usart_putint(wet_threshold);
                        usart_put(0x0D);
                        _delay_ms(100);
                }
                G_mode = 1;

                while(job == 'm'){
                // ***********************************************
                // The main operating loop
                // ***********************************************
                // 1. Start with RCCP cooling (G_mode==1)
```

```
                // 2. DP found => Go to SCP heating (G_mode==4)
                // 3. EP found => Go to SCP cooling (G_mode==3)
                // 4. If time long => Go to RCCP cooling
                // 5. DP found => Go to SCP heating
                // 6. If time long => Go to RCCP heating (G_mode==2)
                //
                // G_mode == 0 => ReInitialize
                // ***********************************************
                        switch (G_mode)
                        {
                                case 0 :
                                        break;
                                case 1 :
                                        RCCPcooling_proc(wet_threshold,
                                                &G_counter,
                                                &G_pwm_dc_set,
                                                &G_current_ep,
                                                &G_current_dp,
                                                &G_current_dp_ep,
                                                &G_DP_counter,
                                                &G_mode);
                                         break;
                                case 2 :
                                        RCCPheating_proc(wet_threshold,
                                                &G_counter,
                                                &G_pwm_dc_set,
                                                &G_current_ep,
                                                &G_current_dp,
                                                &G_current_dp_ep,
                                                &G_DP_counter,
                                                &G_mode);
                                        break;
                                case 3 :
                                        SCPcooling_proc(wet_threshold,
                                                &G_counter,
                                                &G_pwm_dc_set,
                                                &G_current_ep,
                                                &G_current_dp,
                                                &G_current_dp_ep,
                                                &G_DP_counter,
                                                &G_mode,
                                                &G_last_detection_time_H);
                                        break;
                                case 4 :
                                        SCPheating_proc(wet_threshold,
                                                &G_counter,
                                                &G_pwm_dc_set,
                                                &G_current_ep,
                                                &G_current_dp,
                                                &G_current_dp_ep,
                                                &G_DP_counter,
                                                &G_mode,
                                                &G_last_detection_time_C);
                                        break;
                        }

                        //Exit loop and reinitilize or NOT????
                        _delay_ms(100);
                        if (UCSRA & (1<<RXC)){
                                job = usart_receive();
                                break;
                        }
                }
        }
}
```

C.1.2 scp.c

```
#include <stdio.h>
#include <stdint.h>

#include <avr/io.h>
#include <avr/interrupt.h>

#include <util/delay.h>

#include "pwm.h"
#include "define.h"
#include "scp.h"
#include "usart.h"
#include "readout.h"
#include "helpingFunctions.h"

// ========================================
// THE SCP HEATING PROCEDURE
// ========================================
int SCPheating_proc(int wet_thresh, int32_t * G_counter, int * G_pwm_dc_set,
                float * G_current_ep, float * G_current_dp, float *
                    G_current_dp_ep,
                int32_t * G_DP_counter, int *G_mode, int *G_last_det_time){
        float temp = 0.0;
        float temp_arch[TEMP_ARCH_NO] = {0.0};
        float temp_avg = 0;
        float temp_deviation = 0;

        int   state = WET;
        int   reflex_adc;
        int   reflex_avg=0;
        int   duty_cycle = *G_pwm_dc_set - SCP_CP_DETECTION_STEP;
        char output_string[60];
        int   counter = 1;
        int   SCPHeatCounter = 1;
        int32_t  StartCounter = * G_counter;

        PORTC &= (0 << PC2);              //Keep H-Bridge in COOL mode

        //Start heating
        pwm_dc_set(duty_cycle);

        while ( (state == WET) && (*G_mode == 4) ){
                _delay_ms(10);
                temp = temp_read();
                reflex_adc = reflector_read();
                state = mirror_state(reflex_adc, wet_thresh);

                //print results
                sprintf(output_string, "%ld\t %d\t %d\t %d\t %4.2f\t "
                        "%4.2f\t %4d\t %4.2f\t %ld\t %4.2f\n",*G_counter,
                        *G_mode, state, reflex_avg, reflex_adc, temp,
                        *G_current_dp, duty_cycle, temp_deviation,
                        *G_DP_counter, *G_current_dp_ep);
                usart_puts(output_string);

                //Temperature calculations
                tempStats(&counter, temp, &temp_avg, &temp_deviation,
                    temp_arch, SCP_TEMP_SAMPLES_NUMBER);

                //Decrease the Duty Cycle
                if ( (temp_deviation < SCP_DEVIATION_LIMIT ) && (duty_cycle
                    < DC_MAX) && (counter > SCP_TEMP_SAMPLES_NUMBER) ){
                        duty_cycle -= SCP_DC_HEATING_STEP;
```

```
                pwm_dc_set(duty_cycle);
                counter = 1;
            }

            //Mode checking procedure
            if ( (SCPHeatCounter > *G_last_det_time * SCP_NO_DET_FACTOR
                ) && SCPHeatCounter > SCP_NO_DET_LIM ){
                *G_counter = *G_counter + 1;
                *G_pwm_dc_set = duty_cycle;
                *G_mode = 2;

                return 0;
            }


            if (UCSRA & (1<<RXC)){
                break;
            }

            *G_counter = *G_counter + 1;
            counter ++;
            SCPHeatCounter++;
        }

        *G_last_det_time = *G_counter - StartCounter;
        *G_DP_counter = *G_DP_counter + 1;
        *G_current_ep = temp;
        *G_current_dp_ep = *G_current_dp - *G_current_ep;
        *G_pwm_dc_set = duty_cycle + SCP_CP_DETECTION_STEP;
        *G_mode = 3;

        return 0;
}


// ========================================
// THE SCP COOLING PROCEDURE
// ========================================
int SCPcooling_proc(int wet_thresh, int32_t * G_counter, int * G_pwm_dc_set,
            float * G_current_ep, float * G_current_dp, float *
                G_current_dp_ep,
            int32_t * G_DP_counter, int *G_mode, int * G_last_det_time){
        float temp = 0.0;
        float temp_arch[TEMP_ARCH_NO] = {0.0};
        float temp_avg = 0;
        float temp_deviation = 0;

            int  state = FREE;
        int  reflex_adc;
        int  reflex_avg=0;
        int  duty_cycle = *G_pwm_dc_set;
        char output_string[60];
        int  counter = 1;
        int  SCPCoolCounter = 1;
        int32_t  StartCounter = * G_counter;

        PORTC &= (0 << PC2);            //Keep H-Bridge in COOL mode

        //Start cooling
        pwm_dc_set(duty_cycle);

        while ( (state == FREE) && (*G_mode == 3) ){
            _delay_ms(10);
            temp = temp_read();
            reflex_adc = reflector_read();
```

```
                state = mirror_state(reflex_adc, wet_thresh);

                //print results
                sprintf(output_string, "%ld\t %d\t %d\t %d\t %d\t %4.2f\t"
                        "\t %4.2f\t %4d\t %4.2f\t %ld\t %4.2f\n",*G_counter,
                        *G_mode, state, reflex_avg, reflex_adc, temp,
                        *G_current_ep, duty_cycle, temp_deviation,
                        *G_DP_counter, *G_current_dp_ep);
                usart_puts(output_string);

                //Temperature calculations
                tempStats(&counter, temp, &temp_avg, &temp_deviation,
                    temp_arch, SCP_TEMP_SAMPLES_NUMBER);


                //Increase the Duty Cycle
                if ( (temp_deviation < SCP_DEVIATION_LIMIT ) && (duty_cycle
                    < DC_MAX) && (counter > SCP_TEMP_SAMPLES_NUMBER) ){
                        duty_cycle += SCP_DC_COOLING_STEP;
                        pwm_dc_set(duty_cycle);

                        counter = 1;
                }

                //Mode checking procedure
                if ( (SCPCoolCounter > *G_last_det_time * SCP_NO_DET_FACTOR
                    ) && SCPCoolCounter > SCP_NO_DET_LIM){
                        *G_counter = *G_counter + 1;
                        *G_pwm_dc_set = duty_cycle;
                        *G_mode = 1;

                        return 0;
                }


                if (UCSRA & (1<<RXC)){
                        break;
                }

                *G_counter = *G_counter + 1;
                counter ++;
                SCPCoolCounter++;
        }
        *G_last_det_time = *G_counter - StartCounter;
        *G_current_dp = temp;
        *G_pwm_dc_set = duty_cycle;
        *G_mode = 4;

        return 0;
}
```

C.1.3 rccp.c

```
#include <stdio.h>

#include <util/delay.h>

#include <avr/io.h>

#include "rccp.h"
#include "pwm.h"
#include "readout.h"
#include "usart.h"
#include "helpingFunctions.h"
```

```
// ==========================================
// THE RCCP HEATING PROCEDURE
// ==========================================
int RCCPheating_proc(int wet_thresh, int32_t * G_counter, int * G_pwm_dc_set
    ,
             float * G_current_ep, float * G_current_dp, float *
                 G_current_dp_ep,
             int32_t * G_DP_counter, int * G_mode){
        float temp = 0.0;
        float temp_arch[RCCP_TEMP_SAMPLES_NUMBER] = {0.0};
        float temp_avg = 0;
        float temp_deviation = 0;

        int state = WET;
        int reflex_adc;
        int reflex_avg=0;
        int duty_cycle = *G_pwm_dc_set - RCCP_CP_DETECTION_STEP;
        char output_string[60];
        int counter = 1;

        PORTC &= (0 << PC2);              //Keep H-Bridge in COOL mode

        //Start heating
        pwm_dc_set(duty_cycle);

        while ( (state == WET) && (*G_mode == 2) ){
                _delay_ms(10);
                temp = temp_read();
                reflex_adc = reflector_read();
                state = mirror_state(reflex_adc, wet_thresh);

                //print results
                sprintf(output_string, "%ld\t %d\t %d\t %d\t %4.2f\t"
                        "\t %4.2f\t %4d\t %4.2f\t %ld\t %4.2f\n",*G_counter,
                        *G_mode, state, reflex_avg, reflex_adc, temp,
                        *G_current_dp, duty_cycle, temp_deviation,
                        *G_DP_counter, *G_current_dp_ep);
                usart_puts(output_string);

                //Temperature calculations
                tempStats(&counter, temp, &temp_avg, &temp_deviation,
                        temp_arch, RCCP_TEMP_SAMPLES_NUMBER);

                //Decrease the Duty Cycle
                if ( (temp_deviation < RCCP_DEVIATION_LIMIT ) &&
                        (duty_cycle < DC_MAX) &&
                        (counter > RCCP_TEMP_SAMPLES_NUMBER) ){
                        duty_cycle -= RCCP_DC_HEATING_STEP;
                        pwm_dc_set(duty_cycle);
                        counter = 1;
                }

                if (UCSRA & (1<<RXC)){
                        break;
                }
                *G_counter = *G_counter+1;
                counter ++;
        }

        *G_DP_counter = *G_DP_counter + 1;
        *G_current_ep = temp;
        *G_current_dp_ep = *G_current_dp - *G_current_ep;
        *G_pwm_dc_set = duty_cycle + RCCP_CP_DETECTION_STEP;
        *G_mode = 3;
```

```
        return 0;
}


// ========================================
// THE RCCP COOLING PROCEDURE
// ========================================
int RCCPcooling_proc(int wet_thresh, int32_t * G_counter, int * G_pwm_dc_set
    ,
                float * G_current_ep, float * G_current_dp, float *
                    G_current_dp_ep,
                int32_t * G_DP_counter, int * G_mode){
        float temp = 0.0;
        float temp_arch[RCCP_TEMP_SAMPLES_NUMBER] = {0.0};
        float temp_avg = 0;
        float temp_deviation = 0;

        int state = FREE;
        int reflex_adc;
        int reflex_avg=0;
        int duty_cycle = *G_pwm_dc_set;
        char output_string[60];
        int counter = 1;

        PORTC &= (0 << PC2);              //Keep H-Bridge in COOL mode

        //Start cooling
        pwm_dc_set(duty_cycle);

        while ( (state == FREE) && (*G_mode == 1) ){
                _delay_ms(10);
                temp = temp_read();
                reflex_adc = reflector_read();
                //reflex_avg = reflex_average(reflex_adc);
                state = mirror_state(reflex_adc, wet_thresh);

                //print results
                sprintf(output_string, "%ld\t %d\t %d\t %d\t %4.2f\t"
                        "\t %4.2f\t %4d\t %4.2f\t %ld\t %4.2f\n",*G_counter,
                        *G_mode, state, reflex_avg, reflex_adc, temp,
                        *G_current_ep, duty_cycle, temp_deviation,
                        *G_DP_counter, *G_current_dp_ep);
                usart_puts(output_string);

                //Temperature calculations
                tempStats(&counter, temp, &temp_avg, &temp_deviation,
                         temp_arch, RCCP_TEMP_SAMPLES_NUMBER);


                //Increase the Duty Cycle
                if ( (temp_deviation < RCCP_DEVIATION_LIMIT ) &&
                        (duty_cycle < DC_MAX) &&
                        (counter > RCCP_TEMP_SAMPLES_NUMBER) ){
                        duty_cycle += RCCP_DC_COOLING_STEP;
                        pwm_dc_set(duty_cycle);
                        counter = 1;
                }


                if (UCSRA & (1<<RXC)){
                        break;
                }
                *G_counter = *G_counter+1;
                counter ++;
```

```
        }

        *G_current_dp = temp;
        *G_pwm_dc_set = duty_cycle;
        *G_mode = 4;

        return 0;
}
```

C.1.4 helpingFunctions.c

```
#include <stdio.h>
#include <math.h>

#include <util/delay.h>
#include <avr/io.h>

#include "define.h"
#include "usart.h"
#include "pwm.h"
#include "readout.h"

//Function that calculates the Temperature average value and deviation
void tempStats (int * Counter, float Temp, float * TempAvg,
                float * TempDeviation, float TempArch[], int TempArchNumber)
                     {

        //Initialize the temperature archiving
        if (*Counter == 1){
                for(int i=0; i<TempArchNumber; i++){
                        TempArch[i] = Temp;
                }
        }

        //Calculate the average temperature over the last TEMP_ARCH_NO
            temperatures
        for(int i=0; i<TempArchNumber-1; i++){
                *TempAvg += TempArch[i];
        }
        *TempAvg = *TempAvg / TempArchNumber;


        //Store the last TEMP_ARCH_NO temperature measurements
        for(int i=0; i<TempArchNumber-1; i++){
                TempArch[i] = TempArch[i+1];
        }
        TempArch[TempArchNumber-1] = Temp;


        //Calculate the standard deviation of temperature over the last
            TEMP_ARCH_NO temperatures
        *TempDeviation = 0.0;
        for(int i=0; i<TempArchNumber-1; i++){
                *TempDeviation += ( TempArch[i] - *TempAvg ) * ( TempArch[i]
                     - *TempAvg );
        }
        *TempDeviation = sqrt ( *TempDeviation / TempArchNumber );
}


//Function to define the clean mirror reflection
int free_reflex_avg(int n){
        int32_t reflex_avg = 0;
        int reflex_adc = 0;
```

```
        char output_string[60];

        float temp = 0.0;
        float temp_arch[INIT_TEMP_SAMPLES_NUMBER] = {0.0};
        float temp_avg = 0.0;
        float temp_deviation = 0.0;

        int counter = 1;
        int duty_cycle = 20;

        PORTC |= (1 << PC2);            //Turn the H-Bridge to heating mode

        pwm_dc_set(duty_cycle);         //Start Heating
        while  (temp < 40.0) {
                _delay_ms(20);
                temp = temp_read();
                sprintf(output_string, "%d\t %d\t %4.2f\n", counter,
                    duty_cycle, temp);
                usart_puts(output_string);

                //Temperature calculations
                tempStats(&counter, temp, &temp_avg, &temp_deviation,
                    temp_arch, INIT_TEMP_SAMPLES_NUMBER);

                //Increase the Duty Cycle
                if ( (temp_deviation < INIT_DEVIATION_LIMIT ) && (duty_cycle
                     < DC_MAX) && (counter > INIT_TEMP_SAMPLES_NUMBER) ){
                        duty_cycle += INIT_DC_HEATING_STEP;
                        pwm_dc_set(duty_cycle);
                        counter = 1;
                }

                counter ++;
                if (UCSRA & (1<<RXC)){
                        break;
                }
        }

        for (int i=0; i<n; i++){                //Measure average reflection
             on supposedly clean mirror
                _delay_ms(100);
                temp = temp_read();
                reflex_adc = reflector_read();
                reflex_avg += reflex_adc;

                sprintf(output_string, "%d\t %4.2f\t \n", reflex_adc, temp);
                usart_puts(output_string);
        }
        reflex_avg = reflex_avg / n;

        return reflex_avg;                              //Return average
}


//Function to define if the mirror is WET or FREE
int mirror_state(int reflex, int wet_ref) {
        int state;

        if (reflex > wet_ref)
                state = FREE;
        else
                state = WET;

        return state;
}
```

C.2 readout.h

```
#include <util/delay.h>

#include "readout.h"
#include "adc.h"
#include "define.h"
#include "usart.h"


//=============================
//       READOUT CIRCUIT FUNCTIONS
//=============================

//function to read the temperature through the ADC
float temp_read(){
        int adc_value = adc_read(PT_CHANNEL);
        //int adc_value = adc_read();
        double temp=0.0;
        float Rpt=0.0;

        if (adc_value > 0){
                Rpt = ( adc_value * mV_PER_COUNT_2_56V_12BIT + VCC) * R1 /
                        ((TEMP_AMP_GAIN - 1) * VCC - adc_value *
                         mV_PER_COUNT_2_56V_12BIT);
                temp = (Rpt - 1) / 0.00385;
        }
        else{
                usart_puts("**** ERROR in the temperature measurement!");
                usart_put(0x0D);
        }

        return temp;
}


//function to read the reflectance of the mirror through the ADC
int reflector_read(){
        int adc_value;
        int reflex = 0; //The ADC counts of the phototransistor receiver

        // Measurement procedure
        PORTD |= (1 << PD3);                    // LED on
        _delay_ms(10);                          // Wait until stable
        adc_value = adc_read(REFLECTOR_CHANNEL);// measure
        PORTD &= ~(1 << PD3);                                   // LED off

        if (adc_value > 0){
                reflex = adc_value;
        }
        else{
                usart_puts("**** ERROR in the reflector measurement!");
                usart_put(0x0D);
        }

        return reflex;
}
```

C.3 adc.h

```
#include <avr/interrupt.h>

#include "adc.h"
#include "define.h"

void adc_init_frm(void){
        ADCSRA |= (1 << ADPS1) | (1 << ADPS0); // Set the ADC timer to F / 8
        ADMUX  |= (1 << REFS0); // Set the reference voltage to AVCC
        ADCSRA |= (1 << ADEN);  // Enable the ADC
        ADCSRA |= (1 << ADSC);  // Start Conversion
        ADCSRA |= (1 << ADATE); // Set to auto trigger. Enable free running
            mode.
}


void adc_init_sc(void){
        ADCSRA |= (1 << ADPS1) | (1 << ADPS0);  // Set the ADC timer to F /
            8
        ADMUX  |= (1 << REFS0); // Set the reference voltage to AVCC
        ADCSRA |= (1 << ADEN);  // Enable the ADC
        ADCSRA |= (1 << ADIE);
}


int adc_read(int channel){
        int32_t adc_value_sum = 0;
        int  adc_value_over = 0;
        int32_t  adc_value_avg = 0;
        int result = 0;

        //Delete the previous ADC channel
        ADMUX &= 0b11110000;
        //set ADC channel and the Voltage reference
        if (channel == PT_CHANNEL){
                ADMUX  |= (1 << REFS0) | (1 << REFS1);
        }
        else if (channel == REFLECTOR_CHANNEL){
                ADMUX  |= (1 << REFS0) | (1 << REFS1);
                ADMUX |= (1 << MUX0);
        }
        else if(channel == 2)
                ADMUX |= (1 << MUX1);
        else if(channel == 3)
                ADMUX |= (1 << MUX1) | (1 << MUX0);


        //Averaging
        for (int j=0;j< ADC_AVERAGING; j++){
                //Oversampling
                adc_value_sum = 0;
                for (int i=0; i< ADC_OVERSAMPLING; i++){
                        MCUCR |= (1<<SE);               // Set enable sleep
                        ADCSRA |= (1 << ADSC);      // Start Conversion
                        __asm volatile("sleep");    // Go to sleep
                        MCUCR &= ~(1<<SE);              // Clear enable sleep

                        result  =  ADCL;
                        result +=  (ADCH << 8);

                        adc_value_sum += result;
                }
                adc_value_over = adc_value_sum / ( ADC_OVERSAMPLING / 4 );
```

```
                adc_value_avg += adc_value_over;
        }
        adc_value_avg = adc_value_avg / ADC_AVERAGING;

        return (int) adc_value_avg;
}


ISR(ADC_vect){
        MCUCR &= ~(1<<SE); //Clear enable sleep
}
```

C.4 pwm.h

```
#include <avr/io.h>

#include "define.h"

void pwm_init(void) {
        //Use Timer1 for PWM
        DDRD |= _BV(DDD5);
        //Phase Correct PWM with 10bit resolution
        TCCR1A |= (1 << WGM10) | (1 << WGM11);
        //Prescaler = 1. f_PWM = f_clock
        TCCR1B |= (1 << CS10);
        //Set output to LOW level when on compare match
        TCCR1A |= (1 << COM1A1);
}


int pwm_dc_set(int duty_cycle){
        float reg_value;

        // Depending on the resolution use MAX_nBIT
        reg_value = (float) duty_cycle * MAX_10BIT / 1000;
        reg_value += 0.5; // Rounding to the closest the integer
        OCR1A = reg_value;

        return reg_value;
}
```

C.5 usart.h

```
#include <stdio.h>
#include <stdlib.h>

#include <avr/io.h>

#include "usart.h"

void usart_init(unsigned int baud) {
        /* Set baud rate */
        UBRRH = (unsigned char)(baud>>8);
        UBRRL = (unsigned char)baud;
        UCSRA =0x00;
        /* Enable receiver and transmitter */
        UCSRB = (1<<RXEN)|(1<<TXEN);
        /* Set frame format: 8data, 2stop bit, Odd Parity */
        UCSRC = (1<<URSEL)|(1<<USBS)|(1<<UCSZ0)|(1<<UCSZ1)|(1<<UPM1)|(1<<
            UPM0);
}


void usart_put(unsigned char data) {
        /* Wait for empty transmit buffer */
        while ( !( UCSRA & (1<<UDRE)) );
        /* Put data into buffer, sends the data */
        UDR = data;
}


unsigned char usart_receive(void) {
        /* Wait for data to be received */
        while ( !(UCSRA & (1<<RXC)) );
        /* Get and return received data from buffer */
        return UDR;
}


void usart_puts(const char *data_string) {
        while (*data_string != 0x00){
                usart_put(*data_string++);
        }
}

void usart_putint(int number){
        char help_string[6];
        itoa(number, help_string, 10);

        usart_puts(help_string);
}
```

C.6 define.h

```
#ifndef DEFINE_H
#define DEFINE_H

//=============================
// READOUT CIRCUIT DEFINITONS
//=============================
//***** Global Attributes *****
//The maximum of the ADC counts
#define ADC_MAX                         1023
//The system voltage in mV
#define VCC                             5000
//The mV per ADC count when reference is 5V
#define mV_PER_COUNT_5V                 4.883
//The mV per ADC count when reference is 2.56V
#define mV_PER_COUNT_2_56V              2.5
//The mV per ADC count when reference is 5V
//and oversampled 12 bit
#define mV_PER_COUNT_2_56V_12BIT        0.625



//***** PT Cicruit definitions *****
//The resistor in the PT-1000 circuit (KOhm)
#define R1  10.0
#define PT_CHANNEL  0
#define TEMP_AMP_GAIN  13.0
#define V_DEDUCTION  5050


//***** Reflector Cicruit definitions *****
#define REFLECTOR_CHANNEL 1

//***** Mirror State Definitions *****
#define WET 1
#define FREE 0
//ADC counts of water layer formation
#define DEW_STEP 10

//***** ADC Oversampling & Averaging *****
//The number of samples to achieve extra accuracy bits.
//Samples = 4^n, where n are the extra bits.
#define ADC_OVERSAMPLING        16
#define ADC_AVERAGING           16

//=============================
// PWM CIRCUIT DEFINITONS
//=============================
#define MAX_16BIT       65535
#define MAX_12BIT       4095
#define MAX_10BIT       1023
#define MAX_8BIT        255
#define VDD                     4995  //In Volts (V)
#define R_SENSE         1360  //In mOhms



//=============================
// MAIN CIRCUIT DEFINITONS
//=============================
//Maximum allowed duty cyle in thousands.
#define DC_MAX  200
//Initial cooling DC value.
```

```
#define INIT_COOLING_DC 5
//Definition of the wet mirror as a percentage
//of the clean mirror reflectance. This value is
//the percantage
#define WATER_LAYER_ADC 0.99
//The number of temperature points that get archived
#define TEMP_ARCH_NO    50


// ***** Initialization Procedure *****
//Heating step in duty cycle
#define INIT_DC_HEATING_STEP            4
//Cooling step in duty cycle
#define INIT_DC_COOLING_STEP            4
//Temperature deviation allowed to assume stability (oC)
#define INIT_DEVIATION_LIMIT            0.5
//The number of temp points calculated for the statistics
#define INIT_TEMP_SAMPLES_NUMBER        50



// ***** SCP Procedure *****
//Heating step in duty cycle
#define SCP_DC_COOLING_STEP     1
//Cooling step in duty cycle
#define SCP_DC_HEATING_STEP     1
//Step in duty cycle each time a detection happens
#define SCP_CP_DETECTION_STEP   2
//Temperature deviation allowed to assume stability (oC)
#define SCP_DEVIATION_LIMIT     0.6
//The number of temp points calculated for the statistics
#define SCP_TEMP_SAMPLES_NUMBER 50
//After SCP_NO_DET_FACTOR * last_detection_duration exit SCP
//Thios only if detection duration > SCP_NO_DET_LIM
#define SCP_NO_DET_FACTOR       3
#define SCP_NO_DET_LIM          100


// ***** RCCP Procedure *****
//Heating step in duty cycle
#define RCCP_DC_COOLING_STEP            5
//Cooling step in duty cycle
#define RCCP_DC_HEATING_STEP            5
//Step in duty cycle each time a detection happens
#define RCCP_CP_DETECTION_STEP          2
//Temperature deviation allowed to assume stability (oC)
#define RCCP_DEVIATION_LIMIT            0.6
//The number of temp points calculated for the statistics
#define RCCP_TEMP_SAMPLES_NUMBER        50

#endif /* DEFINE_H */
```

C.7 Makefile

```
#############################################################
# Makefile for the project DPsensor
#############################################################

## General Flags
PROJECT = DPsensor
MCU = atmega32
TARGET = DPsensor.elf
CC = avr-gcc

CPP = avr-g++

## Options common to compile, link and assembly rules
COMMON = -mmcu=$(MCU)

## Compile options common for all C compilation units.
CFLAGS = $(COMMON)
CFLAGS += -Wall -gdwarf-2 -std=gnu99          -DF_CPU=1000000UL -Os -funsigned
    -char -funsigned-bitfields -fpack-struct -fshort-enums
CFLAGS += -MD -MP -MT $(*F).o -MF dep/$(@F).d

## Assembly specific flags
ASMFLAGS = $(COMMON)
ASMFLAGS += $(CFLAGS)
ASMFLAGS += -x assembler-with-cpp -Wa,-gdwarf2

## Linker flags
LDFLAGS = $(COMMON)
LDFLAGS +=  -Wl,-Map=DPsensor.map


## Intel Hex file production flags
HEX_FLASH_FLAGS = -R .eeprom -R .fuse -R .lock -R .signature

HEX_EEPROM_FLAGS = -j .eeprom
HEX_EEPROM_FLAGS += --set-section-flags=.eeprom="alloc,load"
HEX_EEPROM_FLAGS += --change-section-lma .eeprom=0 --no-change-warnings


## Libraries
LIBS = -lm -lprintf_flt -lc

## Objects that must be built in order to link
OBJECTS = DPsensor.o

## Objects explicitly added by the user
LINKONLYOBJECTS =

## Build
all: $(TARGET) DPsensor.hex DPsensor.eep DPsensor.lss size

## Compile
DPsensor.o: DPsensor.c
	$(CC) $(INCLUDES) $(CFLAGS) -c  $<

##Link
$(TARGET): $(OBJECTS)
	 $(CC) $(LDFLAGS) $(OBJECTS) $(LINKONLYOBJECTS) $(LIBDIRS) $(LIBS) -
	     o $(TARGET)

%.hex: $(TARGET)
	avr-objcopy -O ihex $(HEX_FLASH_FLAGS)  $< $@
```

```
%.eep: $(TARGET)
	-avr-objcopy $(HEX_EEPROM_FLAGS) -O ihex $< $@ || exit 0

%.lss: $(TARGET)
	avr-objdump -h -S $< > $@

size: ${TARGET}
	@echo
	@avr-size -C --mcu=${MCU} ${TARGET}

## Clean target
.PHONY: clean
clean:
	-rm -rf $(OBJECTS) DPsensor.elf dep/* DPsensor.hex DPsensor.eep
	    DPsensor.lss DPsensor.map


## Other dependencies
-include $(shell mkdir dep 2>/dev/null) $(wildcard dep/*)
```

Bibliography

[1] J.G.Korvink, L.Chandran, T.Boltshauser, H.Baltes , "Accurate 3d capacitance evaluation in integrated capacitive humidity sensors," Sensors and Materials, vol. 4, no. 1, pp. 323 – 335, 1993.

[2] G. Gerlach and K. Sager, "A piezoresistive humidity sensor," Sensors Actuators A, vol. 43, pp. 181–184, 1994.

[3] V. M. Mecea, J. O. Carlsson, P. Heszler, and M. Bârtan, "Development and testing of a high temperature quartz crystal microbalance," Vacuum, vol. 46, no. 7, pp. 691 – 694, 1995.

[4] B. I. K. J. C. N. H. S. Kwon, S. Y. Choi, "A highly stable quartz crystal microbalance sensor and its application to water vapor measurements," Journal of Korean Physical Society, vol. 48, no. 1, pp. 161 – 165, 2006.

[5] E. Radeva, V. Georgiev, L. Spassov, N. Koprinarov, and S. Kanev, "Humidity adsorptive properties of thin fullerene layers studied by means of quartz microbalance," Sensors and Actuators B: Chemical, vol. 42, no. 1, pp. 11 – 13, 1997.

[6] H.-T. Sun, Z.-T. Cheng, X. Yao, and W. Wlodarski, "Humidity sensor using sol–gel-derived silica coating on quartz crystal," Sensors and Actuators B: Chemical, vol. 13, no. 1-3, pp. 107 – 110, 1993.

[7] F. Pascal-Delannoy, B. Sorli, and A. Boyer, "Quartz crystal microbalance (qcm) used as humidity sensor," Sensors and Actuators A: Physical, vol. 84, no. 3, pp. 285 – 291, 2000.

[8] M. Hoummady, C. Bonjour, J. Collin, F. Lardet-Vieudrin, and G. Martin, "Surface acoustic wave (saw) dew point sensor: application to dew point hygrometry," Sensors and Actuators B: Chemical, vol. 27, no. 1-3, pp. 315 – 317, 1995. Eurosensors VIII.

[9] F. Mitschke, "Fiber-optic sensor for humidity," Opt. Lett., vol. 14, no. 17, pp. 967–969, 1989.

[10] W. Kunzler, S. G. Calvert, and M. Laylor, "Measuring humidity and moisture with fiber optic sensors," vol. 5278, pp. 86–93, SPIE, 2003.

[11] S. Luo, Y. Liu, A. Sucheta, M. K. Evans, and R. V. Tassell, "Applications of lpg fiber optical sensors for relative humidity and chemical-warfare-agents monitoring," vol. 4920, pp. 193–204, SPIE, 2002.

[12] A. Alvarez-Herrero, H. Guerrero, and D. Levy, "High-sensitivity sensor of low relative humidity based on overlay on side-polished fibers," Sensors Journal, IEEE, vol. 4, pp. 52 – 56, feb. 2004.

[13] R. S. Jackowicz and W. J. Makulski, "Optimal measurement procedures for a dew point hygrometer system," IEEE Transactions on Instrumentation and Measurement, 1993.

[14] J. Gmbh, Datasheet.

[15] Melcor, "Thermoelectric handbook." www.melcor.com.

[16] C. C. P. Joseph A. Curcio, "The near infrared absorption spectrum of liquid water," Journal of the Optical Society of America, 1951.

[17] F. Toselli, Imaging Spectroscopy. Kluwer Academic Publishers, 1992.

[18] Honeywell, http://sensing.honeywell.com/index.cfm?ci_id=140301&la_id=1&pr_id=152782, Honeywell HOA0708 011 Reflective Sensor, March 2010.

[19] Atmel, http://www.atmel.com/dyn/resources/prod_documents/doc2503.pdf, Atmel ATMega32 microcontroller datasheet, October 2006.

[20] Sensirion, Datasheet SHT7x. http://www.sensirion.com/en/pdf/product_information/Datasheet-humidity-sensor-SHT7x.pdf, 4.3 ed., May 2010.

[21] Sensirion, Datasheet Evaluation Kit EK-H4. http://www.sensirion.com/en/pdf/product_information/Datasheet_EvalKit_Humidity_Sensors_EK-H4.pdf, 1.1 ed., May 2010.

[22] D. Acosta, M. Della Negra, L. Foa, A. Herve, and A. Petrilli, CMS physics: Technical Design Report. Technical Design Report CMS, Geneva: CERN.

[23] "The CMS information site." http://cms.web.cern.ch/cms/index.html, jun 2010.

[24] R. S. Jachowicz, J. Weremczuk, D. Paczesny, and G. Tarapata, "A MEMS-based super fast dew point hygrometer—construction and medical applications," Measurement Science and Technology, vol. 20, p. 124008, December 2009.

[25] W. M. Organization., "Guide to meteorological instruments and methods of observation," Guide to meteorological instruments and methods of observation, 1983.